Universitat Politècnica de València
Departamento de Máquinas y Motores Térmicos

Study of different fuel injection and air management strategies as a tool for emissions control in a compression ignition engine (Diesel engine).

Doctoral Thesis
Presented by:
Daniel Estepa Ruiz
Directed by:
Dr. Santiago A. Molina Alcaide

Valencia, September, 2018

Doctoral Thesis

Study of different fuel injection and air management strategies as a tool for emissions control in a compression ignition engine (Diesel engine).

Presented by: Daniel Estepa Ruiz
Directed by: Dr. Santiago A. Molina Alcaide

Examining Board:

President: Dr. Jose Manuel Luján
Secretary: Dr. María de los Reyes García Contreras
Examiner: Dr. Gabriele Di Blasio

Reviewing Board:

Dr. Gabriele Di Blasio
Dr. Vicent Doménech
Dr. Octavio Armas

Valencia, September, 2018

Resumen.

En la actualidad, la industria del transporte es la encargada de satisfacer las necesidades logísticas del mundo. Los combustibles fósiles continúan siendo la principal fuente de energía de esta industria, y el motor Diésel, una de las tecnologías principales en la transformación de la energía química de estos combustibles en energía mecánica a través del proceso de combustión. Asociado a este proceso de transformación de la energía, un conjunto de efectos indeseados como las emisiones contaminantes o los gases de efecto invernadero han hecho movilizar a la comunidad científica. Dicha comunidad, ha realizado importantes esfuerzos en la investigación de soluciones limpias y eficientes que ayuden a minimizar los efectos indeseados del uso del motor Diésel.

Sumado a los esfuerzos en la investigación, diferentes organizaciones gubernamentales han generado normativas que regulan estas emisiones contaminantes y la industria del motor ha reaccionado integrando soluciones tecnológicas que han hecho evolucionar la configuración original del motor Diésel. Debido a razones principalmente geopolíticas, el desarrollo económico a nivel mundial no se ha dado de manera homogénea, y en la actualidad, existe una disparidad global en cuanto a las exigencias en normativa de emisiones y la implementación de tecnologías para su control, siendo estas afectadas principalmente por sus costos. Es en este contexto donde se enmarca esta tesis doctoral, cuyo objetivo principal es el estudio de diferentes estrategias de inyección y de renovación de la carga como herramienta de control de emisiones en motores de encendido por compresión, teniendo en cuenta el costo de su integración. Se busca poder definir los límites de estas estrategias de bajo costo, determinando así su potencial real en la futura normativa de los mercados emergentes.

Para abordar dicho objetivo, la tesis se ha desarrollado en tres etapas. En la primera, se ha realizado una aproximación teórico-experimental a las estrategias de inyección mediante modelado 3D-CFD y ensayos paramétricos en motor que permiten establecer como los parámetros de inyección responden al objetivo planteado. En la segunda etapa, se han estudiado las estrategias de renovación de la carga. Primero desde el modelado 1D para luego su posterior evaluación mediante su ensayo experimental en motor definiendo de esta manera las ventajas e inconvenientes de cada estrategia. En la tercera y última etapa, se han combinado todas las estrategias previamente estudiadas desde una aproximación experimental. De esta manera se puede alcanzar el objetivo de la tesis doctoral donde se ha comprobado la viabilidad de estas estrategias de bajo costo y se ha determinado su verdadero potencial como herramientas de control de las emisiones contaminantes.

Resum.

En l'actualitat, la indústria del transport és l'encarregada de satisfer les necessitats logístiques del món. Els combustibles fòssils continuen sent la principal font d'energia d'aquesta indústria, i el motor Diésel, una de les tecnologies principals en la transformació de l'energia química d'aquests combustibles en energia mecànica a través del procés de combustió. Associat a aquest procés de transformació de l'energia, un conjunt d'efectes indesitjats com les emissions contaminants o els gasos d'efecte hivernacle han fet mobilitzar a la comunitat científica. Aquesta comunitat, ha realitzat importants esforços en la recerca de solucions netes i eficients que ajuden a minimitzar els efectes indesitjats de l'ús del motor Diésel.

Sumat als esforços en la recerca, diferents organitzacions governamentals han generat normatives que regulen aquestes emissions contaminants i la indústria del motor ha reaccionat integrant solucions tecnològiques que han fet evolucionar la configuració original del motor Diésel. A causa de raons principalment geopolítiques, el desenvolupament econòmic a nivell mundial no s'ha donat de manera homogènia, i en l'actualitat, existeix una disparitat global quant a les exigències en normativa d'emissions i la implementació de tecnologies per al seu control, sent aquestes afectades principalment pels seus costos. És en aquest context on s'emmarca aquesta tesi doctoral, que el seu objectiu principal és l'estudi de diferents estratègies d'injecció i de renovació de la càrrega com a eina de control d'emissions en motors d'encès per compressió, tenint en compte el cost de la seua integració. Se cerca poder definir els límits d'aquestes estratègies de baix cost, determinant així el seu potencial real en la futura normativa dels mercats emergents.

Per a abordar dita objectiva, la tesi s'ha desenvolupat en tres etapes. En la primera, s'ha realitzat una aproximació teòric-experimental a les estratègies d'injecció mitjançant modelatge 3D-CFD i assajos paramètrics en motor que permeten establir com els paràmetres d'injecció responen a l'objectiu plantejat. En la segona etapa, s'han estudiat les estratègies de renovació de la càrrega. Primer des del modelatge 1D per a després la seua posterior avaluació mitjançant el seu assaig experimental en motor definint d'aquesta manera els avantatges i inconvenients de cada estratègia. En la tercera i última etapa, s'han combinat totes les estratègies prèviament estudiades des d'una aproximació experimental. D'aquesta manera es pot aconseguir l'objectiu de la tesi doctoral on s'ha comprovat la viabilitat d'aquestes estratègies de baix cost i s'ha determinat el seu vertader potencial com a eines de control de les emissions contaminants.

Abstract.

Nowadays, the transport industry is responsible for accomplish the world's logistics requirements. Fossil fuels continue to be the main source of energy for this industry, and the Diesel engine, one of the main technologies in the transformation of the chemical energy of these fuels into mechanical energy through combustion. Associated with this process of energy transformation, a set of undesired effects such as pollutant emissions or greenhouse gases have challenged the scientific community that has made significant research efforts aiming clean and efficient solutions.

Added to the scientific community efforts, different governmental organizations have created regulations in order to control these pollutant emissions and the engine industry has reacted by integrating technological solutions that have evolved the original configuration of the Diesel engine. Due mainly to geopolitical reasons, economic development worldwide has not occurred in a homogeneous manner, and currently, there is a global disparity regarding the requirements in emission regulations and the implementation of technologies for their control, mainly driven by their costs. It is in this framework where is set this doctoral thesis, with the main objective to study different injection and air management strategies as a tool for emission control in compression ignition engines, taking into account the cost of their integration. The aim is to be able to define the limits of these low-cost strategies, thus determining their real potential in the future regulations of emerging markets.

To address this objective, the thesis has been developed in three stages. In the first one, a theoretical-experimental approach to the injection strategies has been carried out using 3D-CFD modeling and parametric engine tests which allow us to establish how the injection parameters help to reach the depicted thesis objective. In the second stage, the air management strategies have been studied. First, from the 1D modeling point of view in order to select the best option for this platform, and later to proceed with the experimental validation of this selection. Through the described approach is possible defining the advantages and disadvantages of each air management strategy. In the third and final stage, all previously studied strategies have been combined from an experimental approach. In this way, the evaluation of these cost-effective strategies has been defined and the fully potential as a tool for emissions control has been determined thus the objective of the doctoral thesis could be achieved.

Agradecimientos - Acknowledgements.

Sabiendo de antemano que expresar en texto o en palabras sentimientos de gratitud es una tarea compleja, ya que dichas herramientas limitan la verdadera magnitud de esta característica tan humana. Las siguientes lineas pretenden dar agradecimiento a todas las personas involucradas en la realización de esta tesis doctoral.

A continuación, mencionaré de manera sincera las personas que tanto me han aportado a lo largo de mi formación profesional, todos y cada uno de ustedes tienen un espacio importante en la consecución de este objetivo y son tan participes sin importar el orden en el que son mencionados.

En primer lugar quiero agradecer a Francisco Payri, Jose María Desantes y Jesús Benajes, quienes con su esfuerzo construyeron el centro de investigación CMT motores térmicos permitiéndome así ser parte de este grupo de trabajo, que ha aportado tanto a la investigación de los motores de combustión interna.

Continuando con estos agradecimientos, quiero mencionar a mi tutor de Tesis Santiago Molina y al conjunto de profesores de la linea de Combustión, principalmente a Ricardo Novella, Antonio García, Jose María García y Jose Manuel Pastor, quienes con sus conocimientos hicieron de mi estancia en el grupo de trabajo un aprendizaje constante, compartiendo no solo sus experiencias profesionales sino también personales en este mundo de la investigación y su relación con la industria, siendo cercanos todo el tiempo y estando disponibles en todo momento.

No quiero olvidarme del conjunto de técnicos que me han ayudado en las tareas experimentales (fuente principal de esta tesis doctoral y de mi paso por CMT) brindándome otra óptica de los diversos problemas que me he encontrado, dándome consejos de la vida en la "terreta" y sacando sonrisas en momentos que a veces eran complicados. En este punto quiero personalizar en Miguel Ortíz, Gabriel Alcantarilla, Ricardo Ortega e Iván Ballesteros a lo largo de todo este tiempo fueron un soporte muy importante en todas las tareas realizadas.

Las siguientes lineas van dedicadas a mis compañeros doctorandos, en primer lugar mis compañeros de despacho Dario López por quien guardo una gran admiración y auguré desde que lo conocí un futuro brillante en la investigación, Kevin Thein y Jorge Valero con quienes compartí conocimientos y buenos momentos en el día a día en el centro de investigación. En este punto caben todos los demás compañeros tanto de la linea de combustión, como de las demás lineas de trabajo, para lo cuales no tengo mas que agradecimiento ya que en muchos momentos de dudas fueron siempre un apoyo.

C'est le moment pour remercier tous les membres du groupe advanced engineering chez Volvo group trucks technology. Vous avez apporté des importantes expériences dans l'industrie et des expériences personnelles dans mon séjour à Lyon. Particulièrement, Laurent Beauvir et Iyad Balloul merci pour votre aide pendante la réalisation de mon stage de doctorat.

Quiero dedicar también unas lineas de agradecimiento muy importantes a todos aquellos que hicieron que mi paso por Valencia no fuera "incógnito", y que un "moreno" como yo viviendo en Benimaclet se sintiera un Valenciano más. Partidos de fútbol y sus cervezas, salidas a comer, fallas y todas las demás actividades son todas "escenas" que me llevo guardadas en el carriel paisa.

Para terminar, y no menos importante, quiero dedicar estas lineas finales a toda mi familia, quienes me han hecho sentir su amor y cariño todo el tiempo a pesar de la distancia que nos separa, y durante todos estos años que he estado fuera de mi país. Padre, Madre y hermano saben ustedes que los esfuerzos son el motor de nuestras vidas y son ustedes la energía que me levanta y me lleva adelante ¡GRACIAS!.

A mi familia

Table of Contents

Index of Figures

Index of Tables

Nomenclature

Latin

A_s	Surface area
A/F	Air fuel ratio
$CA50$	Combustion angle 50%
$CA75$	Combustion angle 75%
$CA90$	Combustion angle 90%
C_p	Heat capacity at constant pressure
CR	Compression ratio
C_v	Heat capacity at constant volume
ΔHRL	Fuel released thermal energy
ΔQ	Heat transfer from the gas trapped to the surrounding surfaces
Δm_{bb}	Mass flow due to blow-by
H	Enthalpy
$\dot{m}_{air}$	Total air mass flow
$\dot{m}_f$	Total fuel mass flow injected
n	Engine speed
N_i	mole number of reactants
N_j	mole number of products
P	Pressure
P_{int}	Intake pressure
P_{exh}	Exhaust pressure
R	Universal gas constant
T	Temperature
T_{adb}	Adiabatic flame temperature
u	Flow velocity

Y_{O2}	Oxygen concentration

Greek

α	DOE levels
ρ	Density

Subscripts

air	Referred to atmospheric conditions
ivc	Referred to intake valve closing
evo	Referred to exhaust valve opening
est	Referred to stochiometric conditions
inj	Relative to injection process

Initials and acronyms

BDC	Bottom dead center
$BSFC$	Brake specific fuel consumption
CAD	Crank angle degree
CI	Compression Ignition
CO	Carbon monoxide
CO_2	Carbon dioxide
$Comb_{EFF}$	Combustion efficiency
CFD	Computational Fluid Dynamics
DI	Direct injection
DOC	Diesel oxidation catalyst
DoE	Design of experiments
DPF	Diesel particulate filter
ECU	Electronic Control Unit
EGR	Exhaust Gas Recirculation
EOC	End of combustion
EOI	End of injection
EVO	Exhaust valve opening
GA	Genetic algorithm
H_2O	Water
HC	Hydrocarbon
$HDVs$	Heavy duty vehicles

HRR	Heat release rate
HRL	Heat release law
$HSDI$	High speed direct injection
ICE	Internal Combustion Engine
$iEGR$	internal Exhaust Gas Recirculation
$IMEP$	Indicated mean effective pressure
IP	Injection pressure
$ISFC$	Indicated specific fuel consumption
$ISFC_{GROSS}$	Gross Indicated specific fuel consumption
$ISFC_{NET}$	NET Indicated specific fuel consumption
IVC	Intake valve closing
LIF	Laser-Induced Fluorescence
N_2	Nitrogen
NA	Nozzle angle
NO_x	NO+NO_2
O_2	Oxygen
$PAHs$	Polycyclic aromatic hydrocarbon
$PMEP$	Pumping mean effective pressure
PM	Particulate matter
SCR	Selective Catalytic Reduction
SOI	Start of injection
SOC	Start of combustion
TDC	Top Dead Center
VGT	variable geometry turbocharger

Chapter 1

Introduction

Contents

1.1 Introduction

The chapter 1 is divided into three main sections. The section 1.2 explains the technological and normative framework of this thesis, giving a detailed description of the heavy duty Diesel engine legislation, technologies and challenges. Later, in the section 1.3 are defined the thesis relevance and the objectives helping to complete the context and raising specific activities which are addressed and developed along the thesis document. The last section 1.4 describes the document structure giving a brief description of all the written chapters. This section could be used at the same time as a conceptual summary of this research work.

1.2 Technological and normative framework

1.2.1 The transport sector energy balance

Energy in all its forms is a fundamental property for every human activity. In the modern life, despite the growth of non-fossil energy (such as nuclear and hydropower) the fossil fuels continue as the main source of world energy supply with only a slightly reduction in the last 40 years from 86.7% to 81.4% as described by the International Energy Agency [1]. In the report the CO_2 emissions from fuel combustion [2], the same agency quantifies the use of energy from fossil fuels as the largest source of greenhouse gases. The fossil fuels combustion is the source of the 69% of share of the global anthropogenic greenhouse gases, where 90% corresponds to carbon dioxide (CO_2) emissions. At the same time, the total final energy consumption nearly doubled in this period, and if current trends continue unaltered, it could rise another 70% by 2050.

As described by the the state of clean transportation policy [3], the global transport sector was responsible for almost a quarter of all carbon dioxide (CO_2) emissions produced by human activity in 2010, resulting in the release of 8.8 billion metric tons (Gt) of CO_2 into the atmosphere consuming 47 million barrels per day of oil (mbd). In the Fig. 1.1. could be observed in the transport sector how on-road vehicles accounted for about three-quarters of fuel consumption (35 mbd) and CO_2 emissions (6.5 $GtCO_2$) with almost a half of this numbers generated from heavy-duty vehicles which are mainly driven by heavy duty compression ignition (CI) -Diesel- engines.

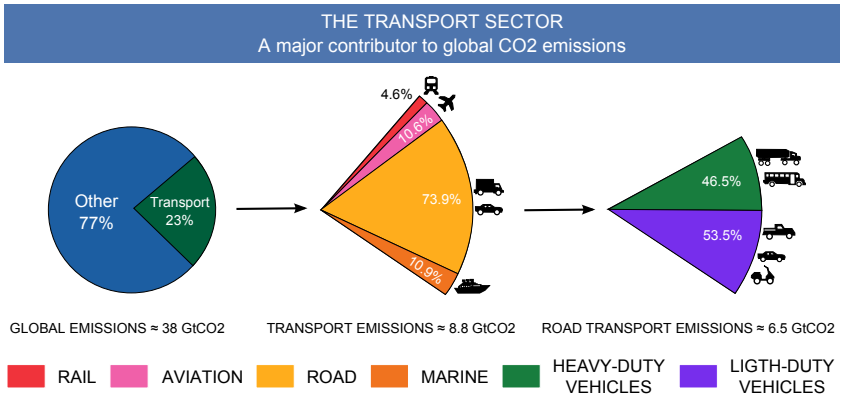

Figure 1.1: Contribution of transport industry in the total CO_2 emissions [3]

1.2.2 The heavy duty CI engine pollutants and legislation

Historically, the higher efficiency of compression ignition (CI) engines than spark ignition (SI) engines has led them to lead heavy-duty transportation with a share greater than 60% over the world as described in the The future of trucks in 2017 [4]. However, in spite of offering improved fuel economy, heavy duty CI engines are major contributor to transport-related pollutant emissions. In the case of NO_x, heavy duty vehicles contribute more than one-third of total transport-related emissions. For Particulate matter (PM) 2.5 emissions, they account for nearly half of total transport-related emissions, all numbers extracted from the same report.

The main pollutants associated to the heavy duty CI engines operation are now described:

- Particulate matter (PM) is a complex aggregate formed by soot, hydrocarbons (HC) resulting from fuel and lubrication, and other minor products. Major concerns for human health from exposure to PM are related to damaging in the breathing and respiratory systems. Transportation sector, composed mostly by internal combustion engines (ICEs) as described in previous section, is responsible of 11% of the particles with diameter of 10 um or less (PM10) and 16% of the PM2.5 emitted to the atmosphere [5].

- Nitrogen oxides (NO_x) cause a wide variety of health and environmental damages. NO_x react with the volatile organic compounds forming ozone at ground level, which causes respiratory illness and other health problems and at the same time they contribute to acid deposition and

eutrophication, which can lead to potential changes in soil and water quality [6]. Since NO_x formation is benefited from high temperatures and lean combustion environments, they suppose a major challenge for heavy duty CI engines.

- Carbon monoxide (CO) is produced from the partial oxidation of the fuel when there is not enough oxygen to produce carbon dioxide (CO_2). It is a dangerous colorless, odorless and tasteless gas which potentially enters the bloodstream and reduces oxygen delivery to the body's organs and tissues [7]. However, CO emissions are not a major concern of CI engines due to the excess of oxygen in the ambient during combustion development.

- Hydrocarbons (HC) are a product of an incomplete combustion of the injected fuel due to rich conditions and low temperatures that can locally be achieved inside the cylinder. Partially oxidized HC and non-burnt HC are usually included inside this group. As the case of carbon monoxide, HC emissions are of less importance than NO_x and PM in Diesel engines.

In this challenging framework, the world authorities have developed regulations about pollutant emissions in heavy duty CI engines which have become increasingly restrictive during the last years. Fig. 1.2 shows the evolution of the European emission standards for heavy duty vehicles in the case of heavy duty Compression-Ignition engines in the left side the NO_x and PM evolution and in the right side the CO and HC ones. It can be seen that the trend from EURO I (1992) to EURO VI (2014) is to decrease the limits of pollutant emissions, specially for nitrogen oxides (NO_x) and Diesel engines have reduced the NO_x limits in 95%, while the maximum soot emissions have been reduced in 98%.

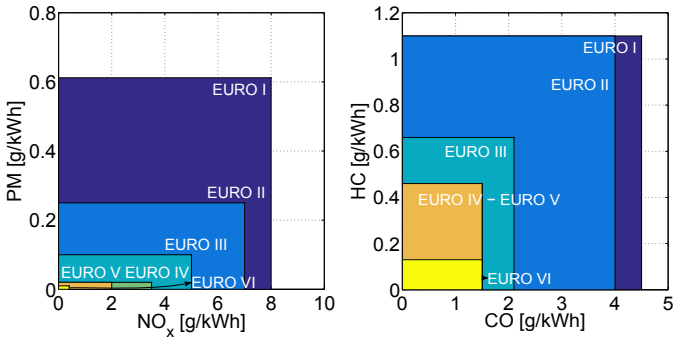

Figure 1.2: European emission legislation historically [3]

In the same way than European authorities, as mentioned before, the world first economies have defined their own emission standards and the heavy duty CI engines have been evolving in order to fulfill the legislation and all the industrial requirements. In the Fig. 1.3 could be seen the evolution of the world emission standards in the same euro standard framework. The world first economies have been concerned about the pollutants in heavy duty CI engines from beginning of the 90s decade [8] and their evolution creates a gap between its policies and the emerging markets policies which have been on back step in the emission legislation exigences.

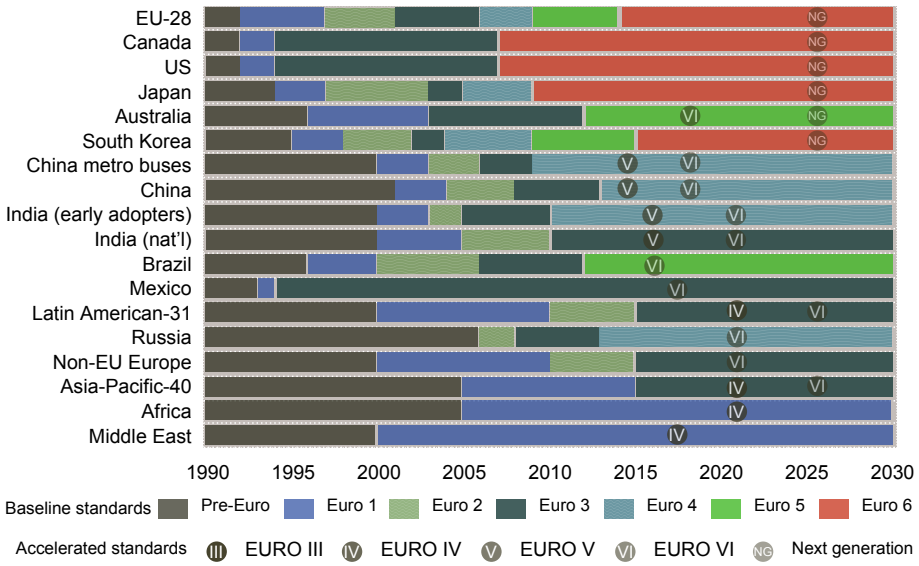

Figure 1.3: Global emissions legislation EURO equivalence [3]

According to Fig. 1.4, it is in this moment when the emerging markets, which traditionally have been one step back in terms of emission legislation requirements, are beginning to increase their exigences in terms of heavy duty vehicles emissions and in this context, to apply the same technological answers than first economies, may lead to increase the total vehicle cost and in the worst scenario the abusive use of the scarce natural resources.

In this actual and complex framework, this thesis gives an overview of the cost-effective combustion systems through modern modeling tools, which are supported by parametric experimental studies, defining the real effectiveness of these cost-effective combustion systems. In the same way, this thesis serves to define the limits of this kind of technological approaches for future regulations in emerging markets.

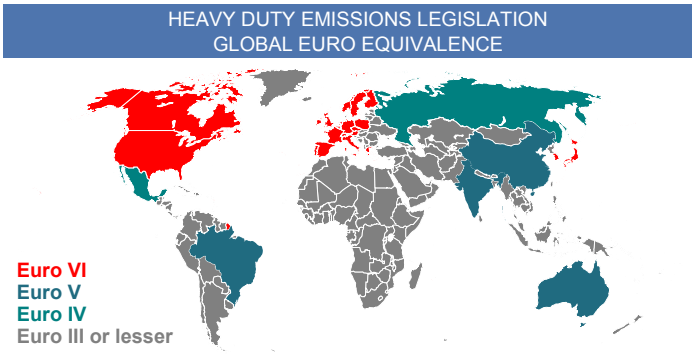

Figure 1.4: Global emissions legislation EURO equivalence

1.2.3 The technological answer to heavy duty CI engine legislation

There are two ways to reduce the pollutant emissions in heavy duty CI engines as described by Novella [9]. On the one hand, the formation of pollutant emissions can be avoided directly during the combustion process. Electronically controlled fuel injection, Exhaust Gas Recirculation (EGR) or different air management configuration through modification of cam profiles were until the EURO IV the solutions adopted by the engine industry to face up the first economies emission regulations. These kinds of emissions control tools could be grouped as the in-cylinder engine control strategies.

On the other hand, the pollutant emissions can be reduced or controlled by means of after-treatment systems located in the exhaust manifold as observed in Fig. 1.5. Selective Catalytic Reduction (SCR) after-treatment systems for the reduction of NO_x [10], Diesel particulate filter (DPF) and Diesel oxidation catalyst (DOC) to remove particulates and unburned hydrocarbons (HC) and carbon monoxide (CO) emissions [11] are the most used after-treatment systems and they are commonly found in the heavy duty vehicles of the first economies to face up the legislation after EURO IV.

As previously mentioned, the after-treatment systems are integrated in the Diesel engine design process, in order to fulfill the EURO V emission limits and later ones. EURO V limit was a challenging first step for the Diesel engine manufacturers which have combined SCR + DOC technologies or DPF + DOC technologies with the aim to accomplish this pollutant control policy. In the second generation of heavy duty Diesel engines integrating after-treatment solutions to fulfill the newest EURO VI limits all the technologies SCR + DPF + DOC are coupled and integrated despite the associated increase of the heavy duty CI engine cost and the use of scarce natural resources.

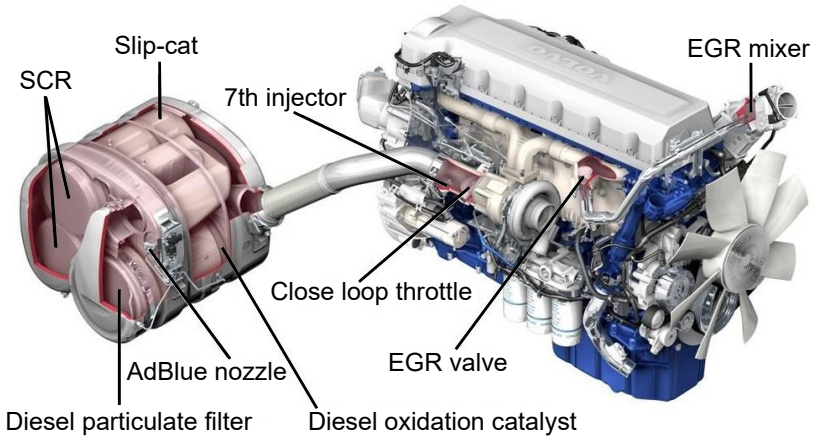

Figure 1.5: Different subsystems of VOLVO D13K460 EURO VI version [12]

1.2.4 The fuel quality constraint

The after-treatment solutions described in the previous section, have associated, additionally to their high cost implementation, an important constraint in the fuel quality requirements. In the emerging markets to guarantee a free sulfur content fuel is a difficult task, the fuel sulfur content which plays a key role in the capacity to reduce the pollutants in the after-treatment systems is higher in these kind of markets making difficult the engine integration of the after-treatment solutions [13]. In this subsection is done a description of each after-treatment device affectation under the presence of sulfur in the fuel quality.

The DOCs are the most common after-treatment emissions control technology found in current Diesel vehicles. DOCs are very similar to the earliest catalysts used for gasoline engines. Oxidation catalysts work by oxidizing CO, HC and the soluble organic fraction of the PM to CO_2 and H_2O in the oxygen rich exhaust stream of the Diesel engine. When sulfur is present in the fuel, DOCs also increase the oxidation rate of SO_2, leading to dramatic increases in sulfate nanoparticle emissions. Sulfate conversion depends on overall catalyst efficiency, with more efficient catalysts capable of converting nearly 100% of the SO_2 in the exhaust to sulfate. Generally, one should restrict the use of DOCs to areas which have fuel sulfur levels of 500 PPM or below. With low sulfur fuel, a DOC can reduce PM emissions by 25 o 30%.

Diesel particulate filters already reliably demonstrate over 95% efficiency with near-zero sulfur fuel use. They are also capable of reducing the total number of particle emissions below those of gasoline engines. One

important area of research the area most impacted by sulfur levels is the passive regeneration or cleaning of the collected particles from the filter surface. Filters need to be cleaned, ideally without human intervention, before reaching capacity in order to maintain vehicle performance and fuel and filter efficiency.The Continuously Regenerating Diesel Particulate Filter (CR-DPF) and the Catalyzed Diesel Particulate Filter (CDPF) are two examples of PM control with passive regeneration. The CR-DPF and CDPF devices can achieve 95% efficiency for control of PM emissions with 3 ppm sulfur fuel. But efficiency drops to zero with 150 ppm sulfur fuel and PM emissions more than double over the baseline with 350 ppm sulfur fuel. The increase in PM mass comes mostly from water bound to sulfuric acid. Soot emission also increase with higher sulfur fuel but even with the 350 ppm sulfur fuel DPFs maintain around 50% efficiency for non-sulfate PM. The systems eventually recover to original PM control efficiency with return to use of near - zero sulfur fuels, but recovery takes time due to sulfate storage on the catalyst. Sulfur also increases the required temperature for regeneration of the filter. In moving from 3 to 30 ppm sulfur fuel, the exhaust temperatures required for regeneration increase by roughly 25°C. The CDPF requires consistently higher temperatures but holds stable above 30 ppm, while the CR DPF requires a very-increasing temperatures.

Two very different technologies NO_x adsorbers and selective catalytic reduction systems are the most likely alternatives for further NO_x control. In the case of NO_x adsorbers or Lean NO_x trap the same compounds that are used to store NO_x are even more effective at storing sulfur as sulfates, and therefore NO_x adsorbers require ultra low sulfur Diesel fuel [14]. In the SCR technologies the case of Zeolite-type catalysts will deactivate very rapidly with high-sulfur fuels. Vanadium-type catalysts are sulfur tolerant. To a certain degree, the SCR activity is increased by the presence of sulfur-oxides as the catalyst surface will be acidified [15].

1.3 Thesis relevance and objectives

Regarding the background shown in the previous section it could be noticed the thesis relevance in a framework of future restrictive regulations in emerging markets. At this juncture and with the defined scope, the main objective of this thesis could be summarized as follows:

Evaluating and defining a cost-effective heavy duty CI engine architecture for emerging markets, in terms of performance and pollutants, in a framework of future restrictive emission regulation.

In order to address the development of this main objective it must be defined a group of sub-objectives which help to describe and technically justify the selected cost-effective solutions, the methodological path followed during the study and the complete simulated and tested results supporting and bringing cohesion to this research work:

- Exploring the different technological approaches used by the CI engine industry and the research community through a complete literature review in order to define the cost-effective solutions applied as emission control.
- Defining a set of experimental and theoretical tools which helps to study, understand and evaluate the real potential of this cost-effective technological solutions.
- Evaluating in a framework of real emission legislation the limits of each cost-effective heavy duty CI engine through the experimental and theoretical tools defined in the previous sub-objective.
- Comparing the results of each emission control cost-effective tools highlighting the limits and the potential of each one, and contrasting it with its troubles and weaknesses.

1.4 Thesis structure

The document structure is organized in seven chapters grouped in 3 blocks. The first chapters block includes this introduction chapter which is the number 1 as could be observed in Fig. 1.6. The chapter 2 is composed of a complete literature review where are depicted the most relevant research works in the fields of formation and pollutants control in heavy duty CI engines and it serves to frame the state-of-the-art of the studied solutions.

Finishing the first block, the chapter 3 defines the different experimental and theoretical tools which are required for the proper analysis of the results, specially when considering the added complexity from the Diesel engine operation. In this chapter, a general description is given over the experimental installation and measurement equipment used in the study, the definition of the general testing methodology and finally, the most relevant modeling tools used to perform the 1D and 3D CFD simulations during the exploration of the cost-effective engine definitions.

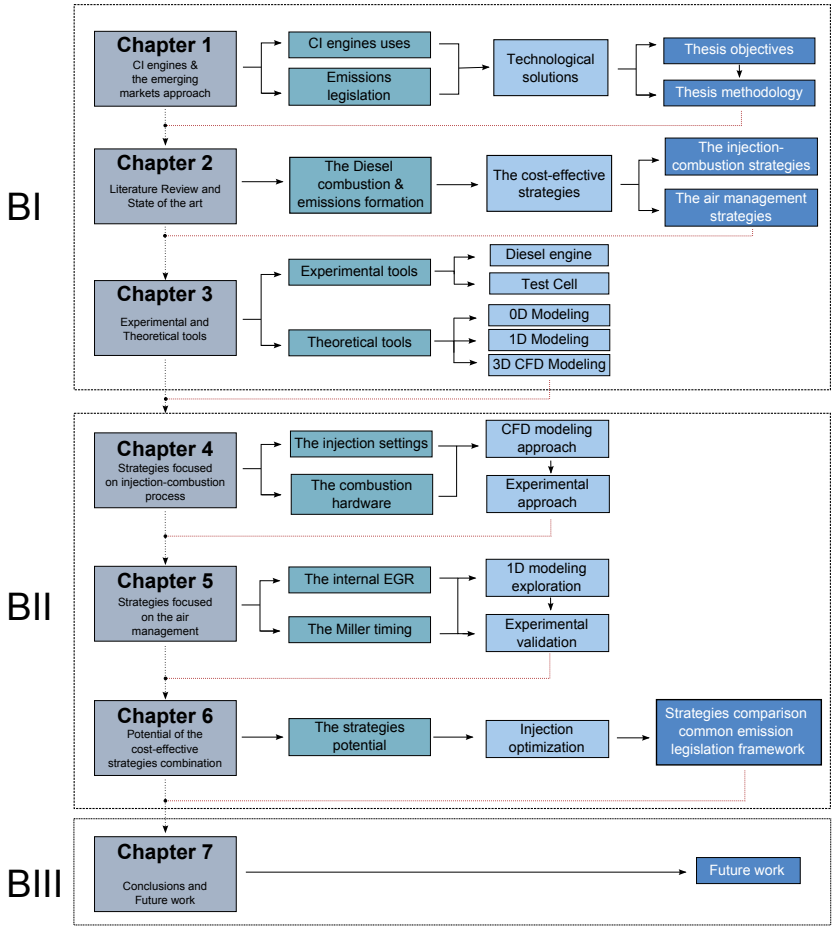

Figure 1.6: Summary diagram of the thesis structure

The second block is composed of the chapter 4 and chapter 5 and chapter 6. In this case chapter 4 and chapter 5, are mainly based in the theoretical modeling tools and the experimental results obtained with the multi cylinder heavy duty CI engine; Chapter 4 comprises the studies related to the analysis and optimization of the injection/combustion settings where a dedicated Design of Experiments (DoE) methodology applied in the 3D CFD modeling combined with traditional parametric engine testing are used to identify cause/effect relations of the injection settings and combustion hardware parameters. This combined approach illustrates the governing phenomena affecting the mixture preparation, the combustion development and the emissions formation processes under this cost-effective engine definition. Chapter 5 is composed of the exploration of the air management strategies, in

first instance the 1D model serves to identify the best configuration of Miller cycle and the internal EGR defining in this way, through the 1D simulations, the optimal cam profiles to be tested. Later, the experimental study of the selected cam profiles is done over the predefined regulations engine operating conditions using the heavy duty CI engine.

The chapter 6 is a synthesis chapter. In this chapter all the engine conditions measured experimentally are placed and compared in a common reference framework. Later, they are weighted as defined in the normative, which allow defining the real limits of each cost-effective engine definition. Along this key chapter, they are given the basis to conclude about the main potential of these solutions in a restrictive emission regulation policy in emerging markets.

The third and last block is composed of chapter 7. This chapter describes the main conclusions of this research work and highlights the most relevant results obtained in this study. In the same way the conclusions are the starting point to propose new possible research directions giving a complete overview of the future work in this research field.

Bibliography

[1] iea International Energy Agency. *Key world energy statistics.* International Energy Agency iea, 2017.

[2] iea International Energy Agency. *CO2 Emissions from Fuel Combustion Highlights.* International Energy Agency iea, 2017.

[3] Miller J. D. and Façanha C. *The State of clean transport policy.* The international council on clean transportation, 2014.

[4] iea International Energy Agency. *The Future of Trucks Implications for Energy and the Environment.* International Energy Agency iea, 2017.

[5] Agency European Environment. *Emissions of primary PM2.5 and PM10 particulate matter.* European Environment Agency, 2010.

[6] air technology center (MD-12) Clean. *Nitrogen oxides (NOx), why and how they are controlled.* Environmental Protection Agency, 1999.

[7] Weaver L. K. "Carbon monoxide poisoning". *Critical Care Clinics*, Vol. 15 n^o 2, pp. 297–317, 1999.

[8] Molina S. A. *Influencia de los parámetros de inyección y la recirculación de gases de escape sobre el proceso de combustión en un motor Diesel.* Doctoral Thesis, Universidad Politécnica de Valencia, Departamento de Máquinas y Motores Térmicos, 2003.

[9] Novella R. *Influencia de los ciclos Atkinson y Miller sobre el proceso de combustión y las emisiones contaminantes en un motor Diesel.* Doctoral Thesis, Universidad Politécnica de Valencia, Departamento de Máquinas y Motores Térmicos, 2009.

[10] Piumetti M., Bensaid S., Fino D. and Russo N. "Catalysis in Diesel engine NOx aftertreatment: a review". *Catalysis, Structure & Reactivity*, Vol. 1 n^o 4, pp. 155–173, 2015.

[11] Serrano J. R., Bermúdez V., Piqueras P. and Angiolini E. "On the impact of DPF downsizing and cellular geometry on filtration efficiency in pre- and post-turbine placement". *Journal of Aerosol Science*, Vol. 113 n^o Supplement C, pp. 20–35, 2017.

[12] Volvo Group Trucks Technology . *VOLVO D13K460 EURO VI version.* Available technical information in http://http://productinfo.vtc.volvo.se/STPIFiles/Volvo/FactSheet/D13K460,

[13] Blumberg K. O., Wals M. P. and Charlotte P. *Low-sulfur gasoline & Diesel: The key to lower vehicle emissions.* The international council of clean transportation (ICCT), 2003.

[14] Association Manufacturers Emission Controls. *Emission Control Technologies for Diesel-Powered Vehicles.* Manufacturers of Emission Controls Association, 2007.

[15] Nova I. and Tronconi E. *Urea-SCR Technology for deNOx After Treatment of Diesel Exhausts.* Springer, 2014.

Chapter 2

Literature review and state of the art

Contents

2.1 Introduction

In order to accomplish the objectives and sub-objectives described in the chapter 1. The first step in the thesis development is to perform a complete literature review. This chapter begins describing the Diesel emissions dilemma. In particular, a description of the conventional Diesel combustion process is discussed, In this way, it is possible to understand the reasons governing the classical trade-off between NO_x and soot emissions, experienced during conventional Diesel operation as the majority of the Diesel engines in emerging markets. Later the state of the art comprising the cost-effective emissions control solutions is defined as well as their characteristics and their ranges of application in an emission legislation framework.

2.2 Conventional Diesel combustion

In the last years significant progress has been made in understanding the Diesel combustion process. In this section, based on the last published research work it is given an overview of the conventional Diesel combustion concept. The main objective is to depict an updated summary of the physical and chemical processes which occurs in the combustion chamber of a direct injection Diesel engine. The conventional Diesel combustion description is done in a qualitative way taking the main conclusions between the different conceptual models developed by the engine research community.

2.2.1 Temporal evolution of the Diesel combustion

In order to simplify a really complex process combining physical and chemical process, the review of Diesel combustion in this subsection is faced time dependent describing the main processes occurring inside the cylinder. Beginning at the moment when the fuel leaves the injector nozzle and is injected into the combustion chamber, at this moment it exist a high density and high temperature environment that promotes mixing, evaporation, and ignition of the fuel-air mixture. Later if it is the case of a single injection strategy timed relatively close to the top-dead-center (TDC) with a sufficiently long duration, the analysis of the injection rate and the heat release rate (HRR) allow identifying the different phases of the combustion process following the chronological order, as presented in Fig. 2.1.

The HRR is obtained from the analysis of the cylinder pressure using a 0-D model based on the application of the first law of thermodynamics CALMEC

which is discussed in chapter 3, in the theoretical tools section. The HRR helps to describe the phenomena which the chemical energy contained within the fuel is released. The main phases of Diesel combustion are conventionally defined as follows:

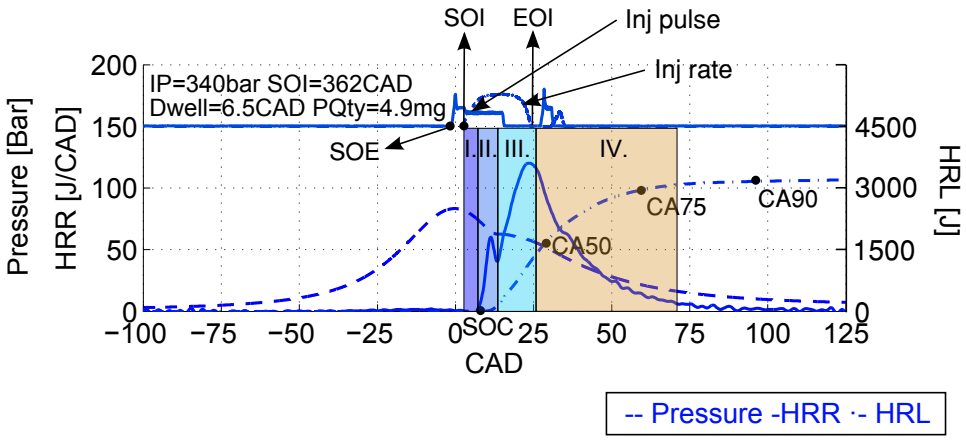

Figure 2.1: Conventional Diesel combustion phases

- *Ignition delay:* The first stage is a defined period between the start of injection (SoI) and the start of combustion (SoC). This is the elapsed time between the moment when the first fuel droplet enters into the combustion chamber environment and the time where the energy release starts to grow significantly. During the first phase the fuel is injected with no apparent or low HRR increase, as shown in Fig. 2.1. Fuel injection begins slightly before TDC, where the in-cylinder gases are hot and dense. The liquid-fuel spray mixes with the ambient gases, which provide the thermal energy to vaporize the fuel. The forming hot mixture of vaporized fuel and ambient gas is very unstable and chemical pre-reactions of low intensity start to develop. These small reactions will lead to the spontaneous self-ignition of the mixture, unleashing highly exothermic reactions until the chemical rate of the heat release eventually exceeds the vaporization energy rate. This point marks the start of the high temperature phase of the HRR, which is distinguished by a measurable pressure increase, that defines the end of the ignition delay and the start of combustion.

- *Premixed combustion:* The next phase in Diesel combustion is the premixed one, in this case the ignition reactions rapidly accelerate propagating to all the vaporized fuel injected during the delay that was

premixed during the time lag before ignition, consuming the available oxygen in the overall fuel-rich mixtures. The burning of this premixed mixture is primarily controlled by chemical kinetics so the energy is released at a fairly high rate, producing the first characteristic peak on the HRR trace. After the premixed burn, the HRR typically decreases to a lower level until reaching a relative minimum (time derivative of HRR equal to 0), which indicates the end of the premixed combustion phase and the transition towards the mixing-controlled stage or diffusion phase.

- *Fast mixing-controlled combustion:* In the third Diesel combustion phase, the injection and combustion processes continue to develop simultaneously, at this moment the mixing process of the injected fuel continue to be driven mainly by the momentum flux induced by the spray. The heat is assumed to be released at the same rate as the fuel mixes with air, and a diffusion flame is established. The reaction zone is located where the fuel-air mixture reaches stoichiometric conditions. If the injection duration is long enough, the flame structure stabilizes reaching quasi-steady conditions, which are kept until the end of the injection (EoI).

- *Slow mixing-controlled combustion:* The last Diesel combustion phase, when the injector needle starts to close a transitory state in the injection rate begin, until the injector holes are finally closed, and the introduction of mass and momentum disappears. The amount of mixture remaining in the chamber continue to burns but a slower rate, which is characterized by the HRR progressive decaying, as shown in Fig. 2.1. Combustion looses intensity and the flame change from the quasi-stationary structure to more random configurations, until the flame finally quenches and the whole combustion process is finished (EoC).

In last decades, the engine research community has provided different tools for making detailed measurements of the Diesel combustion process and define the structure of Diesel flames. Optically accessible engines and constant volume vessels combined with the development of laser imaging diagnostics allow Dec et al. [1] to propose a conceptual model for conventional Diesel combustion, which was subsequently extended by Flynn et al. [2], and became widely accepted by the scientific community as an important foundation for the understanding and modeling of the in-cylinder processes responsible for Diesel engine performance and pollutant emissions characteristics. Although a more accurate description of the temporal sequence is obtained compared

to what was previously introduced with the traditional time evolution of the HRR, most of the new contribution actually concerns the spatial resolution of the related physical and chemical processes.

2.2.2 Spacial evolution of the Diesel combustion

Early injection, ignition and stabilization: Before the start of combustion, the different processes in the spray formation are driven by physical phenomena until the moment when the oxygen content of the mixture triggers the first chemical reactions modifying both its physical and chemical environment. Several experiments and studies related to the injection and spray characterization are performed under non-reactive atmospheres in order to isolate the physical aspects from the chemical ones. For instance, the internal flow characterization of the injector, which has been widely studied by Gimeno et al. [3] and Hermens et al. [4], focuses on the study of the associated fuel pressure drops and efficiency losses, starting from the rail and arriving to the nozzle orifice outlet, which are credited for the major part to liquid friction but also to complex phenomena like cavitation, which is extensively detailed in the works of Salvador et al. [5].

At the beginning of the fuel injection event, the liquid fuel atomizes into small droplets which possibly vary their configuration by coalescence before their vaporization. The fuel mixes with air in a process which is mainly controlled by the momentum flux created by the pressure drop between the injector nozzle and the combustion chamber, then, a spray forms and goes through a succession of purely physical processes which breaks down into liquid fuel atomization, air entrainment and fuel vaporization. First, the liquid phase atomizes and then each spray penetrates into the combustion chamber, expanding into a roughly conical shape, as the in-cylinder gases (typically air or a mixture of air with combustion gases) entrained into the spray increases with downstream distance from the injector. Such processes are also very similar to those when injecting the same spray into an atmosphere of inert gases. The works of Correas [6], López [7] or Ruiz [8] provide in-depth discussions about the physical processes leading to liquid atomization and their modeling.

The increasing of penetration in the chamber causes the equivalent ratio to vary along the spray axis approximately inversely with the downstream distance as proposed by Naber et al. [9]. The equivalence ratio is defined as the ratio of local fuel ambient charge mass ratio to the stoichiometric fuel-ambient mass ratio. During this process, enough energy is entrained to heat up and evaporate the liquid fuel. At some distance downstream of the injector

nozzle, all of the fuel enters the vapor phase establishing the location of the termed "liquid length" as discussed by Naber et al. [9] and Siebers et al. [10] The liquid length can be reliably predicted to find the location where the fuel-ambient ratio is such that the thermal energy added to the jet by the entrained gas is sufficient to fully-vaporize the fuel a process well described by Siebers et al. [10] and Desantes et al. [11]

Fig. 2.2. shows a sequence of idealized schematics of the early stages of the Diesel combustion event originally presented by Dec et al. [1] and Flynn et al. [2], which has been slightly modified to include contributions from later Kosaka et al. [12] investigations . The sequence begins immediately after the start of fuel injection and show the development of a liquid jet, continuing through the premixed burn and up to the start of quasi-steady combustion. Some of the changes that were made compared to the original model of Dec [1], is that the new representation includes formaldehyde (representative of the first-stage ignition), and soot and its precursors (PAHs) are presented in a single color (red). The crank angle instants selected for the sequence are also marked in the apparent HRR profile shown on top of the figure.

For the first three crank angle degrees (from 0 to 5 ms) of the fuel injection, the liquid fuel (dark brown) and vapor fuel (light brown) penetrate together, until the fuel is fully vaporized stabilizing the liquid length at around 25 mm, from where the vapor fuel continues to penetrate beyond the liquid forming a sheath of vaporized fuel-air mixture around the periphery of the jet and at the leading edge of the jet. Fuel heating and vaporization causes a local cooling effect in the spray region, inhibiting temporally the ignition chemistry and consuming energy. As additional hot air is entrained into the jet, temperatures within the jet increases up to a level from which the first stage of ignition begins, and from that point, the mixture switches to an unstable state and chemical reactions of hydrocarbon oxidation propagate to the surroundings. The onset of this chain reaction technically marks the end of what is called the "physical induction phase" of ignition.

At this point of the discussion, it is important to remark that the detailed chemical kinetics of ignition itself is controlled by fuel molecule structure, oxygen content and temperature. Furthermore, typical Diesel fuels are composed of a mixture of thousands of chemical species, including single and multiple-ring aromatics, olefins, and branched- and straight-chain alkanes. The large fraction of long, straight-chain alkane species are responsible for much of the two-stage ignition chemistry characteristic of Diesel fuels.

The first-stage ignition period begins with the first detectable chemical activity in terms of chemiluminescence or rise in pressure, and progresses

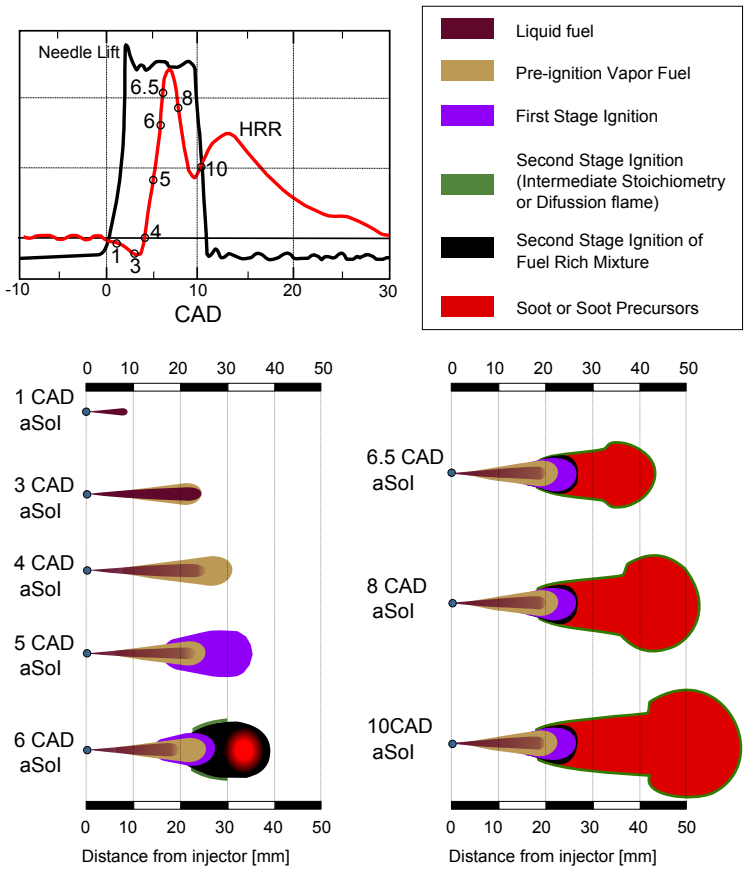

Figure 2.2: Conventional Diesel spray developement

until the rapid increase in the rate of heat release, which defines the start of the premixed burn and second-stage of ignition. It is worth to note that the duration of the first stage ignition period can vary depending on the resolution of the hardware employed for the measurement, and on the selected criteria used to consider the HRR as "significant" to mark the beginning of the premixed burn. This period is usually referred to in the literature as "low-temperature ignition". Short time after ignition, near the peak HRR of the premixed burn, the OH layer grows and forms a diffusion flame on the periphery of the fuel rich, high-temperature downstream region of the jet. The flame front moves, on one side downstream of the spray towards the jet tip, and on the other, towards the nozzle until the balance between the flame front speed and the velocities within the spray is found and "quasi-steady conditions" are reached.

Finally, it is worth to note that during the processes of second-stage ignition, the liquid length decreases somewhat, likely due to local temperature rise at the start of combustion, including a temperature increase because of compression heating from the premixed burn. Several different interpretations can be found in the literature about this transition from premixed-to diffusive phase, if the reader wants to have a more thorough description it is referred to the research carried out by Dec and Coy [13], and more recently by Higgins [14].

Quasi-steady period: After the initial transient of the spray penetration and ignition processes described in the previous subsection, the Diesel ignited spray establishes and progresses until reaching its natural maximum length being the moment when it is defined the "quasi-steady" period (during which the characteristic description of the combusting jet does not change), while the combustion is sustained by the convective and diffusive contribution of fuel and oxygen. For the operating conditions depicted in the schematics shown in Fig. 2.2, quasi-steady conditions are established around 10 crank angle degrees after the start of injection. A more detailed schematics of Dec conceptual model during the "quasi-steady" period is introduced in Fig. 2.3. As discussed by Dec et al. [1], this schematic shows some hypothesized features in addition to those actually determined from laser optical techniques.

As it is depicted in Fig. 2.3 a first zone could be identified (zone I), in the region located between the nozzle exit and the lift-off length. All the physical processes related to atomization, air entrainment and mixture vaporization, which were previously described, basically take place in this first zone. This region behave like a non-reactive and evaporative spray although the physical mixing process can be altered by the presence of the diffusive flame downstream this zone. After the lift-off length, the flame adopts the typical structure of a diffusion flame, as depicted in the zone II, where the internal structure of the jet is occupied by combustion products partially oxidized in a premixed rich zone, surrounded by the stoichiometric diffusive reaction surface which impedes the oxygen to flow towards the core of the spray.

Because the flame is lifted, fuel and air are premixed upstream of the diffusion flame, and Dec hypothesized that a standing premixed reaction zone would form near the lift-off length, as depicted in Fig. 2.3, where the rich combustion reactions would consume all the oxygen entrained in the first nonreactive region. The degree of premixing of fuel with ambient gases upstream of the lift-off length is critical for soot formation in the spray as discussed by Chartier et al. [15]. The amount of entrainment upstream of the premixed combustion zone increases with increasing lift-off length, so that the

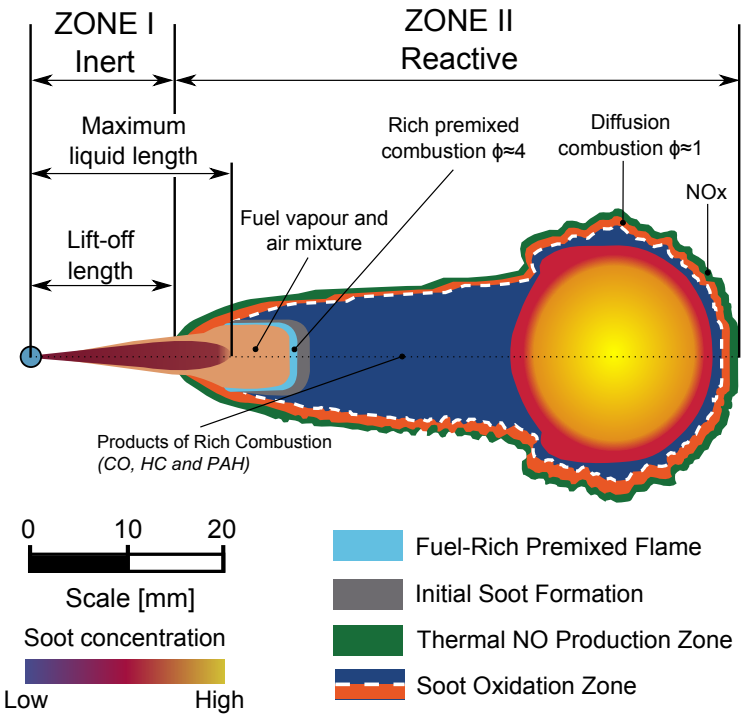

Figure 2.3: Diesel Quasi-Steady spray description

equivalence ratio of the mixture entering the standing reaction zone decreases with increasing lift-off length. Soot formation decreases as the equivalence ratio at the lift-off is reduced, until reaching a threshold of equivalence ratio near to 2, from which no soot formation appears in the jet a behavior explained by Picket et al. [16], and Siebers et al. [17]. The magnitude of the lift-off length and the equivalence ratio at the lift-off are affected by many factors, including ambient gas temperature, density, oxygen concentration, injection pressure, orifice diameter, and also fuel properties [17]. Under typical Diesel conditions, the equivalence ratio at the lift-off length is well above the threshold for soot formation, so that the jet is typically filled with soot, as shown in Fig. 2.3.

Flynn et al. [2] estimate that in the quasi-steady spray, the temperature of the liquid fuel rises by mixing with hot air from its injection temperature of approximately 350 K to a temperature of 650 K to 700 K before it enters the region surrounded by the diffusion flame. Inside the diffusion flame the recirculated products of partial combustion can be entrained into the jet, causing a rapid increase to about 825 K where oxidation reactions can be completed rapidly. The energy released by the initial low temperature fuel oxidation reactions are sufficient, given the local rich conditions of the

mixture, to cause the local temperature to rise well above 1150 K. This is the temperature threshold where reaction rates increase sharply leading to the complete consumption of all available oxygen and driving local temperatures up to 1600 K.

Only 10% to 15% of the fuel energy is released in this rich premixed reaction zone, and the resulting combustion products (typically a mixture of CO, partially burned fragments of hydrocarbons and PAH's) are transported through the interior of this zone toward the boundary of the stoichiometric diffusion flame, increasing their temperature through radiative and convective heat transfer from the flame. When moving downstream along the axis of the reacting Diesel jet, the soot concentration increases with longer residence time at these locally fuel-rich and high temperature conditions. As the fuel fragments and partially oxidized products approach the diffusion flame, they become hotter as they arrive to a very thin reaction zone, where the remaining 90% to 85% of the heat of combustion is released and local temperatures reach levels close to the adiabatic flame temperature at stoichiometric conditions. More precisely, the intermediate combustion products including hydrocarbons and soot, complete their oxidation into carbon dioxide and water when finding the adequate amount of oxygen by diffusion into the burning flame from the exterior of the flame sheath.

Laser imaging performed by Dec et al. [18] and also by Kosaka et al. [19] confirm how the soot particles are observed within the inner area of the flame, surrounded by the reaction surface, traced by the existence of the OH radical fluorescence. In the same work Dec et al. [18] confirm that soot particles almost disappears in the outside region of the flame, indicating the complete oxidation of soot which is dominated by the OH radical at stoichiometric conditions, as they travel across the flame front. In the LIF measurements of Dec, nitrogen oxides formation is observed initially in a relatively thin surface surrounding the exterior of the diffusion burning interface, consistent with the ideal conditions of high temperature (around 2700 K) and oxygen excess that are required for the appearance of this species [20]. NO formation is rapid in zones of high OH concentration and in magnitude it mirrors the OH behavior, therefore, OH can provide an indirect and qualitative indication of likely NO distributions and regions of formation, which is useful due to the diagnostic difficulties associated with direct optical detection of NO. Once NO_x has been formed, it can diffuse both into and away from the diffusion flame sheath. It is worth to comment that even when approximately two thirds of the tail pipe NO_x is created during the vigorous portion of heat release, since the NO thermal formation path is a relatively slow chemical process, around 33%

of the NO_x is formed during the late-stage of combustion happening in the expansion process.

The original conceptual model of Dec for conventional Diesel combustion was applied only through the quasi-steady period, prior to the end of injection, so it did not describe late-cycle processes occurring after the end of injection. However, the end of the injection event is associated with relevant processes both from mixing and combustion point of view, which also affect the formation and destruction of pollutants, and therefore, the final emissions level.

Late stage, mixing and combustion ending: The final phase of the Diesel combustion comprises the time period after the fuel injection ends (EoI) until the remaining fuel burns and the combustion process is completely extinguished (EoC). This period was previously identified in the HRR by the progressive decay in the energy release, which corresponded to the slow mixing-controlled stage of combustion.

When the injector needle starts to close a transitory state begins, which is marked by the ramp-down in the injection rate that finishes when the nozzle holes are completely closed, and the introduction of mass flow rate and momentum that previously sustained the diffusive flame finally stops. Arregle et al. [21] and [22] describe that even when the spray momentum is not introduced any longer, the amount of mixture remaining in the chamber continue to mix with air, partly due to the existing turbulence in the combustion chamber given by swirl and piston displacement, but primarily by the residual energy coming from the injection process. For Diesel sprays at typical engine conditions, the mixtures produced after the transient ramp-down near EoI have not been investigated in great detail as in the case of the quasi-steady conditions. Two early studies done by Kim et al. [23] and also by Bruneaux [24] at constant-volume spray chambers, that primarily investigated downstream spray mixing at non reactive evaporating conditions through in-cylinder vapor-phase fuel imaging, showed that the equivalence ratio in the near-injector region appears to rapidly decrease after the EoI. Moreover, fuel concentrations within the transient jet were apparently lower than the observed during the period sustained by the injection. Even when the importance of the transient after EoI for conventional Diesel combustion is still not well established.

Focusing on the combustion characteristics during this late-stage, Musculus et al. [25] studied the regions of the fuel spray that undergo second-stage combustion after the EoI, through high-speed chemiluminescence

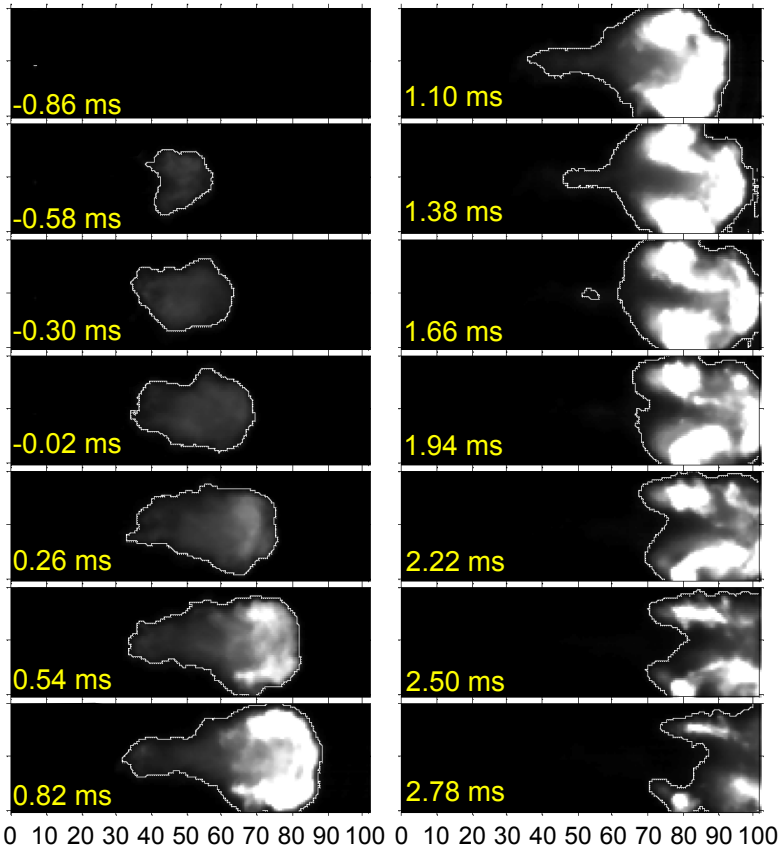

Figure 2.4: Spray at end of injection in a low oxygen (12%) environment [25].

imaging in a reacting environment with 12% of oxygen concentration at the constant volume chamber. Fig. 2.4 shows a time-sequence from a single injection event at this EGR rate. The start of second-stage combustion begins at approximately 0.6 ms before EoI, yielding a negative ignition dwell. An approximate boundary for the reaction zone is indicated by the white contour line overlaid on the image. For the conditions used in this study, the sequence shows that the head of the spray continues to penetrate across the chamber, but there is little change in the near-injector second-stage combustion reaction zone during the time of injection. Thus, the near-injector reaction zone remains approximately the same until about 0.8 ms after EoI and the reaction zone does not return back toward the injector. Instead, the reaction zone begins to thin at the edges of the jet by 0.8 ms and then moves downstream by 1.1 ms after EoI. The fact that the second stage combustion reaction does not return back to the injector means that upstream fuel-lean mixtures located

near the nozzle do not burn to completion. Then, the formation of fuel-lean mixtures near the injector after EoI may therefore play a significant role in inhibiting their complete combustion, acting as a source of HC emissions, particularly in high EGR or highly diluted conditions, as the ones used in Musculus studies.

From these experimental observations, Musculus suggests that the evolution of the reactive zone after the EoI is strongly dependent on the speed of the end-of-injection transient, which will later affect late cycle HC emissions. For instance, injectors with faster end of injection transients may maintain high axial velocities until very near EoI, that would more effectively stabilize the downstream reaction zone so that it could not return back upstream.

2.3 Emissions control strategies in Diesel engines

As described in the section 2.2 Diesel engine pollutants like Soot, hydrocarbons (HC) and carbon monoxide (CO) are formed in heavy duty engines due to mixing challenges and incomplete fuel combustion, while NO_x is formed from high-temperature combustion conditions. In the current section different emissions control strategies to reduce the Diesel engine emissions as could be observed in Fig. 2.5 are discussed. The most important approaches include reducing pollutants formation could be classified in In-cylinder engine control strategies and the After treatment technologies an interesting comparison of both approach could be found in the research work developed by Beatrice et al. [26].

2.3.1 In-cylinder engine controls

Advanced technological approaches can manipulate in-cylinder combustion dynamics to minimize the formation of these pollutants, reducing engine-out emissions. The temperature, speed, and composition of the air entering the chamber influence burn conditions, as does the fuel delivery timing and strategy. Engine redesigns, which do not add significant hardware costs but do require investment in Research and development, seek to improve combustion efficiency through engine geometries that improve mixing of air and fuel. Three strategies to reduce engine-out emissions do add hardware costs: improved fuel injection, improved air handling, and exhaust gas recirculation (EGR).

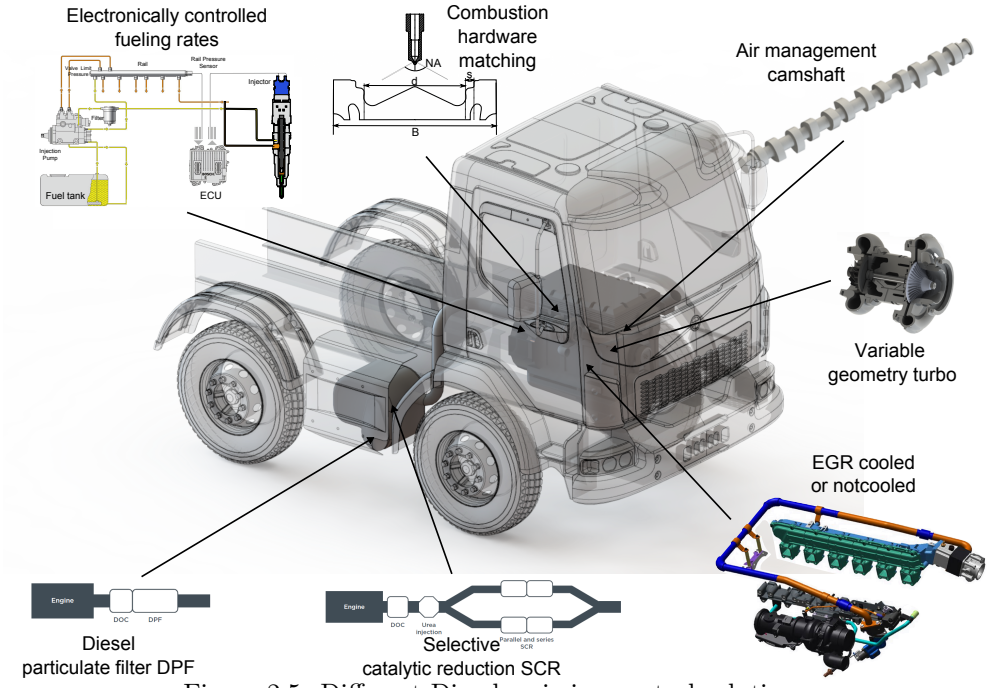

Figure 2.5: Different Diesel emission control solutions

2.3.1.1 Fuel injection systems

Fuel injection pressure, rate, and timing are all used to control both NO_x and Soot. High pressure injection reduces the size of the fuel droplets (atomizing the fuel) and improves fuel penetration into the cylinder, resulting in better mixing of air and fuel. Fuel systems can further improve fuel mixing and the combustion process with redesigned nozzles and piston bowls. This leads to more complete fuel combustion that both reduces particle formation and improves fuel economy. Electronic controls of injection allow precise and variable fuel timing and metering. In conventional fuel injection systems that employ a single injection event for every engine cycle, the timing of the fuel injection can favor either NO_x or Soot control. Early fuel injection increases combustion pressures and temperatures, improves fuel efficiency, reduces Soot, and increases NO_x emissions. Delayed injection of fuel reduces NO_x emissions due to lower temperatures, but also reduces fuel efficiency and increases Soot emissions.

2.3.1.2 Air handling technology

The air management system of an engine must control the motion, temperature, and pressure of the air entering the chamber, ensure that it is clean, and ensure that it contains both sufficient oxygen for complete combustion and enough diluent to control the combustion temperature. Increasing the pressure of the air entering the chamber increases the air density, allowing better combustion in the brief time available. Tuning these parameters minimizes production of both Soot and NO_x. As part of the air handling system, turbochargers boost the intake air pressure. Traditional turbochargers achieve this at mid to low engine power ratings, but their narrow operational range leaves low-speed and high-torque operations with less air than required for the most efficient combustion. Variable geometry turbochargers (VGTs) improve upon traditional turbochargers by providing the right amount of air under a wider range of engine operating conditions, including at low speed and high torque.

2.3.1.3 Exhaust gas recirculation systems

An EGR system recirculates a portion of exhaust gas back to the engine's cylinders. This provides diluent to the air handling system and reduces NO_x formation by lowering peak combustion temperature within the cylinder. Coolers are often included for further temperature control. EGR is the most widely used technology for in-cylinder NO_x reduction in Diesel-powered engines. The EGR fraction (i.e., the share of recirculated exhaust gas in the total intake charge) is tailored to each engine operating condition and, in the latest systems, varies from 0 to 40% of the incoming air. EGR systems can be high-pressure or low pressure, each with trade-offs and varying effectiveness under different operating conditions.

2.3.2 Aftertreatement

Aftertreatment systems treat NO_x, Soot, HC, and CO in the exhaust stream. Selective catalytic reduction (SCR), using urea as a reagent, controls NO_x emissions in the exhaust line. The DPF and the Diesel oxidation catalyst (DOC) control Soot in the exhaust stream; they are also effective at reducing HC and CO emissions. These technologies can also be used in combination with other strategies to reduce other pollutant emissions. For example, DOCs can support SCR, and SCR systems enable in-cylinder strategies to reduce Soot emissions.

2.3.2.1 Selective catalytic reduction systems

SCR systems introduce ammonia to react with NO_x over a catalytic surface, producing nitrogen and water. It is possible for SCR systems to achieve high NO_x conversion efficiency over a relatively wide temperature range. Use of SCR allows the engine to be tuned for higher efficiency, generating lower Soot emissions and higher engine out NO_x levels, which can then be treated by the SCR system. Lower Soot emissions are a result of reducing average particle size, thus reducing the mass of particles but not the number.

2.3.2.2 Diesel oxidation catalysts

The DOC oxidizes HC, CO, and the soluble organic fraction of Soot. In conventional heavy-duty Diesel engines, the oxidation efficiency of these components is high due to the presence of excess oxygen in the exhaust. However, the contribution to total Soot of the soluble organic fraction component is typically no more than 20%-25% on a mass basis. Because DOCs are not able to control the solid carbonaceous fraction of Soot, they have virtually no impact on the number of particles emitted. DOCs require 500 ppm or lower sulfur in Diesel fuel. DOCs also play a fundamental role in SCR operations they oxidize nitrogen oxide into nitrogen dioxide, leading to improved conversion rates in the SCR and in regeneration of passive DPFs.

2.3.2.3 Diesel particulate filters

DPFs physically trap the solid carbonaceous fraction of Soot, including black carbon. Wallflow DPFs, which force the exhaust flow through a typically ceramic substrate, achieve Soot reduction efficiency higher than 95% due to their ability to accumulate the solid fraction of Soot, including ultra fine particles. The process of removing the accumulated Soot is called filter regeneration, and it can be passive or active. Passive regeneration burns the deposited material using nitrogen dioxide as an oxidizer. The nitrogen dioxide is formed from nitrogen oxide oxidation on an oxidation catalyst, which may be located upstream of the DPF or washcoated onto the filter itself. Active regeneration requires late fuel injections or fuel burners upstream of the DPF to regenerate the trap.

2.4 Cost effective emissions control strategies

The final step in the analysis focuses in different emission control technologies cost. For each regulatory emission legislation in EURO VI development, the total incremental costs could be estimated by matching the technologies required for that stage with their costs as could be observed in Fig. 2.6. As the strategies and technologies used to meet Euro VI are in a implemented in a cumulative integration the cost of compliance of EURO VI emission standard per 12 L Diesel engine is U$6,937 extracting the data from the ICCT report costs of emission reduction [27].

The costs presented here represent updated estimates of manufacturer compliance costs. These include costs for materials research and development but not for manufacturers certification or warranty. They also do not include the operational costs or savings incurred by vehicle owners including improved fuel economy, added cost of Diesel exhaust fluid and low or ultralow sulfur fuel, and any adjustments in maintenance costs.

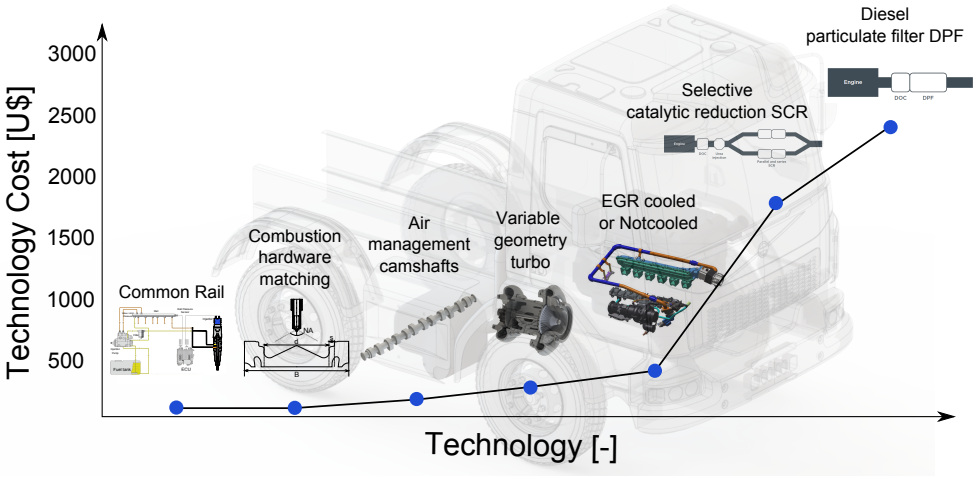

Figure 2.6: Cost of different Diesel emission control solutions

These estimates improve on past assessments that projected the technology needs to meet upcoming regulatory stages. The analysis is informed by publicly available data on in-cylinder and aftertreatment technologies that are in widespread commercial use, and cost factors have been adjusted based on industry review. Nonetheless, these values are only approximations, as information on the exact costs of most engine and aftertreatment technology is protected as a trade secret.

From Fig. 2.6 could be observed than the pollutant control strategies with lower cost from the evaluated ones are the in-cylinder engine control strategies

specially the injection combustion strategies and the air management ones. In a restrictive cost framework in which they are the emerging markets the full potential of these cost effective strategies must be explored in order to define their real limits and to avoid possible extra cost due to aftertreatement integration in the final heavy duty Diesel definition. This kind of approach was done in the research work of Beatrice et al. [28] but in this case the emission legislation framework was the Rail Diesel Engines giving a qualitative results of the emission control strategies.

In next subsection the injection-combustion and the air management which from now in this document are the cost-effective emission control strategies are described by a literature review exploring their characteristics, engine technological implementation and their associated potential.

2.4.1 The injection-combustion strategies

The pollutant control strategies focused in the injection-combustion processes are classified into the in-cylinder strategies as described in previous subsection. In this case the objective is to take advantage of the different parameters controlled by the electronically driven Diesel injection, or the geometrical parameters in the design of the combustion chamber, in order to search the best compromise between the engine efficiency and the engine emissions. Several studies dealing with the control of parameters affecting the injection/combustion process, as well as their effect on engine efficiency and emissions can be found in the literature to accomplish this task.

2.4.1.1 The injection parameters

The electronically driven Diesel injection which technologically is called common rail gives place to more complex and precise injection control, allowing the use different injection pressures, modify injection phasing and multiple injection strategies as could be observed in Fig. 2.8.

Beginning by the injection pressure, the spray mixing properties are improved by higher injection pressure. In Diesel engines, the penetration length increase at higher injection pressure, determining the fuel-air mixing rate and the air utilization as described by Mohan et al. [29]. Currently, modern Diesel injection pressure ranges are between 2000 bar and 2500 bar, but in the emerging markets definition these limits are in the 1600 or 1800 bar. In general, faster fuel injection leads to faster combustion, with a subsequent increase in the indicated and brake efficiency, along with a reduction in the

Soot formation; however, higher injection pressure leads also to an increase in NO_x formation as the work performed by Su et al. [30] due to an enhancement of the combustion process, and hence higher gas temperature. Dodge et al. [31] have highlighted that very high injection pressure can also penalize the Brake Specific Fuel Consumption(BSFC), due to higher power requirements of the injection pump; moreover, working at high pressure increase the wear of the injection system.

In the Fig. 2.7 could be observed the comparison of the injection rate under different conditions of injection pressure. For a defined injected fuel mass there is a significant reduction in injection duration under the high injection pressure compared with the low injection pressure which accelerate the combustion process improving the engine efficiency but worsening the NO_x emission.

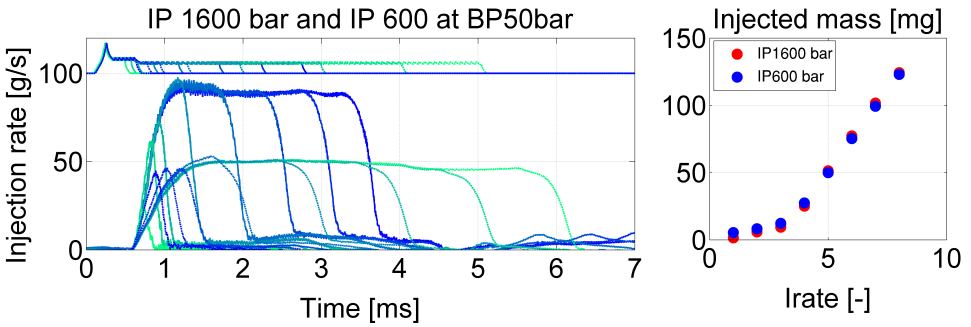

Figure 2.7: Injection rate measurements

In terms of injection phasing the modification of Start of Injection (SoI) affects the combustion phasing and HRR shape, through the change in the premixed/diffusion fuel energy balance released. Thus, the ignition delay is affected by the injection timing as a result of changes in the air pressure and temperature near TDC. Advancing the SoI use to produce higher in-cylinder pressure evolution and increases the indicated effciency; however, the higher temperature peaks lead to more NO_x formation. Delaying the SoI helps to control NO_x formation, but usually has a penalty on Soot formation as proposed by Agarwa et al. [32]

The modern injection system technology allow multiple injection strategies in this case as observed in Fig. 2.8 pilot injections are useful to reduce noise and NO_x emissions with low effect on engine performance as demonstrated in the works of Badami et al. [33] and Hiwase et al. [34]. On the other hand, coupled post injections with high pressure are useful to complete the combustion of the Soot, and a later post injection helps to the regeneration of the particulate filter and the NO_x adsorption catalyst as described by Mohan et al. [29].

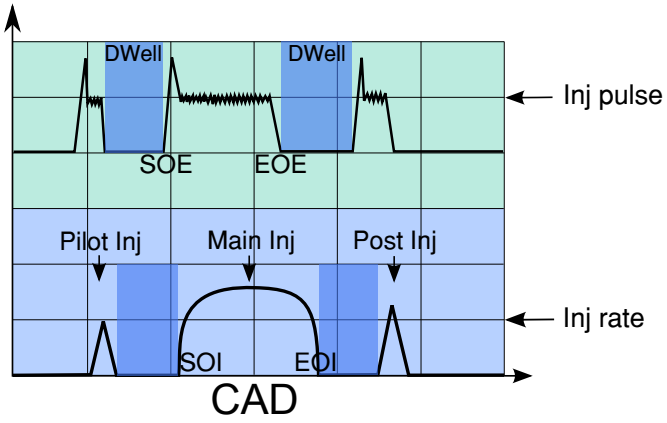

Figure 2.8: Injection parameters

However, these strategies use to have negative effects on consumption, since late combustion is not useful from the indicated efficiency point of view.

Nishimura et al. [35] studied the effects of fuel injection rate on combustion and emission in a DI Diesel engine. They found that pilot injection helps to simultaneously reduce NO_x and noise, with a slight increase in Soot emission. With the use of boot shaped injection rates, they achieve an important reduction in both, Soot and combustion noise. Their results emphasize the benefits of using injection rate control as a key strategy to reduce emissions. Since the injection rate is highly dependent on the injection pressure, Kohketsu et al. [36] examined the feasibility of using a variable pressure injection system, based on two common rails. They reproduced a boot shaped injection rate, and found that the use of this system improves the fuel consumption as well as NO_x and Soot emissions trade-off. According to these authors, it seems that boot injection rate effects are more important at high speed and load operating points than at medium speed and load operating points [37], [38].

2.4.1.2 The injection-combustion hardware

The combustion chamber geometry plays an important role in boosting the in-cylinder air motion which in turn helps in air-fuel mixing and combustion processes. Park et al. [39] studied the optimum combustion chamber geometry for a Diesel engine using a micro-genetic algorithm. Through this optimization, a shallow chamber geometry was developed; this led to a 35 % improvement in the gross indicated specific fuel consumption.

In the past Zhang et al. [40] studied the influence of combustion chamber geometry on flame speed by considering three different chamber shapes for a

large bore Diesel engine equipped with a low-pressure injection system. They found that adopting a re-entrant chamber, the combustion is enhanced during the expansion stroke, preventing the diffusion of the flame in the squish region and giving lower smoke levels. As far as the mean combustion velocity is concerned, it increases with the combustion chamber radius and is lower in the case of flat-bottom bowls.

Diesel engine combustion chamber geometries for both small and large bores were optimized using the KIVA code integrated with the genetic algorithm by Wickman et al. [41]. They optimized three chamber geometry related variables along with six engine operating variables for two engines and found that both engines (i.e., with small-bore and large-bore engines) favored a relatively large diameter and shallow piston bowls for their bowl geometry along with long injection duration, a small hole diameter, and a moderate swirl ratio for their engine operating conditions. Ge et al. [42] also performed optimization for an HSDI (high speed direct injection) engine for passenger cars using a multi-dimensional CFD (computational fluid dynamics) code and multi-objective genetic algorithm methodology.

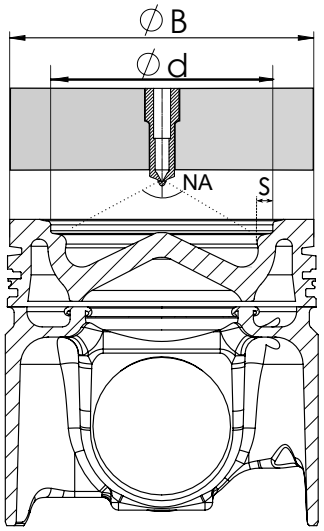

Figure 2.9: Geometric parameters in the combustion chamber design

Reitz and his research group applied a computer code (KIVA-GA) to optimize the combustion chamber geometry together with several engine input parameters (e.g. EGR, injection profile, etc.). In those studies, the bowl geometry was defined by three input variables (bowl diameter, bowl depth and central crown height of the piston) allowing only open chamber profiles to be investigated. Moreover, the larger number of parameters included in

the GA optimization makes the interpretation of results quite complicated preventing straightforward interpretation of the effect of combustion chamber geometry on engine performance and emissions.

The research work proposed by Lee et al. [43] brings the opportunity to distinguished the most common procedure in order to evaluate the injection combustion hardware. In this case the combination of the 3D CFD simulations which mathematical methods of optimization could lead to define an specific configuration for an specific engine application. As could be observed in Fig. 2.9 the main geometrical factors which are evaluated in the majority of the different studied research work are: the Piston diameter (B), the Bowl diameter (d), the re-entrant profile (S), the Nozzle angle (NA) and the movement of air in the cylinder (Swirl).

As described by deRisi et al. [44], the effect of combustion chamber shape on the engine performance is very complex due to its influence on the flow field and the air-spray interaction and the results in literature confirm that it is difficult to define an optimized combustion chamber, because of the influence of engine specification and injection system.

2.4.2 The Air management strategies

As proposed in the previous subsections the air management strategies classified into the cost effective pollutant control tools are now explored evaluating different research works published by the scientific community. In this case between all the possibilities of valve timing configuration the Miller camshaft profile and the iEGR profile are the chosen ones due to high potential in pollutant control as is described in this literature review.

2.4.2.1 Miller camshaft profile

The basic principle underlying the Miller process is that the effective compression stroke can be made shorter than the expansion stroke by suitable shifting of the inlet valve timing delaying or advancing it as observed in Fig. 2.10. When both the engine output and boost pressure are kept constant, this will reduce the cylinder filling and the pressure and temperature in the cylinders will be lower.

The original purpose of the Miller process was to increase the power density of engines without exceeding their mechanical and thermal limits. In the last years, attention turned to how it could be used to reduce the temperature in

the cylinder for a constant engine output, and to using this positive effect to minimize NO_x formation.

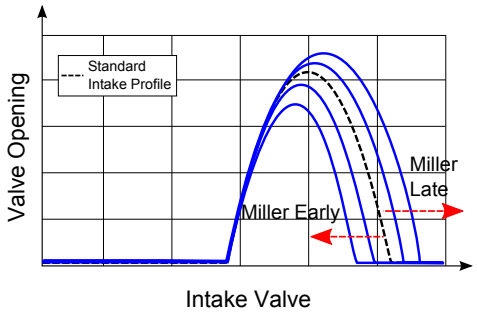

Figure 2.10: Conceptual Miller description

In an ideal cycle late or early closing of the intake valves are equivalent, In real cycles however there are differences. With early closing the intake valves must start to close very early; therefore, the differences between the cylinder pressure and the boost pressure is larger due to throttling; in the case of late closing the intake and the discharge of a portion of the charge air also involves some throttling losses. Which if these two effects is the more dominant will depend of the valve geometry and cam profile an example is observed in Fig. 2.11. With late closing is also necessary to consider the heat transfer, the charge air which is forced back has already been heated up in the cylinder and this heat is stored in the intake duct until the intake valve opens again in the next cycle. This partly reduces the theoretical cooling of the cylinder charge, compared with early closing.

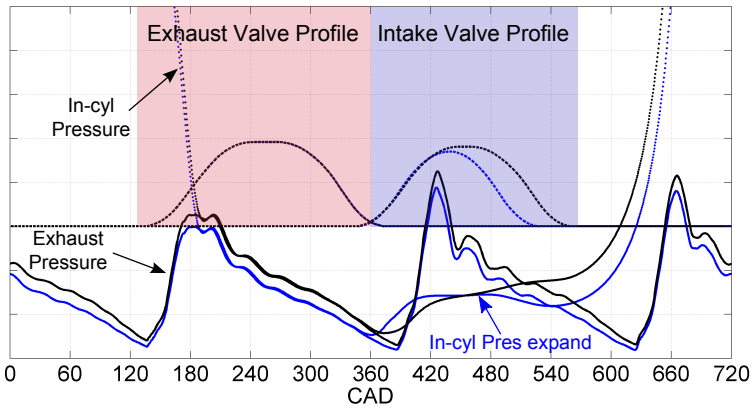

Figure 2.11: Miller instantaneous description

Focusing in NO_x emission, the application of Miller timing in internal combustion engines has been widely studied and it is a demonstrated way to reduce the NO_x emission formation. Recently Verschaeren et al. [45] studied the Miller strategy in a heavy marine engine with an inline system pump injection system. In this study, the Miller strategy is applied in 2 operating conditions at low speed combined with different external EGR rates and obtaining an important reduction of NO_x emission (between 15% to 25%), with a small increment of fuel consumption. Boulouchos et al. [46] proposes after researching in a 9 cylinder heavy duty Diesel engine of 1420 kW of power with Miller timing, the reduction in NO_x emission between 20% to 30% without penalties on fuel consumption and soot emission over the whole load in a low speed operating point.

Benajes et al. [47] as well as Gonca et al. [48] obtained reductions on NO_x emissions between 15% to 25% through modeling and experimental studies in a single cylinder engine using Miller timing (advancing the IVC) and EGR strategies applied combined. This research indicated this important reduction in NO_x emission but a slightly reduction on engine efficiency due to lower compression ratio. In the same way the work performed by Wang et al. [49] where the advancing of IVC was progressively evaluated in a 2 cylinder 1.2L naturally aspirated small Diesel engine showing reductions until 13% of NO_x emissions at full load.

Using a simulated 1D model Millo et al. [50] studied the combination between EGR and Miller timing but in this case, due to the mass losses caused by the the earlier intake closing, the intake pressure was increased in order to recover the original intake mass flow rate. In this work was found an important reduction of NO_x (until 35%) without affect or penalize the fuel consumption.

2.4.2.2 iEGR camshaft profile

In a conventional Diesel engine without any particular type of EGR system could be noticed the iEGR effect, it is common under certain operating conditions, that a small portion of gases backflux trough the intake valve which leaves the cylinder during the period of valve overlapping. The gases back flow gases coming from the cylinder have been generated in the combustion process of the previous cycle and therefore contain a high fraction of burned gas. These gases will be re-admitted into the cylinder at the next intake time. In the same way in the conventional Diesel operation and under certain engine operating conditions, it is possible to have a gases backflux entering into the cylinder through the exhaust valve at the end of the exhaust time when the piston

begins its down stroke and a new intake period begins. In this time period during a short time interval, the exhaust valve remains open (delaying to close the exhaust). The composition of this gas is also high in burned gases. Both 2 effects that can occur simultaneously in normal Diesel operation cause than the mass of gas trapped in the cylinder in an operating cycle containing a burned gas portion, thus appearing in an involuntarily way the effect of the iEGR.

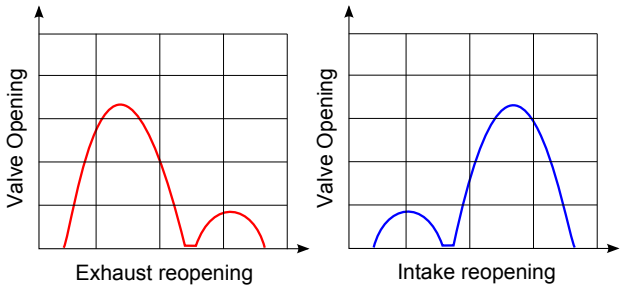

Figure 2.12: Conceptual iEGR description

As described by Luján [51] this phenomenon establishes the basis for the production of iEGR. In fact, if the exhaust valve is opened during the intake process, there will be an entry of gases into the cylinder through the exhaust valve as observed in Fig. 2.12, so that the intake process will be carried out with the addition of fresh gas through the admission plus the burned gas from the exhaust. This effect can be carried out by altering the profile of the camshaft re opening the exhaust valve a few seconds after its normal closing as could be noticed in Fig. 2.13. The level of exhaust gas recirculation produced in this case will depend on the time period of opening of the exhaust valve, its re breathing opening and the difference between the in cylinder pressure and the exhaust manifold pressure in a close point to the exhaust valve.

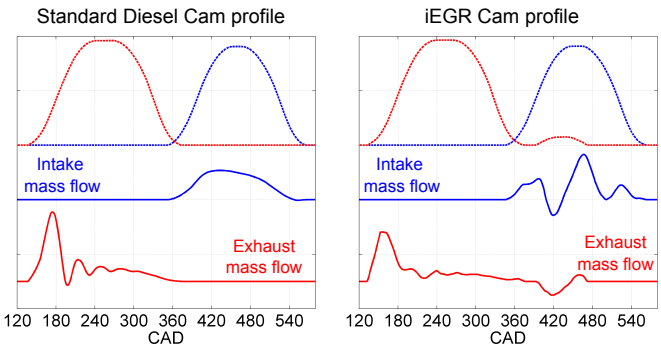

Figure 2.13: iEGR instantaneous flow

The same effect of iEGR could be produced through the modification of the intake valve profile. If the intake valve is reopened while the exhaust event time, part of burnt gases will be introduced in the intake duct taking a part in the intake manifold, these gases will be introduced again in the cylinder in a later cycle in the same way than exhaust valve reopening.

The advantages of producing this kind of iEGR are the simplicity and cost-effectiveness of the solution due to easy machining of the profile without modification of any other engine hardware. Added to the mentioned advantage there is the capacity to produce higher levels of EGR for any engine operating condition with a convenient design of the cam profile. Beside the advantages of the iEGR there are some cons like the difficult process to design an adequate cam profile having in account the wave behavior in the manifolds and the rigidity of a imposed quantity of EGR after the iEGR cam profile design.

In terms of pollutants control the iEGR is mainly used to reduce the NO_x formation modifying the oxygen concentration in the combustion chamber as studied by Balaji et al. [52]. The strategy is performed by opening the exhaust valve during the the intake stroke, allowing to part of hot exhaust gases to enter to the cylinder if the pressure balance in the intake and exhaust manifolds allows it. This strategy was explored by Millo et al. [53] in a small 2 cylinder Diesel engine obtaining NO_x emission reduction between 25% and 50%.

The main advantage of this form of EGR (internal) could be summarized in the simplicity and economy of producing the exhaust gas re-circulation compared to the complexity of all the components required to realize the external EGR (cooled or not) strategy as proposed by Meistrick et al. [54] and Shi et al. [55].

One fact to take in account when the iEGR strategy is performed is the opposite effect of opening the exhaust valve during the intake stroke. From one side, the oxygen concentration reduction helps to reduce the NO_x formation, but for other side the hot iEGR increases the in-cylinder temperature. This is one of the disadvantages of iEGR that added with the difficulty controlling the amount of iEGR trapped and also the reduction of the intake charge density, may cause excessive Soot emissions as is described by Schwoerer et al. [56]

In both mentioned cases the Miller and iEGR camshaft profiles were studied from the single cylinder engine, multi cylinder engine and the theoretical modeling point of view. In this work the objective is to investigate the engine performance under both strategies separately in a 6 cylinder heavy duty Diesel engine by changing the camshaft hardware profile in order to have the desired intake valve closing (for Miller timing) and the desired opening of the exhaust valve during intake process (for iEGR profile).

Bibliography

[1] Dec J. E. "A Conceptual Model of DI Diesel Combustion Based on Laser-Sheet Imaging*". *SAE International*, 1997.

[2] Flynn P. F., Durrett R. P., Hunter G. L., zur Loye A. O., Akinyemi O. C., Dec J. E. and Westbrook C. K. "Diesel Combustion: An Integrated View Combining Laser Diagnostics, Chemical Kinetics, And Empirical Validation". *SAE International*, 1999.

[3] Gimeno J. *Desarrollo y aplicacion de la medida del flujo de cantidad de movimiento de un chorro diesel*. Doctoral Thesis, Universidad Politécnica de Valencia, Departamento de Máquinas y Motores Térmicos, 2008.

[4] Hermens S. *Influence of diesel injector nozzle geometry on the injection and combustion process*. Doctoral Thesis, Universidad Politécnica de Valencia, Departamento de Máquinas y Motores Térmicos, 2008.

[5] Salvador F.J. *Estudio teórico experimental de la iflnuencia de la geometría de la tobera de inyección sobre las caracteristicas del flujo interno y del chorro*. Doctoral Thesis, Universidad Politécnica de Valencia, Departamento de Máquinas y Motores Térmicos, 2003.

[6] Correas D. *Estudio Teórico-Experimental del chorro libre diesel isotermo*. Doctoral Thesis, Universidad Politécnica de Valencia, Departamento de Máquinas y Motores Térmicos, 1998.

[7] López J.J. *Estudio Teórico-Experimental del chorro libre diesel no evaporativo y de su interacción con el movimiento del aire*. Doctoral Thesis, Universidad Politécnica de Valencia, Departamento de Máquinas y Motores Térmicos, 2003.

[8] Ruiz S. *Estudio Teórico-Experimental de los procesos de atomización y de mezcla en los chorros diesel D.I.* Doctoral Thesis, Universidad Politécnica de Valencia, Departamento de Máquinas y Motores Térmicos, 2003.

[9] Naber J. D. and Siebers D. L. "Effects of Gas Density and Vaporization on Penetration and Dispersion of Diesel Sprays". *SAE International*, 1996.

[10] Siebers D. L. "Scaling Liquid-Phase Fuel Penetration in Diesel Sprays Based on Mixing-Limited Vaporization". *SAE International*, 1999.

[11] Desantes J. M., López J. J., García J. M. and Pastor J. M. "Evaporative Diesel Spray Modeling". *Atomization and Sprays*, Vol. 17 n^o 3, pp. 193–231, 2007.

[12] Kosaka H., Aizawa T. and Kamimoto T. "Two-dimensional imaging of ignition and soot formation processes in a diesel flame". *International Journal of Engine Research*, Vol. 6 n^o 1, pp. 21–42, 2005.

[13] Dec J. E. and Coy E. B. "OH Radical Imaging in a DI Diesel Engine and the Structure of the Early Diffusion Flame". *SAE International*, 1996.

[14] Higgins B., Siebers D. L. and Aradi A. "Diesel-Spray Ignition and Premixed-Burn Behavior". *SAE International*, 2000.

[15] Chartier C., Aronsson U., Andersson, Ö.and Egnell R., Collin R., Seyfried H., Richter M. and Aldén M. "Analysis of Smokeless Spray Combustion in a Heavy-Duty Diesel Engine by Combined Simultaneous Optical Diagnostics". *SAE International*, 2009.

[16] Pickett L. M., Manin J., Genzale C. L., Siebers D. L., Musculus M. P. B. and Idicheria C. A. "Relationship Between Diesel Fuel Spray Vapor Penetration/Dispersion and Local Fuel Mixture Fraction". *SAE International Journal of Engines*, Vol. 4 n^o 1, pp. 764–799, 2011.

[17] Siebers D. L. and Higgins B. "Flame Lift-Off on Direct-Injection Diesel Sprays Under Quiescent Conditions". *SAE International*, 2001.

[18] Dec J. E. and Tree D. R. "Diffusion-Flame / Wall Interactions in a Heavy-Duty DI Diesel Engine". *SAE International*, 2001.

[19] Kosaka H., Nishigaki T., Kamimoto T., Sano T., Matsutani A. and Harada S. "Simultaneous 2-D Imaging of OH Radicals and Soot in a Diesel Flame by Laser Sheet Techniques". *SAE International*, 1996.

[20] Dec J. E. and Canaan R. E. "PLIF Imaging of NO Formation in a DI Diesel Engine1". *SAE International*, 1998.

[21] Arrègle J., López J. J., García J. M. and Fenollosa C. "Development of a zero-dimensional Diesel combustion model. Part 1: Analysis of the quasi-steady diffusion combustion phase". *Applied Thermal Engineering*, Vol. 23 n^o 11, pp. 1301–1317, 2003.

[22] Arrègle J., López J. J., García J. M. and Fenollosa C. "Development of a zero-dimensional Diesel combustion model: Part 2: Analysis of the transient initial and final diffusion combustion phases". *Applied Thermal Engineering*, Vol. 23 n^o 11, pp. 1319–1331, 2003.

[23] Kim T. and Ghandhi J. B. "Quantitative 2-D Fuel Vapor Concentration Measurements in an Evaporating Diesel Spray using the Exciplex Fluorescence Method". *SAE International*, 2001.

[24] Bruneaux G. "Mixing Process in High Pressure Diesel Jets by Normalized Laser Induced Exciplex Fluorescence Part I: Free Jet". *SAE International*, 2005.

[25] Musculus M. P. B., Lachaux T., Pickett L. M. and Idicheria C. A. "End-of-Injection Over-Mixing and Unburned Hydrocarbon Emissions in Low-Temperature-Combustion Diesel Engines". *SAE International*, 2007.

[26] Beatrice C., Rispoli N., Di Blasio G., atrianakos G., Kostoglou M., Konstandopoulos A. G., Imren A., Denbratt I. and Palacin R. "Emission Reduction Technologies for the Future Low Emission Rail Diesel Engines: EGR vs SCR". *SAE Technical Paper-*, 2013. 2013-24-0087.

[27] Posada F., Chambliss S. and Blumberg K. *Costs of emission reduction technologies for heavy-duty Diesel vehicles.* The international council on clean transportation, 2016.

[28] Beatrice C., Rispoli N., Di Blasio G., Konstandopoulos A. G., Papaioannou E. and Imren A. "Impact of Emerging Engine and After-Treatment Technologies for Improved Fuel Efficiency and Emission Reduction for the Future Rail Diesel Engines". *Emiss. Control Sci. Technol*, 2016. DOI 10.1007/s40825-016-0035-1.

[29] Mohan B., Yang W. and Chou S. K. "Fuel injection strategies for performance improvement and emissions reduction in compression ignition engines A review". *Renewable and Sustainable Energy Reviews*, Vol. 28, pp. 664–676, 2013.

[30] Su T. F., Chang C. T., Reitz R. D., Farrell P. V., Pierpont A. D. and Tow T. C. "Effects of Injection Pressure and Nozzle Geometry on Spray SMD and D.I. Emissions". *SAE International*, 1995.

[31] Dodge L. G., Simescu S., Neely G. D., Maymar M. J., Dickey D. W. and Savonen C. L. "Effect of Small Holes and High Injection Pressures on Diesel Engine Combustion". *SAE International*, 2002.

[32] Agarwal A. Kumar, Srivastava D. K., Dhar A., Maurya R. K., Shukla P. C. and Singh A. P. "Effect of fuel injection timing and pressure on combustion, emissions

and performance characteristics of a single cylinder diesel engine". *Fuel*, Vol. 111, pp. 374–383, 2013.

[33] Badami M., Mallamo F., Millo F. and Rossi E. E. "Influence of Multiple Injection Strategies on Emissions, Combustion Noise and BSFC of a DI Common Rail Diesel Engine". *SAE International*, 2002.

[34] Hiwase S. D., Moorthy S., Prasad H., Dumpa M. and Metkar R. M. "Multidimensional Modeling of Direct Injection Diesel Engine with Split Multiple Stage Fuel Injections". *Procedia Engineering*, Vol. 51, pp. 670–675, 2013.

[35] Nishimura T., Satoh K., Takahashi S. and Yokota K. "Effects of Fuel Injection Rate on Combustion and Emission in a DI Diesel Engine". *SAE International*, 1998.

[36] Kohketsu S., Tanabe K. and Mori K. "Flexibly Controlled Injection Rate Shape with Next Generation Common Rail System for Heavy Duty DI Diesel Engines". *SAE International*, 2000.

[37] Desantes J. M., Benájes J., Molina S. and González C. A. "The modification of the fuel injection rate in heavy-duty diesel engines: Part 2: Effects on combustion". *Applied Thermal Engineering*, Vol. 24 n^o 17, pp. 2715–2726, 2004.

[38] Desantes J. M., Benájes J., Molina S. and González C. A. "The modification of the fuel injection rate in heavy-duty diesel engines. Part 1: Effects on engine performance and emissions". *Applied Thermal Engineering*, Vol. 24 n^o 17, pp. 2701–2714, 2004.

[39] Park S. W. "Optimization of combustion chamber geometry for stoichiometric diesel combustion using a micro-genetic algorithm". *Fuel Processing Technology*, Vol. 91 n^o 11, pp. 1742–1752, 2010.

[40] Zhang L., Ueda T., Takatsuki T. and Yokota K. "A Study of the Effects of Chamber Geometries on Flame Behavior in a DI Diesel Engine". *SAE International*, 1995.

[41] Wickman D. D., Senecal P. K. and Reitz R. D. "Diesel Engine Combustion Chamber Geometry Optimization Using Genetic Algorithms and Multi-Dimensional Spray and Combustion Modeling". *SAE International*, 2001.

[42] Ge H.W., Shi Y., Reitz R. D., Wickman D. D. and Willems W. "Optimization of a HSDI Diesel Engine for Passenger Cars Using a Multi-Objective Genetic Algorithm and Multi-Dimensional Modeling". *SAE International Journal of Engines*, Vol. 2 n^o 1, pp. 691–713, 2009.

[43] Lee S. and Park S. "Optimization of the piston bowl geometry and the operating conditions of a gasoline-diesel dual-fuel engine based on a compression ignition engine". *Energy*, Vol. 121, pp. 433–448, 2017.

[44] de Risi A., Donateo T. and Laforgia D. "Optimization of the Combustion Chamber of Direct Injection Diesel Engines". *SAE International*, 2003.

[45] Verschaeren R., Schaepdryver W., Serruys T., Bastiaen M. and Vervaeke, L.and Verhelst S. "Experimental study of NOx reduction on a medium speed heavy duty diesel engine by the application of EGR (exhaust gas recirculation) and Miller timing". *Energy*, Vol. 76 n^o 0, pp. 614–621, 2014.

[46] Boulouchos K. and Stebler H. "Combustion Features and Emissions of a DI-Diesel Engine with Air Path Optimization and Common Rail Fuel Injection". *SAE Technical Paper*, 1998. 981931.

[47] Benajes J., Molina S., Novella R. and Belarte E. "Evaluation of massive exhaust gas recirculation and Miller cycle strategies for mixing-controlled low temperature combustion in a heavy duty diesel engine". *Energy*, Vol. 71, pp. 355–366, 2014.

[48] Gonca G., Sahin B., Parlak, A.and Ust Y., Ayhan, V.and Cesur I. and Boru B. "Theoretical and experimental investigation of the Miller cycle diesel engine in terms of performance and emission parameters". *Applied Energy*, Vol. 138, pp. 11–20, 2015.

[49] Wang Y., Zeng S., Huang J., He Y., Huang X., Lin L. and Li S. "Experimental investigation of applying miller cycle to reduce NOx emission from diesel engine". *Proceedings of the Institution of Mechanical Engineers, Part A: Journal of Power and Energy*, Vol. 219 n^o 8, pp. 631–638, 2005.

[50] Millo F. and Mallamo F. "The Potential of Dual Stage Turbocharging and Miller Cycle for HD Diesel Engines". *SAE Technical Paper-*, 2005. 2005-01-0221.

[51] Luján JM. *Recirculación interna de gases de combustión en motores Diesel sobrealimentados*. Doctoral Thesis, Universidad Politécnica de Valencia, Departamento de Máquinas y Motores Térmicos, 1998.

[52] Balaji J., Ganesh Prasad M. V., L. Navaneetha R.., Bandaru B. and Ramesh A. "Modelling and Experimental Study of Internal EGR System for NOx Control on an Off-Road Diesel Engine". *SAE Technical Paper-2014-01-2645*, 2014. doi:10.4271/2014-01-2645.

[53] Millo F., Mallamo F., Arnone L., Bonanni M. and Franceschini D. "Analysis of Different Internal EGR Solutions for Small Diesel Engines". *SAE Technical Paper-*, 2007. 2007-01-0128.

[54] Meistrick Z., Usko J., Shoyama K., Kijima K., Okazaki T. and Maeda Y. "Integrated Internal EGR and Compression Braking System for Hino's E13C Engine". *SAE Technical Paper*, 2004. 2004-01-1313.

[55] Shi L., Cui Y., Deng K., Peng H. and Chen Y. "Study of low emission homogeneous charge compression ignition (HCCI) engine using combined internal and external exhaust gas recirculation (EGR)". *Energy*, Vol. 31 n^o 14, pp. 2665–2676, 2006.

[56] Schwoerer J., Dodi S., Fox M., Huang S. and Yang Z. "Internal EGR Systems for NOx Emission Reduction in Heavy-Duty Diesel Engines". *SAE Technical Paper-2004-01-1315*, 2004. doi:10.4271/2004-01-1315.

Chapter 3

Experimental and theoretical tools

Contents

3.1 Introduction

A brief description of all the tools used in the research work both theoretical and experimental are present in this chapter. The objectives of using each experimental or theoretical approach to overcome in the cost-effective engine emissions control are highlighted. In the same way, the characteristics and limitations coupled with the uncertainties and the hypothesis are described in order to have some reliable data of all the implemented strategies. The chapter is divided in two main sections. The section 3.2 explains the most relevant characteristics of the experimental equipment, giving a detailed description of the main components in a research test cell facility and the heavy duty Diesel engine installed on it. Moreover, the testing methodology used in the experiments is discussed. The second section 3.3 describes the fundamentals of the theoretical tools used to perform the analysis of the combustion process and the air management study. In this case the 0D modeling, 1D GT Power model and 3D CFD modeling characteristics are explored and described in order to have a complete overview of the strategies effects in the Diesel engine behavior.

3.2 Experimental tools

3.2.1 Heavy duty Diesel engine

The engine used in this research is a heavy duty six-cylinder, four-stroke, overhead camshaft, common rail injection system, water cooled, turbocharged with inter-cooler, direct injection Diesel engine. The engine is a VOLVO TRUCKS production engine, precisely the MDE8 model EURO III-VI, Tier3 Compliant. The basic specification of the engine are included in Table 3.1 and the more specific data as the injection-combustion hardware characteristics as the piston bowl geometry are also given in Fig. 3.1.

3.2.1.1 Injection system characteristics

The common rail injection system produced by the Bosch company is a system where the pressure generation and fuel injection are separate which means that the pump generates the high pressure that is available for all injectors through a common gallery called rail, which can be controlled independent of the engine revolution. The fuel injection pressure, the start and end of injection and the number and timing of the injections are precisely

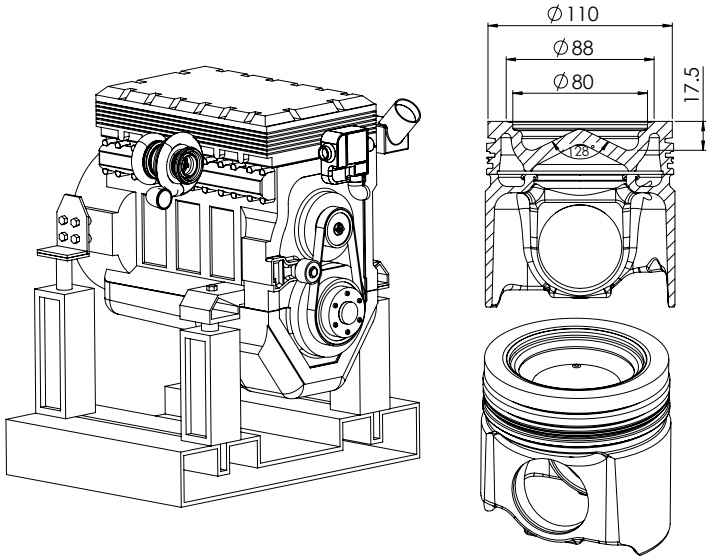

Figure 3.1: Volvo MDE8 Engine and Piston Bowl geometry

defined by the ECU, from information obtained through various sensors installed in the engine. It is this kind of injection system observed on Fig. 3.2 which gives flexibility and entails complexity in the moment to optimize and find the precisely settings that improves the fuel economy and the engine emission [1].

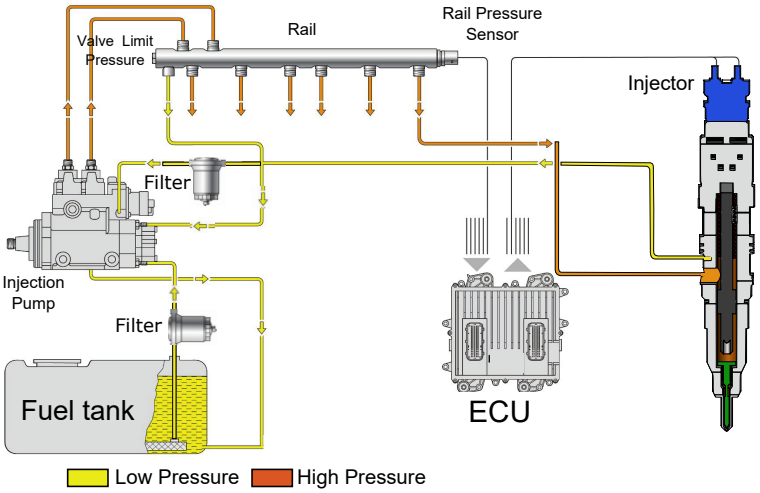

Figure 3.2: Common rail injection system Volvo MDE8 Engine

Cylinders	6 in line
Strokes	4
Bore	110 mm
Stroke	135 mm
Displacement	7800 cm
Nominal CR	16.5:1
Fuel injection system	Common-Rail
Valves per Cylinder	4
Rated speed	2200 rpm
In-cylinder max pressure	175 bar
Bowl Volume	61.27 cm^3
Connecting rod length	212.15 mm
Crank length	67.5 mm

Table 3.1: Volvo MDE8 Engine characteristics

Particularly in the MDE8 engine the fuel feeding is lateral with high pressure connector tube and the return lines goes through the engine block connecting all the injectors returns in a common line. The injection system main characteristics and injector nozzle geometry specification are described on Table 3.2.

Nozzle hole diameter	0.199 mm
Number of holes	7
Max IP	1600 bar

Table 3.2: Injection system characteristics

3.2.1.2 Engine operating conditions

The MDE8 Volvo engine which has an operation map as described in Fig. 3.3 must be divided in load and speed operating zones where some strategical points must be selected in an emission standard framework. In this case, the selected engine standard emission is the ISO 8178 specifically the definition of C1 cycle [2]. This cycle is composed of 8 modes comprising two engine speed labeled as A and B and three or four load conditions labeled as the represented load percentage as observed in Fig. 3.3. Normally, in the case of on-road application the European stationary cycle (ESC) which is

composed of 13 operating points (triangles in Fig. 3.3) should be the emission framework for this MDE8 platform but in order to simplify the number of tests and with the aim to integrate the recommendations of the manufacturer which was leading this research project, it was chosen the C1 cycle as the reference for the operating conditions selection.

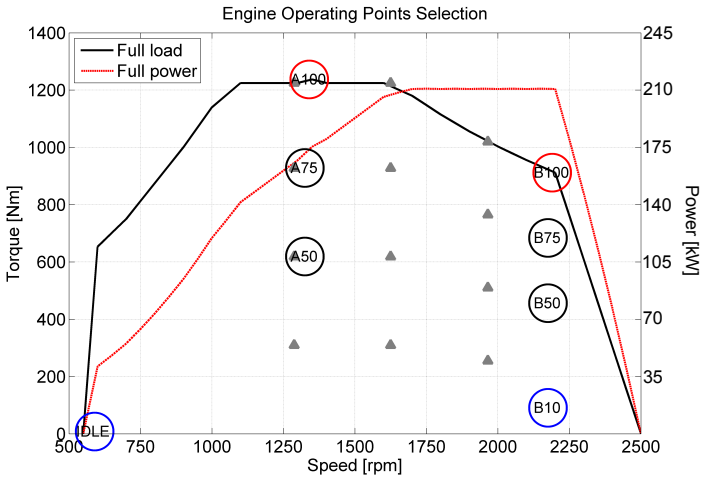

Figure 3.3: C1 Cycle engine operating points

3.2.2 Research test cell facility

The previously described Diesel engine is installed in a full equipped facility which allows to regulate, control and measure different engine variables as observed on Fig. 3.4. Different pressures, temperatures and speeds are acquired through two different acquisition system dividing the variables by its time dependence in average and instantaneous variables. Additionally to the engine function variables the measurement of the engine emission is essential to completely characterize the engine operating condition under the influence of a particular tool of emission control. The complete list of the measured variables is described on Table 3.3.

The auxiliary systems installed in the test cell for engine operation and control identified on Fig. 3.4 such as the torque and speed regulation unit (Dynamometer brake), the intake and exhaust systems (air inter-cooler), and the engine cooling system (water inter-cooler) could be identified in the test cell scheme and will be described in next subsections.

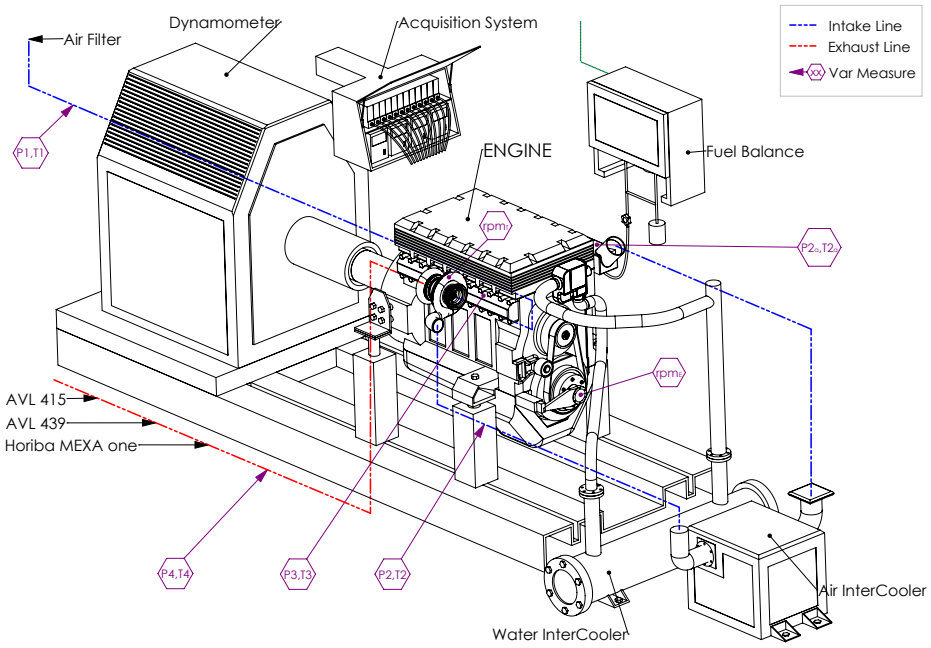

Figure 3.4: Engine and test cell equipment distribution

Variable measured	Description	[Units]
P1 and T1	Pressure and temperature before compressor	[bar] [^{o}C]
P2 and T2	Pressure and temperature after compressor	[bar] [^{o}C]
P2a and T2a	Pressure and temperature at intake manifold	[bar] [^{o}C]
P3 and T3	Pressure and temperature at exhaust manifold	[bar] [^{o}C]
P4 and T4	Pressure and temperature at after turbine	[bar] [^{o}C]
rpmT	Turbo speed	[rpm]
rpmE	Engine speed	[rpm]
Torque	Engine torque	[Nm]

Table 3.3: Description of the measured average variables

3.2.2.1 Regulation and control equipment

Torque and speed regulation system: This system allows to stabilize the engine in a defined operating condition controlling both the engine speed as the engine torque. The main component of this system is the Dynamometer brake which is in charged of the dissipation of engine power. In this kind of brake could be installed different kind of engines with a maximal power of 400

kW giving flexibility in terms of brake cooling because it does not depends on a water supply due the air cooling system installed on it. Dynamometer brake systems has an interesting function as motor which could be used to characterize the engine behavior in motoring conditions thus without combustion, defining the torque required to get over the friction of the mechanical system.

Intake and exhaust system: With the engine installed in the test cell and adapted on the Dynamometer brake to be motored or braked on combustion test, the second system in the regulation and control is composed of two sub-system.

The first sub-system is the intake line which is in charge of filter, condition, measure and drive the fresh air to the intake manifold. The intake line is composed of the air filter which serve to separate the small particles suspended in the air, later the filtered air mass is measured through an air mass flow meter before the compressor inlet. The air after the compressor which its temperature was increased must pass through the inter-cooler where the air temperature is regulated to the desired value in the intake manifold.

The second sub-system is the exhaust line which serve to drive the exhaust gases from turbine outlet to the atmosphere. Is in this line where all the sample lines from gases analyzers are installed with the objective to limit the distance between the place of the sample and the analyzer.

Engine Cooling system: The engine cooling and oil pumps are driven by the engine power leading the heat flux generated by the six cylinders combustion to the heat exchanger where through the test cell water circuit the engine water temperature is maintained constant at 90^{o}C respectively, by means of PID controllers. This values is the one defined for the engine at standard operation. Additionally, the coolant and lubricant temperatures are acquired at the inlet and outlet of the engine, being the last ones used as control variables.

3.2.2.2 Measuring and acquisition systems

The data acquisition systems are used to collect the information from the different measuring equipment and sensors. Due to the different nature of the data acquired during the engine tests, the test cell is equipped with two types of acquisition systems. They can be classified depending on the kind

Variable measured	Description	[Units]
P2a	Pressure intake manifold	[bar]
P3	Pressure exhaust manifold	[bar]
P4	Pressure after Turbine	[bar]
PCYL	Incylinder Pressure	[bar]
Ipulse	Injection pulse	[A]

Table 3.4: Description of the measured instantaneous variables

of variable which is acquired in average and instantaneous variables. The averages variables are acquired through a low frequency acquisition system while the instantaneous uses a high frequency system.

High sampling frequency (Instantaneous variables): The high frequency data acquisition is carried out by means of a Yokogawa DL708E [3] oscillographic recorder with 8 modules of 16 bits A/D. The oscilloscope is connected to a PC, which stores the engine variable transferred from the Yokogawa system the engine variable recorded could be observed on Table 3.4. Regarding its sampling frequency, the angle encoder installed on the crankshaft of the engine sends a pulse to a control box every 0.2 CAD. This pulse serves as the clock timer for the oscilloscope. Additionally, this crank angle encoder sends one reference pulse every revolution, which serves to reference the top dead center (TDC) of the engine. With the pulses every 0.2 CAD acting as clock timer and the reference pulse as trigger, the oscilloscope acquires the data from the sensors at a sampling frequency of 36 kHz.

Low sampling frequency (Mean variables): The low sampling frequency system is used to acquire and store the most important data related to each operating conditions, the engine and test cell monitoring variables, and the experimental average measurements obtained from sensors, dedicated equipment and gas analyzers. These variables are acquired at a frequency of 1 Hz, independently on the engine speed, over a typical measurement period of 1 minute where they are averaged. This is an acquisition system widely used in the automobile industry. This system is called PUMA 5 Compact and is developed by the Austrian company AVL. The measured data is visualized on the test bench during engine operation using a personalized interface, and it is conveniently stored in a file for post-processing and posterior analysis.

The PUMA 5 system allows monitoring of variables which are subject to an upper or lower limit. If the variables values exceeds some of these limits

the system reacts by executing a defined order such as an acoustic alarm, message per screen or even the engine stop like a security measure in the engine operation.

3.2.2.3 Instrumentation description

After the MDE8 Diesel engine description and the research test cell facility overview, this section aims to explain the main instrumentation and measuring equipment used in the experimental facility. Additionally, the measuring range as well as the precision of the different sensors and equipment could be found in this section. A summary of all the information referred to the sensors could be observed in Table 3.5.

Variable measured	Device	Manufacturer and model	Accuracy
In-Cylinder pressure	Piezoelectric sensor	Kistler 6125C	± 1.5 bar
Intake/Exhaust pressure	Piezoresistive sensor	Kistler 4045A10	± 25 mbar
Different Temperatures	Thermocouple	TC direct K type	± 2.5ºC
Different Temperatures	Thermoresistances	Pt100	± 0.3ºC
Crank Angle,Engine Speed	Encoder	AVL 364	± 0.02CAD
Cam profile	Linear transducer	WA HBM	± 0.002mm
NO_x,CO,HC,O_2 Conc	Gas analyzer	Horiba Mexa One	4%
Filter smoke number	Smoke meter	AVL 415s	± 0.025 FSN
Soot opacity	Opacimeter	AVL 439	± 0.01 %
Diesel fuel mass flow	Fuel balance	AVL733S	± 0.2%
Air mass flow	Air flow meter	Sensyflow MT400	± 0.1%

Table 3.5: Test cell instrumentation accuracy

Torque crank angle and engine speed measurement: The engine torque is measured by means of a load cell installed in the torque shaft between the engine flywheel and the Dynamometer brake. The nominal torque for this load cell is 2000 Nm, a value far above of the typical values measured in the present investigation. The precision of this transducer is 1%. In the case of engine speed is measured through an optical encoder installed in the Dynamometer brake while the engine crank angle is measured by means of an AVL 364 [4] optical angle encoder installed on the crankshaft of the engine. In addition, the encoder provides a synchronization signal (one signal per engine revolution), which allows to positioning the top dead center (TDC). As commented before, this synchronization signal is used as trigger for the high speed acquisition system (Instantaneous variables).

Mass flow measurement: the air mass flow is measured by Sensyflow FMT500I [5] which is a thermal flow meter for gases. The measuring principle (hotfilm anemometer) allows the direct determination of mass flow and gas temperature. taking the standard density of the gases into consideration, the standard measure is directly acquired by the PUMA 5 low frequency system.

The fuel mass flow is measured by an AVL 733S [6] fuel balance. The gravimetric fuel balance performs the measurement by means of a capacitive sensor, providing a signal which depends on the instantaneous fuel mass located inside the measuring vessel. The measuring range of the model used in this work ranges from 0 to 160 kg/h and its measure is directly acquired by the PUMA 5 low frequency system

Mean pressure and temperature measurement: In order to measure the mean pressure of the fluids over the whole locations of the research test cell installation (intake, exhaust and cooling systems), several piezoresistive absolute pressure transducers Kistler 4045A10 [7] have been used. The most remarkable characteristics of these transducers are the great thermal stability and the reduced measurement drift. The measuring range of these sensors is from 0 to 10 bar.

Regarding mean temperature acquisition, several thermocouples type K without covering (in the case of the clean gas) and covered (in the case of the exhaust gas), have been installed. The measuring range of those thermocouples is from 0 to 1100 °C, with a precision of 2.5 °C. The upper temperature limit is far above of that experienced in the engine tests.

Other kind of temperature transducers are the thermoresistances Pt100 type which have been used to measure the oil and water temperatures. The measuring range of those sensors is from -200 to 850 °C, with a precision of 0.3 °C. One of the main characteristics of this type of thermoresistances are the great sensibility and linearity in all the measuring range.

All this signals are directly acquired by the PUMA 5 low frequency system (mean variables acquisition system).

Instantaneous pressure transducers: The in-cylinder pressure signal is the most important data needed to perform the combustion diagnosis and analysis. To acquire this signal, a non-cooled piezoelectric transducer Kistler 6125 [8] with measuring range from 0 to 250 bar is used. The signal generated from the pressure sensor is conditioned by a Kistler 5011B10 charge amplifier

before arriving to the high frequency acquisition system being referenced with the crank angle (Instantaneous variable acquisition system).

The instantaneous pressure at the intake and exhaust manifolds uses a water-cooled piezoresistive transducers manufactured by Kistler (4045A10), whose measuring range is from 0 to 10 bar. The pressure signal is conditioned before its acquisition by means of a Kistler 4603A10 charge amplifier before arriving to the high frequency acquisition system being referenced with the crank angle (Instantaneous variable acquisition system).

Horiba gas analyzer: The engine emissions are sampled close to the turbine outlet and drive to the Horiba MEXA-7100DEGR [9] gaseous emissions bench. It is a device actually composed of different gas analyzers which function under different measuring principle depending on the engine emission to be characterized:

- The CO and CO_2 are quantified by means of a NDIR (Non Dispersive InfraRed detector). Both CO and CO_2 absorb a specific wavelength of infrared light, which is transferred into concentration values. CO emissions up to 10 % and CO_2 up to 20 % can be measured with a precision of ± 4 %.
- NO_x is determined based on the chemiluminescence principle. First NO_x is reduced to NO, second the exhaust gas with NO is mixed with ozone (O3). This reaction creates activated NO^*_2 which luminesces broadband visible to infrared light as it reverts to its lower energy state ($NO^*_2 \rightarrow NO_2 + \text{light}$). This light is detected and converted to NO_x concentration. The NO_x can be measured in the range of 0 to 5000 ppm with a precision of ± 4 %.
- The HC concentration is measured using the same ionization principle. A hot sample of the exhaust gas is burned in combination with a mixture of hydrogen, helium and synthetic air. When the hydrocarbons burn, they produce ions which in presence of an electric field, produce an ionization current proportional to the quantity of carbon atoms. The HC emissions can be measured up to 10000 ppm with a precision of ± 4 %.
- The O2 concentration is measured considering the paramagnetic properties of oxygen. The range of oxygen concentration that can be measured is between 0 and 25 with a precision of ± 4 %

  Before starting each test session, a calibration procedure for each analyzer is carried out using reference gases. These reference gases

have a composition that is representative for the typical emissions range observed for several engines. The AF ratio (air/fuel ratio) and lambda are calculated by the Horiba equipment based on the composition of the exhaust gas.

This device could be treated as a mean variable output then it is acquired by the PUMA 5 low frequency system.

AVL Smoke meter: The soot content of the exhaust gas is measured with an AVL 415 [10] smoke meter. In this filter-type smoke meter, a defined quantity of exhaust gas passes through a clean filter paper. In particular, three samples of a 1 liter volume each, with paper-saving mode, they were collected for each engine test recorded. The smoke meter utilizes an optical reflectometer to determine the amount of blackening of filter paper by the soot contained in the fixed volume of exhaust gas. The blackening on the filter paper is detected by a photoelectric measuring head and translated to FSN (Filter Smoke Number) on a scale from 0 (filter without blackening) to 10 (filter completely blacked). The detection limit of this device is 0.002 FSN and the resolution is 0.001 FSN. Soot measurements in FSN are transformed to soot concentration (mg/m3) considering the correlation proposed by AVL manufacturer [10]. Later, soot concentration on mass basis (mg/kg) can be obtained considering a constant exhaust gas density of 1.165 kg/m3. This device could be treated as a mean variable output then it is acquired by the PUMA 5 low frequency system and its used in the static point by point measurements.

AVL 439 Opacimeter: The AVL 439 [11] Opacimeter is a device used to measure the smoke opacity value from the attenuation of visible light in the device measuring chamber, the smoke density value is in effect the result of black smoke (Carbon), blue smoke (hydrocarbon vapor) and white smoke (water vapor). With its high accuracy, dynamics, reliability the main advantage of this equipment is the measure time resolution which allows to have a description of the “instantaneous” smoke emission. The measurement value output is the opacity on a scale from 0 to 100% . The detection limit of this device is 0.1 %. This device could be treated as an “instantaneous” variable output and it is used in the transient tests characterization.

3.2.3 Experimental procedures description

3.2.3.1 Camshaft profiles measurement

As previously discussed, one of the objectives of the thesis work is to explore different air management strategies as a tool of emission control, for this purpose an experimental setup in order to perform the different camshaft profile characterization was needed. The mechanical arrangement to characterize each tested profile was directly mounted over the engine cylinder head and it allows to measure and verify experimentally the simulated profiles. The key component in this arrangement is a WA HBM [12] linear displacement transducer which allows to measure the cam profile using the lift of intake and exhaust valves as is shown in Fig. 3.5 later it is acquired and referenced with the crank angle helped by the High sampling frequency acquisition system.

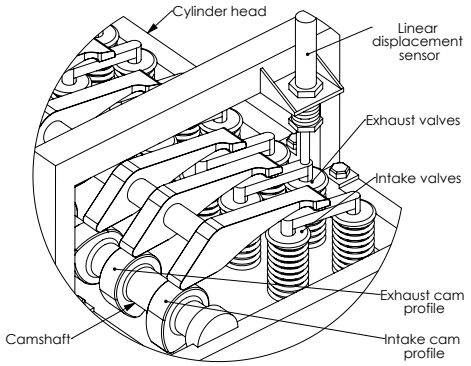

Figure 3.5: Mechanical arrangement to characterize camshaft profiles

The first measured camshaft profile was the standard profile as observed in Fig. 3.6 which is used as the basis to propose the studied alternatives (Miller and iEGR).

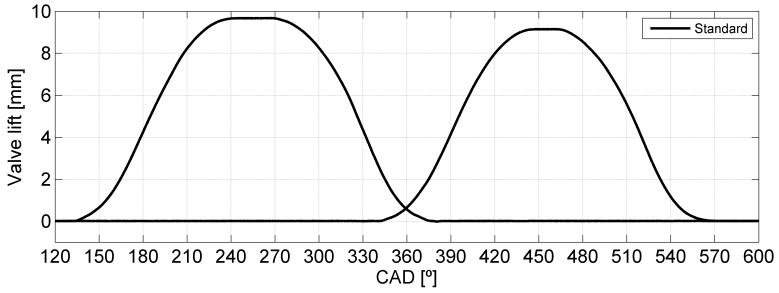

Figure 3.6: Measured standard camshaft profile

3.2.3.2 Standard testing routine

The research test cell facility provides a great flexibility in the control of engine parameters which take part during the tests. The engine operation not only requires a fine control over the different previously described systems (Torque and speed, intake and exhaust, engine cooling), but also the proper management and control of the injection system. As a consequence, the greater complexity in the experimental facility added to the larger number of engine settings that has to be simultaneously controlled and registered, may difficult the errors detection in the tests and the determination of any deviation in the measurement equipment.

Therefore, it is very important to define a specific routine to identify and rapidly detect possible sources of experimental errors before and during test execution [13]. Accordingly, to improve the accuracy and guarantee the quality of the experimental results presented on this investigation, the correct functioning and repeatability of the experimental facility have been carefully checked every testing day, by following a strict monitoring and detection protocol as described in Fig. 3.7.

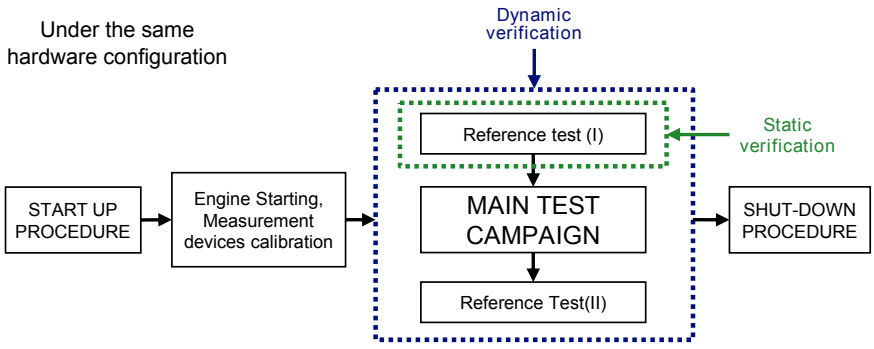

Figure 3.7: Description of the testing procedure

In this case as could be observed in Fig. 3.8 for A50 Reference operating condition, 8 engine parameters are compared under 30 different testing days. The red range symbolizes the variation range defined at each engine parameter and the main variations could be noticed in the engine emissions measurement. In the case of engine parameters all the registered values are inside the defined ranges.

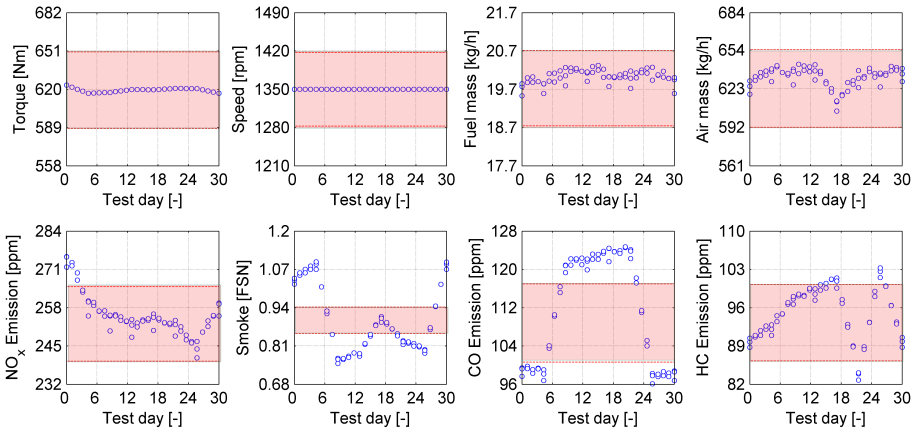

Figure 3.8: A50 Reference point under standard camshaft configuration

3.3 Theoretical tools

The theoretical tools serve to process, analyze and improve the quality of the raw experimental data. This tools help to generate additional information that contribute to better understand all the engine involved process as the air management or combustion process. To select the suitable theoretical tools, it is necessary to consider several aspects:

- Necessary inputs for the models (all information is provided by the experimental facility?)
- Hypothesis of the theoretical approaches.
- Matching between their output information and the objectives of the study.
- Validity and accuracy of the results obtained through it.

In this section are discussed the main characteristics of the three theoretical tools used in this investigation. Specifically, the general hypotheses and principles of the 0-D combustion diagnosis code which are described in subsection 3.3.2. Later, the main details about the 1D modeling methodology, set-up and validation through GT Power software in subsection 3.3.3. finishing by the computational fluid dynamic (CFD) modeling which are discussed on subsection 3.3.4.

3.3.1 0D Engine maps

The engine operating maps described in this section are applied in the exploration of air management strategies as emission control tools. The objective of these maps is to compare the potential of each cam profile strategy in a common reference framework [14].

In order to generate these maps the iEGR quantity is located in the 'X' axis and the A/F ratio in the 'Y' axis. Under the hypothesis of complete combustion it is possible to represent in this axis the ISO lines of constant Y_{O2-ivc} and Y_{O2-evo} which could be obtained from equations 3.1 and 3.2.

$$Y_{O2-ivc} = Y_{O2-air} \cdot \left(1 - iEGR \cdot \frac{(A/F)_{est}}{A/F}\right) \tag{3.1}$$

$$Y_{O2-evo} = Y_{O2-air} \cdot \left(1 - \frac{(A/F)_{est}}{A/F}\right) \tag{3.2}$$

Where Y_{O2-air} is the oxygen mass concentration in the air which is constant and equal to 0.23196 or 23.196% and $A/Fest$ is stoichiometric Air/Fuel ratio which has a constant value and equal to 14.567. The $iEGR$ rate is included as decimal in order to maintain the units coherence.

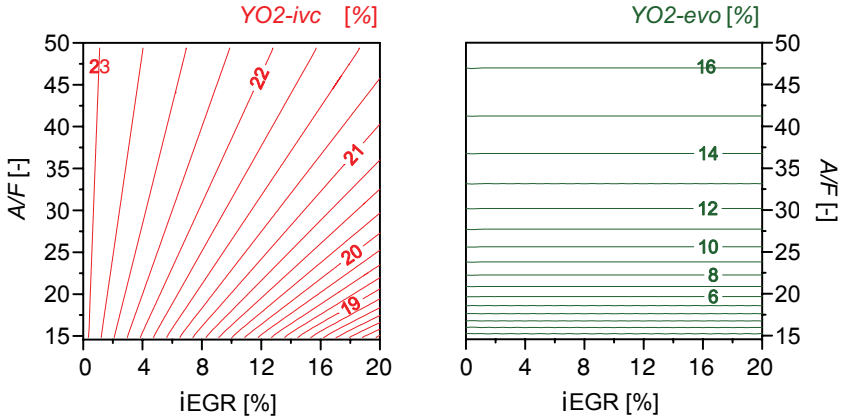

Figure 3.9: Engine maps YO2 intake and exhaust concentration

The Y_{O2-ivc} and Y_{O2-evo} ISO lines in the Fig. 3.10 only depends on fuel Stoichiometry ($(A/F)_{est}$), thus the engine particular operating conditions don't affect this lines behavior.

Now the injection conditions must be considered through the engine load or fuel mass flow. The total mass at the intake valve closing is related with

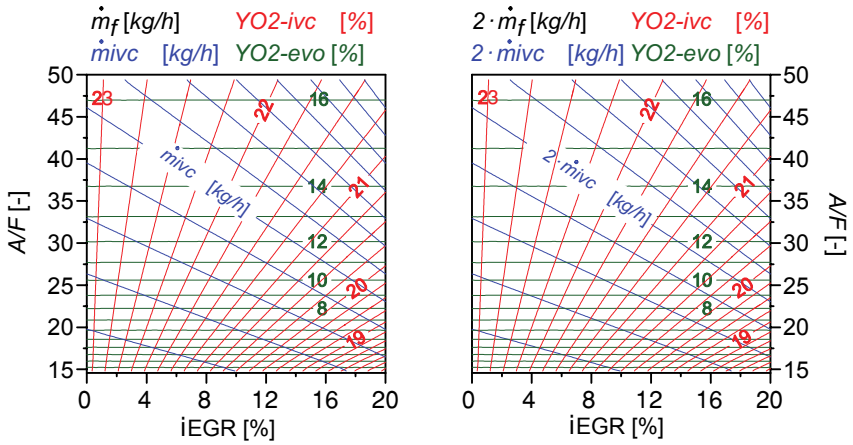

Figure 3.10: Engine maps YO2 intake and exhaust concentration

the engine load as function of A/F and the $iEGR$ rate. As described by the equation 3.3 the total mass flow through intake manifold are represented by the iso lines with negative slope grouped in the engine maps as could be observed in Fig. 3.10.

$$\dot{m}_{air} = \dot{m}_{ivc} \cdot (1 - iEGR) \xrightarrow{\substack{Dividing \\ by\ \dot{m}_f}} A/F = \frac{\dot{m}_{ivc}}{\dot{m}_f} \cdot (1 - iEGR) \tag{3.3}$$

with $\dot{m}_{ivc}$ is the total mass flow at the intake valve closing and $dotm_f$ is the total fuel mass flow injected to the engine. The $iEGR$ is included as decimal in order to maintain the units coherence.

The main hypothesis in order to get constant iso lines of $\dot{m}_{ivc}$ is the minimal affectation of mixture temperature under the low rate of trapped $iEGR$ less than 20%.

3.3.2 0D CALMEC model for combustion diagnosis

The combustion diagnosis codes use the experimental in cylinder pressure signal obtained through the high sampling frequency as input data and, after averaging, filtering, and referring to absolute pressure and crank angle values, solve the heat release law (time evolution of heat release fraction), and the instantaneous gas temperature average along the combustion chamber by combination of both the first principle of thermodynamics and the equation of state.

These kind of models are typically zero-dimensional and single-zone models, hence, do not take into account the air entrainment, vaporization of fuel droplet and spatial variation of mixture composition and temperature. The single-zone models are advantageous because of their simplicity and their wide usage in engine testing for monitoring global combustion parameters. However, the analysis of global combustion parameters such as the start of combustion or the combustion phasing is still valid since they are directly related to the instantaneous evolution of the energy released by the progress of the combustion, independently from the local conditions where this energy is being released.

The combustion diagnosis code used in the present investigation was developed at CMT-Motores Térmicos and is called CALMEC [15] and [16]. The general hypotheses of the model are briefly described and discussed next:

- The pressure is supposed homogeneous in the combustion chamber. This hypothesis is generally accepted since the fluid and the flame propagation velocity are lower than the speed of sound.
- The fluid that evolves inside the combustion chamber is considered as a mixture of air, gaseous fuel and burned products. Despite that in this model a uniformity of charge composition and mixture temperature are taken into account, it is important to remark that a maximum of three species (air, gaseous fuel and burned products) are considered to evaluate the thermodynamic conditions of the mass trapped in the cylinder.
- An ideal gas behavior is assumed for the mixture that evolves in the combustion chamber. It is reasonable to accept this assumption for the air and burned products, however, it could seem not adequate for the gaseous fuel. In this sense, Lapuerta [17] compared the results from the combustion analysis model using different state equations for the gaseous fuel. The results confirmed that the differences in mean temperature and HRL are small enough to accept the hypothesis.
- The internal energy is calculated considering the mean gas temperature. This is the hardest hypothesis since burned products are much hotter than mean temperature at the combustion beginning, even though later they become closer.
- The heat transmitted to the walls is calculated utilizing a modified heat transfer coefficient obtained with Woschni's expression [18]. An additional heat transfer nodal model is used to calculate the different wall temperatures (piston, liner, cylinder head) [19].

Taking into account the previous hypotheses, CALMEC raises the first law of thermodynamics to open systems considering the fuel injection and blow-by flow. Thus, the equation is solved in steps of time defined by the resolution of the in-cylinder pressure measurement.

$$\Delta HRL = m_c \cdot \Delta u_c + \Delta Q + p \cdot \Delta V - (h_{f,iny} - u_{f,g}) \cdot \Delta m_{f,ev} + R_c \cdot T_c \cdot \Delta m_{bb} \quad (3.4)$$

- $\mathbf{\Delta HRL}$. This term corresponds to the fuel released thermal energy assuming a constant heating power in the combustion process.
- $\mathbf{m_c \cdot \Delta u_c}$. This is the sensible internal energy variation of the gas trapped in the control volume. Lapuerta [17] proposes, this term is calculated by means of a specific correlation for each species. For each temporal step, these correlations are solved as a function of the mean temperature in the control volume while pondering by the mass fraction of each specie.
- $\mathbf{\Delta Q}$.This term accounts the heat transfer from the gas trapped in the control volume to the surrounding surfaces of the piston, liner, cylinder head and valves. The model does not consider the possibility of fuel impinged in the wall. The instantaneous heat transfer coefficient between the gas and the different surfaces is based on Woschni with some improvements detailed in Payri et al. [20]. For the calculation of the different wall temperatures a nodal heat transfer model is implemented.
- $\mathbf{p \cdot \Delta V}$. This term represents the total work made by the gas trapped in the control volume during the calculation period. For the instantaneous calculation of the combustion chamber volume, a mechanical deformations model is considered. This sub model takes into account both the pressure made by the gas on the piston head and the inertial forces generated by the alternative movement of the masses.
- $\mathbf{(h_{f,iny} - u_{f,g}) \cdot \Delta m_{f,ev}}$. This term includes all the energetic considerations associated to the fuel injection process i.e. the flow work, the heat needed to reach the evaporation temperature and the heating-up process of the vapor fuel until reaching the combustion chamber temperature.
- $\mathbf{R_c \cdot T_c \cdot \Delta m_{bb}}$. Finally, the energy lost due to the blow-by through the piston rings is also considered. The blow by mass is calculated using an isentropic nozzle model to simulate the gas evolution from the combustion chamber to the oil sump.

The Fig. 3.11 shows the kind of data obtained from CALMEC that will be used to perform the combustion diagnosis. In particular, the figure shows the instantaneous evolution of the heat release law (HRL), rate of heat release (HRR), in-cylinder pressure and simulated fuel injection rate. Based on this results, it can be obtained several time representative parameters to describe the injection and combustion events [21]. The combustion parameters that will be typically used in next chapters are defined below:

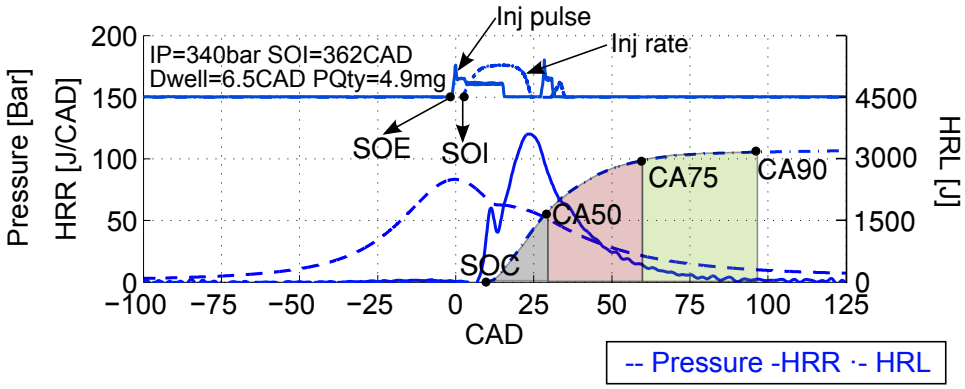

Figure 3.11: Main combustion parameters obtained with CALMEC

- Start of injection (SOI): Defined as the instant in which the injection event begins. This parameter is based on a simulated injection rate, which takes into account the hydraulic and electric delay of the injector after the start of energizing (SOE).

- Ignition delay: Defined as the time elapsed from the diesel start of injection (SOI) up to the start of combustion (SOC).

- Start of combustion (SOC): Defined as the crank angle position in which the cumulative heat release (HRL) has reached 5%.

- CA50, CA75 and CA90: Crank angle degree in which the 50%, 75% and 90% of the total heat release has been released during the combustion process, respectively. The crank angle is referred to the top dead center (TDC).

- Combustion duration: Defined as the time elapsed from the start of combustion (SOC) up to the CA90.

3.3.2.1 Adiabatic flame temperature estimation

As it was previously described, the 0D model CALMEC used for calculating the HRR is based on the assumption of an uniform temperature along the combustion chamber. However, as it was discussed in the literature review, the formation and destruction of pollutants is driven by physical and chemical processes affected by the evolution of local conditions, in terms of mixture composition and temperature. So, to qualitatively compare some general trends observed in the pollutants, specially in terms of NO_x, it appears more appropriate to estimate the maximum temperature achieved during the combustion process [22].

A good qualitative indicator of the maximum local combustion temperature would be to estimate the adiabatic flame temperature (T_{adb}), assuming that the combustion process in a diesel engine is adiabatic and that the reaction is complete. The adiabatic temperature can be defined for two different processes; considering a combustion at constant pressure, or at constant volume. The following hypothesis have to be made for the calculation of the adiabatic flame temperature. This calculation was incorporated to the CALMEC software standard results.

- The combustion develops at approximately constant pressure at each time-step of the calculation. This is a simplification to the characteristic mixing-controlled combustion process occurring in a diesel engine. So if a fuel-air mixture is burnt in an adiabatic process at constant pressure, then the absolute enthalpy of the reactants in the initial state (at unburnt temperature) should be equal to the absolute enthalpy of the products at the end of the reaction (at adiabatic temperature).

$$H_{reac}(T_{unburnt}) = H_{prod}(T_{adb}) \tag{3.5}$$

  This term $H_{reac}(T_{unburnt})$ is the reactives enthalpy at unburnt temperature and $H_{prod}(T_{adb})$ is the products enthalpy at adiabatic temperature.

- The maximum adiabatic flame temperature occurs in a region of local equivalence ratio equal to stoichiometric. This hypothesis is true for diffusive diesel combustion, where the flame develops in a thin reaction zone at stoichiometric mixture conditions.

- The thermodynamic system is considered at all times as a mixture of ideal gases. Then, it is possible to calculate the properties of the mixture,

including the enthalpy, like the weighted sum of each species, with the equations

$$\begin{aligned} H_{reac}(T_{unburnt}) &= \sum_{i=1}^{k} N_i \cdot \overline{h}_i(T_{nuburnt}) \\ H_{prod}(T_{adb}) &= \sum_{j=1}^{m} N_j \cdot \overline{h}_j(T_{ad}) \end{aligned} \tag{3.6}$$

the term N_i is the mole number of reactant i i and N_j is the mole number of product j in the mixture and $\overline{h}_i(T_{unburnt})$ is the specific enthalpy of reactant i y $\overline{h}_j(T_{adb})$ is the specific enthalpy of product j. These specific enthalpies of each species are calculated according to the next equations (3.7).

$$\begin{aligned} \overline{h}_i(T_{unburnt}) &= \overline{h}^o_{i,form} + \int_{T=298}^{T=T_{sq}} \overline{c}_{p,i}(T) \cdot dT \\ \overline{h}_j(T_f) &= \overline{h}^o_{j,form} + \int_{T=298}^{T=T_{ad}} \overline{c}_{p,j}(T) \cdot dT \end{aligned} \tag{3.7}$$

the terms $\overline{h}^o_{i,form}$, $\overline{h}^o_{j,form}$ corresponds to the enthalpy of formation at standard conditions ($T = 298.15\ K$ and $p = p_{ref}$) and $\overline{c}_{p,i}(T)$, $\overline{c}_{p,j}(T)$ the specific heat capacity at constant pressure, calculated by polynomial equations.

- N-dodecane ($C_{12}H_{26}$) is used as surrogate fuel, since their properties are well known and reasonably similar to those of diesel fuel.
- To close the calculation it is necessary to estimate an initial temperature of the reactants ($T_{unburnt}$) at each calculation interval. So the temperature of the reactants is assumed to evolve adiabatically as the pressure in the chamber increases due to the combustion process and piston movement.

Finally, a 13-species equilibrium approach at constant pressure was resolved to arrive at the maximum adiabatic flame temperature, as developed by Way [38]. Since the composition of the products has to be calculated at each time-step, but they depend on the calculated value, the adiabatic temperature is resolved following an iterative calculation process.

3.3.3 1D GT Power model in air-management conditions simulation

For this research work, particularly for the air-management strategies applied in the emissions control, a 1D model is required in order to determine the evolution of the different thermodynamic variables along the intake and exhaust processes [23]. A summary of the information that could be obtained through a 1D model is listed below:

- The pressure looses in all elements of the system, especially in those where it is important, such as filters, inter-coolers or aftertreatement systems.
- The energy losses caused by heat transfer, especially in the exhaust system and in the heat exchangers.
- The effects of flow compressibility in those areas where it can reach high speed as in the cylinder valves. The model serves to determine the flow inertia phenomena which are also important in the region of the cylinder valves.
- The pulsating flow produced by the sequential opening of the intake and exhaust valves is transmitted to the different elements of the system. These pulsations in the exhaust manifold have a greater amplitude than in the intake system they are useful to improve the engine volumetric performance reducing the pumping work.

A commercial software called GT Power, used in most of the automotive companies serve to build the complete 1D model for a specific platform with the aim to explore the engine behavior under the different camshafts configuration. This model allows the calculation of non-reactive flows in the engine determining the previously described results under the next hypothesis [24]:

- The gas flow in all the tubes is considered one-dimensional and the volumes are taken like no dimensional. The action wave model simplifies the problem geometry in tubes where only the length is considered and the volumes where the gas properties maintain uniform properties.
- The flow is considered non-homoentropic thus the momentum losses due to friction and the energy loss due to heat transfer are considered. On the other hand, the viscosity of the gas is not taken into account thus there are not losses by internal friction on the gas.

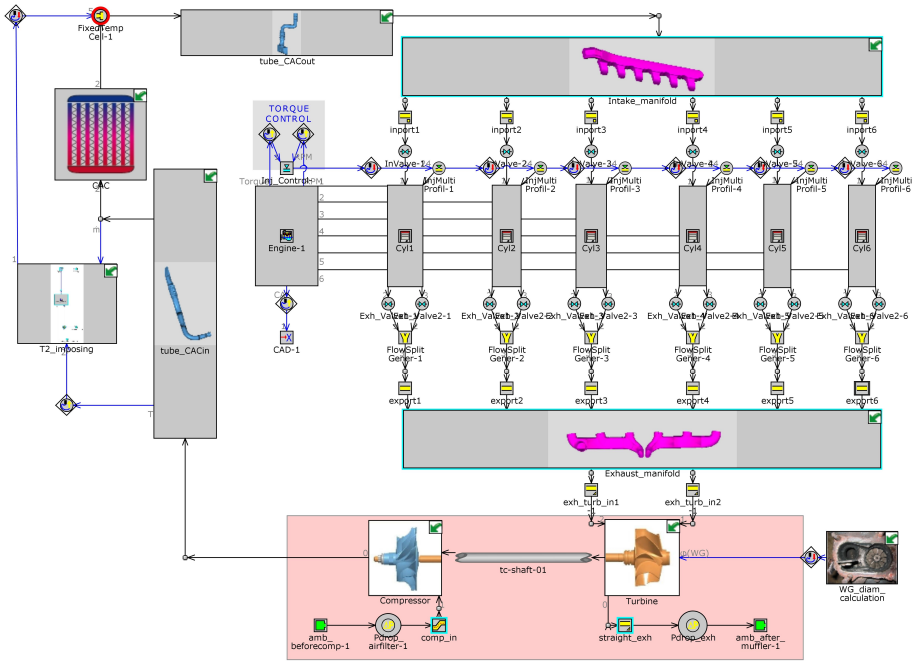

Figure 3.12: MDE8 Engine GT power model

- It is assumed a nonviscous, perfect ideal gas, in spite of the evident differences between the gas composition in the intake or the exhaust. The nonviscous flow condition allows transforming the Navier-Stokes equations into a Euler equations system where the second-order partial derivative are canceled.

The governing equations for the 1D model software are: Continuity 3.8, Momentum 3.9 and Energy 3.10.

$$\frac{dm}{dt} = \sum \dot{m} \tag{3.8}$$

$$\frac{d\dot{m}}{dt} = \frac{dpA + \sum(\dot{m}u) - 4C_f \frac{\rho u|u|}{2} \frac{dxA}{D} - C_p(\frac{\rho u|u|}{2})A)}{dx} \tag{3.9}$$

$$\frac{d(me)}{dt} = p\frac{dV}{dT} + \sum(\dot{m}H) - hA_s(T_{fluid} - T_{wall}) \tag{3.10}$$

With m is the mass, t is the time, $\dot{m}$ is the mass flux, dp is the pressure differential across dx, A is the area, u is the velocity at the boundary, C_f is the

skin friction coefficient, ρ is the density, dx is the discretization length, D is the equivalent diameter, C_p is the pressure loss coefficient, e is the internal + the kinetic energy, p is the pressure, V is the volume, H is the total enthalpy ($H = e + \frac{p}{\rho}$), h is the heat transfer coefficient, A_s is the heat transfer surface area, T_{fluid} is the fluid temperature, T_{wall} is the wall temperature.

As mentioned above, the primary solution variables are mass flow rate, density, and internal energy. The values of mass flow, density and internal energy at the new time are calculated based on the conservation equations. The right hand side of the equations is calculated using values from the previous time step [25]. This yields the derivative of the primary variables and allows the value at the new time to be calculated by integration of that derivative over the time step. To ensure numerical stability, the time step must be restricted to satisfy the Courant condition.

The small time steps required by this method make the method undesirable for simulations that are relatively long (on the order of minutes in real time). But is well suited for highly unsteady flow where a high degree of resolution is already required to capture the extremes of the flow behavior. This method will produce more accurate predictions of pressure pulsations that occur in engine air flows and fuel injection systems and is required when prediction of pressure wave dynamics is important.

At each time step, the pressure and temperature are calculated in the following way:

1. Continuity and energy equations yield the mass and energy in the volume.

2. With the volume and mass known, the density is calculated yielding density and energy.

3. The equations of state for each species define density and energy as a function of pressure and temperature. The solver will iterate on pressure and temperature until they satisfy the density and energy already calculated for this time step. It is also possible for species change (i.e. combustion, cavitation: liquid to vapor, etc.). The mass transfer between species is also accounted for during this iteration.

3.3.3.1 GT Power engine 1D model validation

With the engine one-dimensional model configured in GT Power software as shown in Fig. 3.12. The calibration with experimental data was performed

in the full load conditions A100 and B100 as can be observed in Fig. 3.13. The combustion efficiency and heat release rate directly came from the experimental data and the in-cylinder heat transfer process was calculated with the WoschniGT model. At each operating condition, the gross indicated mean effective pressure (IMEP) and in-cylinder pressure trace were firstly calibrated with adjustments on the intake and exhaust pressures achieved by the accurately calibration of the discharge coefficients in the valves and the efficiency of turbine and compressor. It could be seen that the statistic relative differences are generally less than 5% for the five criteria defined as calibration parameters: net and gross IMEP, BSFC, Pint, Pexh and Pmax and also the measured and simulated in-cylinder pressure traces also show good agreements.

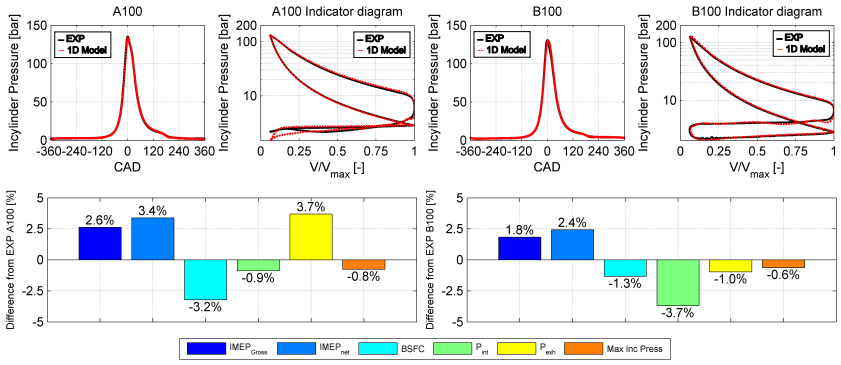

Figure 3.13: 1D model validation

3.3.4 3D StarCD CFD model for injection-combustion simulation

Despite the accurate information which could be obtained through empirically modeling the engine processes, as in classical thermodynamically-based analyses, comprehensive computer codes are now extensively used in engine research to capture some fundamental details of the combustion phenomenon.

The 3D CFD modeling has become a key tool in the optimization process of modern IC engines, as for the development of advanced combustion concepts, specially because it provides a more accurate prediction and study of the behavior of pollutant emissions compared to simplified multi-zone models or chemical kinetics reactor simulations.

Particularly in this research work the CFD modeling serve to characterize the combustion process in the MDE8 engine under different combustion parameters which affects directly the emission formation as the combustion chamber geometry or the injection settings.

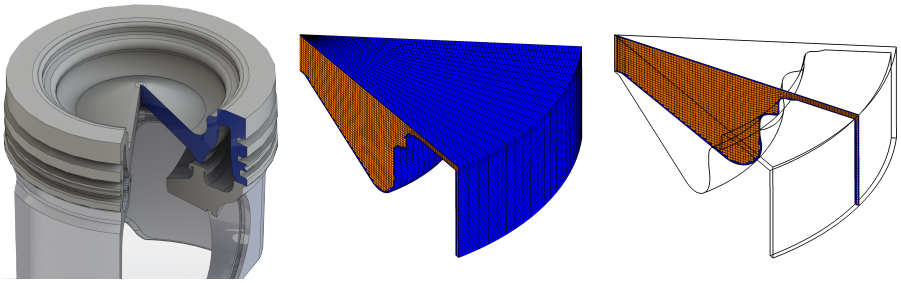

Figure 3.14: Axisymmetric MDE8 Piston bowl section used in the CFD model

The 3D CFD simulations of the engine combustion system were performed in The StarCD code version 4.18 [26]. Each simulation case was calculated as a closed cycle combustion, this is from the closure of the intake valves to the opening of the exhaust valves from 245 to 491 CAD (with the TDC at 360 CAD). The axisymmetry of the combustion chamber as described in the Fig. 3.14. allows to create a sector mesh comprising 180990 cells at BDC with periodic boundary conditions after performing a grid convergence study. The axisymmetry hypothesis is commonly used in the CFD combustion modeling as the works performed by Chan et al. [27], Zheng et al. [28] or Briani et al. [29] in order to simplify the number of cells and the computational time-cost.

The simulations were calculated with 12 cores each with an average time cost of 24 h per simulation. The combustion model was the ECFM-CLEH [30] and [31]. Concerning pollutants, NO_x were calculated using a built-in NO_x NORA model, which is based on the tabulation of equilibrium values of three NO_x species and their relaxation times following a perturbation [32].

A sectional method based on a description of sections containing soot particles of equal volume was used for soot formation and oxidation [33]. Concerning the physical sub-models, the diesel spray was simulated with the standard Droplet Discrete Model available in StarCD. Spray atomization and break-up were simulated by means of the Huh & Gosman [34] and Reitz & Diwakar [35] models, respectively. Diesel fuel physical properties were given by the DF1 fuel surrogate [36]. In these simulations, turbulent flow was modeled by means of the RNG kϵ model [37], with wall-functions based on the model from Angelberger [38] in order to account for wall heat transfer.

OpCon	P_{ivc} [bar]	m_{ivc} [g/cc]	T_{ivc} [K]	T_{wpis} [K]	T_{wlin} [K]	T_{whead} [K]	YO_2 [-]	YN_2 [-]	Y_{EGR} [-]	YH_2O [-]
A100	3.78	3.88	364	558	442	558	0.23	0.76	0.0077	0
B100	3.84	3.69	389	647	424	568	0.23	0.75	0.0196	0

Table 3.6: Boundary conditions at IVC

An implicit scheme was used for time discretization, while divergence terms used the second order Monotone Advection and Reconstruction Scheme (MARS) [26]. Velocity pressure coupling was solved by means of a Pressure-Implicit with Splitting of Operators (PISO) algorithm [39]. The IMEP of the closed cycle can only be compared against experimental data in relative values, so in order to compare in absolute values, the pressure profiles from bottom dead center (BDC) to intake valve closing (IVC) and from Exhaust Valve Opening (EVO) to BDC were taken directly from experimental results, and adjusted in each simulation according to the corresponding operating conditions.

The reference values used for the CFD model boundary and initial conditions for the selected engine operating points are shown in Table 3.6.

3.3.4.1 CFD model validation

The CFD model calibration was done in the full load operating conditions as observed on Fig. 3.15. The model is calibrated and validated with experimental data comparing them with 6 engine output parameters, each one representative in performance or emissions and classified by their time dependence as “instantaneous” parameters or “average” parameters the same classification explained in the previous sections in the experimental acquisition system.

The “instantaneous” parameters compared in the calibration process are the recorded in-cylinder pressure signal and the HRR calculation trace which serve to determine the accuracy of time dependent variables obtained through the 3D CFD model. It is worth clarifying that in the case of the CFD model, the injection rate modeled is compared with the injection electric pulse measured in the experimental facility, hence the observed differences. In the case of “average” parameters the CA90, and ISFC are compared with the aim to calibrate the combustion process and the NO_x emission and the Soot emissions helps to calibrate the pollutant formation models.

As depicted in Fig. 3.15. It could be identified a good accuracy in five of the six selected control parameters. In terms of CA90, NO_x, ISFC, pressure and HRR traces the model shows a prediction representative of the engine experimental behavior perhaps the soot emissions are overestimated.

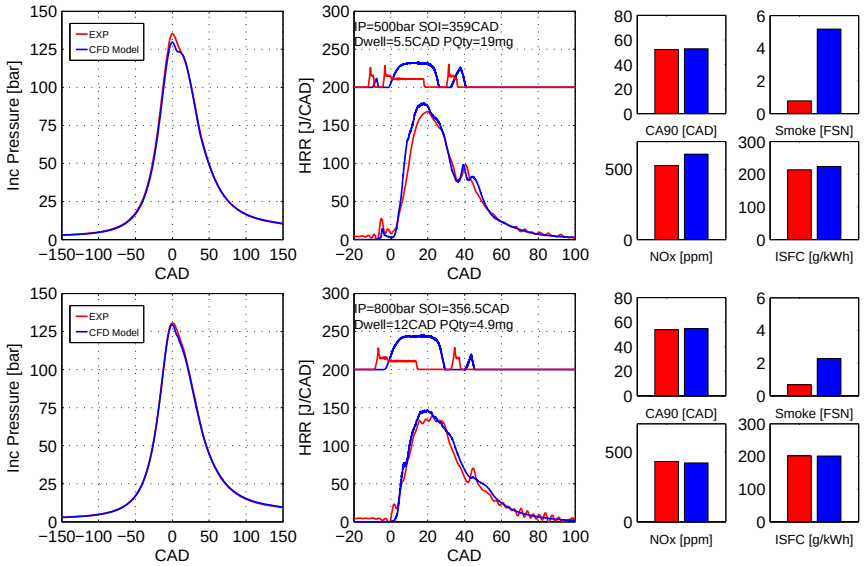

Figure 3.15: A100 and B100 CFD model Calibration

As described by Hernández [40] the understanding of the physical and chemical phenomena leading to the formation of soot particles is incomplete. The chemistry of soot is very complex, in the sense that the initial formation and later growth of soot particles depends on extremely complex chemical paths involving typically hundreds of species and chemical reactions. Even though these mechanisms have been partially deciphered, there are still aspects yet to be discovered. Moreover, soot particles adopt complicated shapes when they start to interact together by coalescence, which is not easy to model.

Mainly due to these reasons not greater efforts were dedicated to improve the soot model predictions, and the study of the combustion soot production is centered in the obtained experimental results.

Bibliography

[1] Molina S. A. *Influencia de los parámetros de inyección y la recirculación de gases de escape sobre el proceso de combustión en un motor Diesel.* Doctoral Thesis, Universidad Politécnica de Valencia, Departamento de Máquinas y Motores Térmicos, 2003.

[2] International standards ISO. *ISO 8178-4 recopricating internal combustion engines - exhasut emissions measurement.* ISO International standards, 2007.

[3] *Yokogawa DL708E oscillographic recorder.* Available technical information in http://www.yokogawa.com.

[4] *AVL 364 angular encoder.* Available technical information in http://www.avl.com.

[5] *Sensyflow FMT500IG hotfilm anemometer.* Available technical information in http://www.abb.com.

[6] *AVL 733S fuel balance.* Available technical information in http://www.avl.com.

[7] *Kistler 4045A10 transducer.* Available technical information in http://www.kistler.com.

[8] *Kistler 46125c transducer.* Available technical information in http://www.kistler.com.

[9] *Horiba MEXA 7100 DEGR exhaust gas analyzer.* Available technical information in http://www.ats.horiba.com.

[10] *AVL 415 Smoke meter.* Available technical information in http://www.avl.com.

[11] *AVL 439 Smoke meter.* Available technical information in http://www.avl.com.

[12] *Linear Transducer WAL by HBM.* Available technical information in https://www.hbm.com.

[13] Benajes J., López J. J., Novella R. and García A. "Advanced methodology for improving testing efficiency in a single-cylinder research Diesel engine". *Experimental Techniques, doi: 10.1111/j.1747-1567.2007.00296.x*, 2007.

[14] Novella R. *Influencia de los ciclos Atkinson y Miller sobre el proceso de combustión y las emisiones contaminantes en un motor Diesel.* Doctoral Thesis, Universidad Politécnica de Valencia, Departamento de Máquinas y Motores Térmicos, 2009.

[15] Armas O. *Diagnóstico experimental del proceso de combustión en motores Diesel de inyección directa.* Doctoral Thesis, Universidad Politécnica de Valencia, Departamento de Máquinas y Motores Térmicos, 2005.

[16] Martín J. *Aportación al diagnóstico de la combustión en motores Diesel de inyección directa.* Doctoral Thesis, Universidad Politécnica de Valencia, Departamento de Máquinas y Motores Térmicos, 2007.

[17] Lapuerta M., Ballesteros R. and Agudelo J. R. "Effect of the gas state equation on the thermodynamic diagnostic of diesel combustion". *Applied Thermal Engineering*, Vol. 26 n^o 14-15, pp. 1492–1499, 2006.

[18] Woschni G. "A universally applicable equation for the instantaneous heat transfer coefficient in the internal combustion engines". *SAE Paper 670931*, 1967.

[19] Torregrosa A. J., Olmeda P., Degraeuwe B. and Reyes M. "A concise wall temperature model for DI Diesel engines". *Applied Thermal Engineering*, Vol. 26 n^o 11-12, pp. 1320–1327, 2006.

[20] Payri F., Olmeda P., Martín J. and García A. "A complete 0D thermodynamic predictive model for direct injection diesel engines". *Applied Energy*, Vol. 88 n^o 12, pp. 4632–4641, 2011.

[21] Monsalve J. *Dual-Fuel Compression ignition: Towards clean, highly efficient combustion*. Doctoral Thesis, Universidad Politécnica de Valencia, Departamento de Máquinas y Motores Térmicos, 2016.

[22] de Lima D. *Analysis of combustion concepts in a poppet valve two-stroke downsized compression ignition engine designed for passenger car applications*. Doctoral Thesis, Universidad Politécnica de Valencia, Departamento de Máquinas y Motores Térmicos, 2016.

[23] Galindo J., Serrano J. R., Arnau F. J. and Piqueras P. "Description and analysis of a one-dimensional gas-dynamic model with independent time discretization". *Proceedings of the ASME Internal Combustion Engine Division 2008 Spring Technical Conference*, 2008.

[24] Gamma Technologies INC. *GT Suite Flow theory manual Version 7.5*. Gamma Technologies, Inc., 2014.

[25] Fjällman J. *GT-Power Report*. KTH Mechanics., 2014.

[26] SIEMENS Corp. *Release notes Star-CD 4.26*. SIEMENS,Corp., 2016.

[27] Chan T. L. and Cheng X. B. "Numerical Modeling and Experimental Study of Combustion and Soot Formation in a Direct Injection Diesel Engine". *Energy & Fuels*, Vol. 21 n^o 3, pp. 1483–1492, 2007.

[28] Zheng Z. and Yao M. "Mechanism of Oxygen Concentration Effects on Combustion Process and Emissions of Diesel Engine". *Energy & Fuels*, Vol. 23 n^o 12, pp. 5835–5845, 2009.

[29] Briani M., Fraioli V., Migliaccio M., Di Blasio G., Lucchini T. and Ettorre D. "Multi-Dimensional Modeling of Combustion in Compression Ignition Engines Operating with Variable Charge Premixing Levels". *SAE Technical Paper-*, 2011. 2011-24-0027.

[30] Subramanian G., Vervisch L. and Ravet F. "New Developments in Turbulent Combustion Modeling for Engine Design ECFM-CLEH Combustion Submodel". *SAE International*, 2007. 2007-01-0154.

[31] Abouri D., Zellat M., Duranti S. and Ravet F. "Advances in combustion modeling in Star-CD:Validation of ECFM CLE-H model to engine analysis". *SAE International*, 2008.

[32] Vervisch P.E., Colin O., Michel J.B. and Darabiha N. "NO Relaxation Approach (NORA) to predict thermal NO in combustion chambers". *Combustion and Flame*, Vol. 158 n^o 8, pp. 1480–1490, 2011.

[33] Marchal C. *Soot formation and oxidation modelling in an automotive engine*. Doctoral Thesis, Université d'Orléans, year = 2008.

[34] Huh KY. and Gosman AD. "A phenomenological model of diesel spray atomization.". *Proceedings of the international conference on multiphase flows*, 1991.

[35] Reitz R.D. and Diwakar R. "Structure of High-Pressure Fuel Sprays". *SAE International*, 1987. 870598.

[36] Habchi C., Lafossas F. A., Béard P. and Broseta D. "Formulation of a One-Component Fuel Lumping Model to Assess the Effects of Fuel Thermodynamic Properties on Internal Combustion Engine Mixture Preparation and Combustion". *SAE International*, 2004. 2004-01-1996.

[37] Yakhot V. and Orszag S. A. "Renormalization group analysis of turbulence. I. Basic theory". *Journal of Scientific Computing*, Vol. 1 n^o 1, pp. 3–51, 1986.

[38] Angelberger C., Poinsot T. and Delhay B. "Improving Near Wall Combustion and Wall Heat Transfer Modeling in SI Engine Computations". *SAE International*, 1997. 972881.

[39] Issa R. I. "Solution of the implicitly discretised fluid flow equations by operator-splitting". *Journal of Computational Physics*, Vol. 62 n^o 1, pp. 40–65, 1986.

[40] Hernández Vera I. *Soot modeling in flames and Large-Eddy Simulations of thermo-acoustic instabilities*. 2011.

Chapter 4

Strategies focused on injection-combustion process

Contents

4.1 Introduction

Electronically controlled fuel injection system technologically called common rail described in 3.2.1.1 allows controlling multiple injection strategies such as: control of injection timing, pilot injection, post injection and injection pressure. Dealing with this flexibility raise the challenge to manage with all this parameters in the design and calibration process of the combustion system in the heavy duty CI engines. Added to the geometrical configuration of the combustion chamber, this injection parameters bring the opportunity to optimize the combustion system achieving really low levels on emissions and improvements on engine efficiency hence in a framework of restrictive legislation for emerging markets optimizing this injection variables is an interesting cost-effective measure to control pollutants keeping the legislation levels.

4.2 The injection parameters exploration

In this section two approaches to deal with the injection parameters are explored: In one hand the study of the injection pressure, the start of main injection, the Dwell and the Post quantity (parameters defined in Fig. 3.11) through the 3D CFD model configured and validated in section 3.3.4 an approach similar than performed by Shy et al. [1]. or Khoobbakht et al. [2]. In the other hand the experimental exploration of these strategies using the multicylinder CI engine and the described test cell facility in section 3.2.2 applying parametrical tests over a group of engine operating conditions selected according to the emission legislation discussed in chapter 3.

4.2.1 The injection parameters study CFD approach

The first activity in this subsection was to select between all the operating conditions the highest in terms of mechanical requirements of the engine. A medium speed full load, as well as high speed full load (A100 and B100 respectively) were the selected operating conditions as could be observed on Fig. 4.1. Both conditions are included in the regulations then there is a double interest in simulate the strategies in these points.

Later, after the definition of the interest operating conditions it must be identified their injection settings determined as the standard settings in the Table 4.1 for A100 engine point and 4.2 for the B100 one. The main start of injection angle, the Dwell between Main and Post injection, the Post

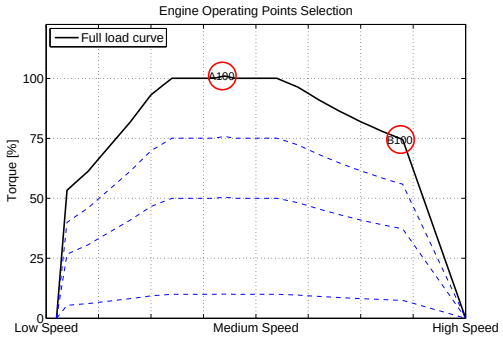

Figure 4.1: Engine operating conditions for CFD simulations

quantity and the injection pressure are all the injection parameters identified and studied for these operating conditions.

In order to deal with all the injection parameters through the 3D CFD simulation approach, the study comprises the definition of the injection parameters relation helped by a design of experiments methodology DoE as studied by Beatrice et al. [3] or Taghavifar et al. [4]. In this case, a response surface method (central composite design) was selected to determine the combination of each factor for each the 3D CFD simulation. These kind of strategies are widely used by researchers in order to define the relation of the parameters as the work performed by Reitz et al. [5] or Shi et al. [6]. In Tables 4.1 and 4.2 could be observed a row dedicated to the maximum and minimum range of each factor as well as the number of intermediary levels of each factor defined trough α.

	NoI [-]	Main SoI [CAD]	Dwell [CAD]	Post Qty [mg/cc]	IP [bar]
standard	3	359	5.5	19	500
min	3	356	4.5	14.6	400
max	3	362	6.5	22.6	800
α		2	2	2	2

Table 4.1: A100 DoE: Injection settings factors and ranges

In a central composite design of 4 factors and α=2 there are 5 levels of each factor. From DoE theory for this kind of experiments a totally of 25 tests (in this case simulations combining the parameters) are comprised to statistically reproduce the entrance parameters relation and its influence in the selected engine outputs. In the section appendix 4.A, a detailed explanation of the DoE methodology under central composite design is described.

	NoI [-]	Main SoI [CAD]	Dwell [CAD]	Post Qty [mg/cc]	IP [bar]
standard	2	356.5	12	4.9	820
min	2	353.5	13.6	2.4	600
max	2	359.5	7.6	7.3	1400
α		2	2	2	2

Table 4.2: B100 DoE: Injection settings factors and ranges

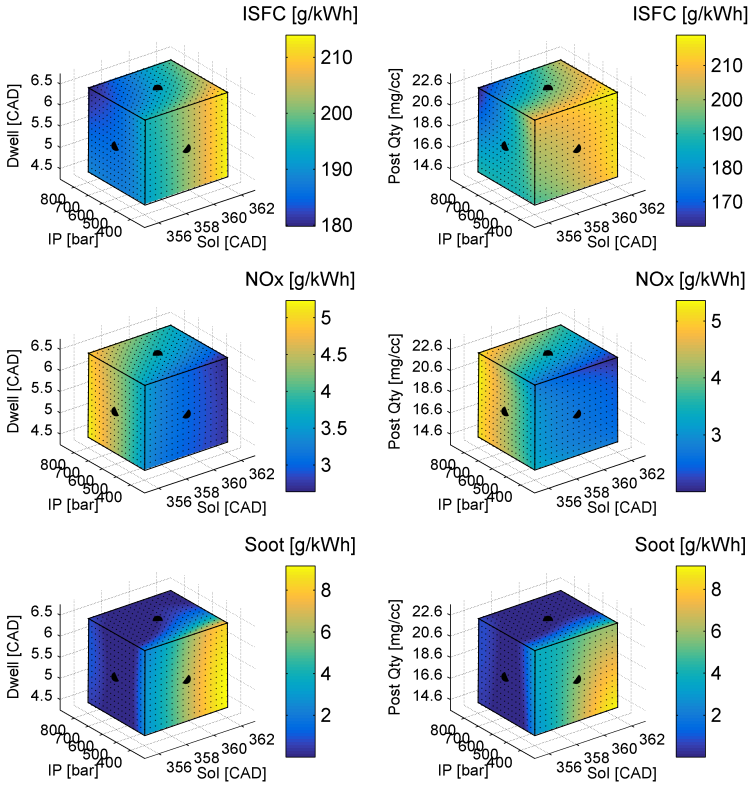

Figure 4.2: A100 injection settings exploration CFD results

The results of the injection settings study could be observed in Figs. 4.2 and 4.3. The figures depict each DoEs variable as an axis in the 3D cubes grouped in next structure: in the left column the SoI, IP and Dwell are compared while in the right one the SoI, IP are related with the Post Qty. The colormap of each cube face traces the evolution of the studied engine output (ISFC, NO_x and soot) regulated in modern Diesel engines [7] and it is a very effective way

to understand the DoE parameters interactions and their influence in each engine output.

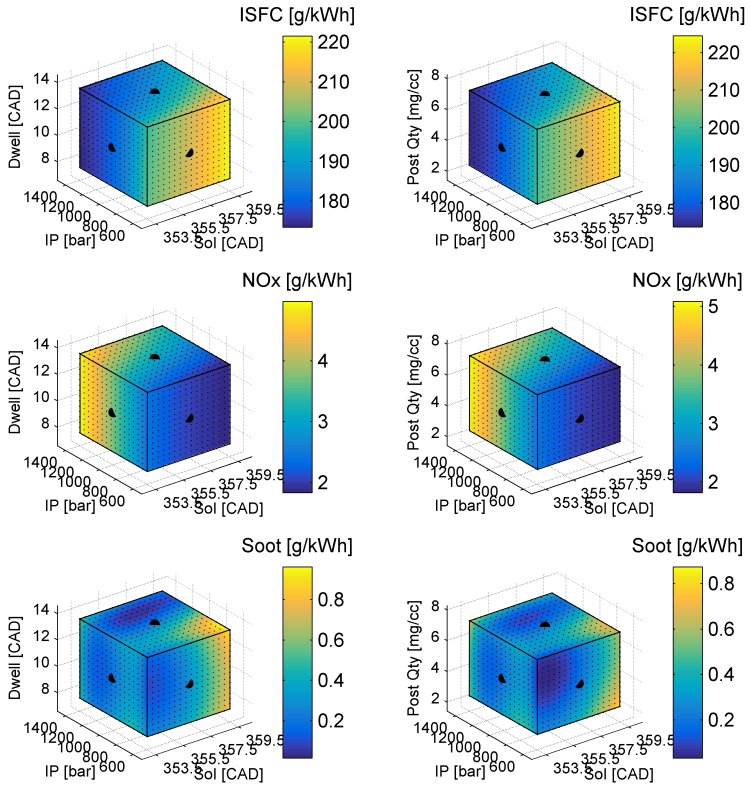

Figure 4.3: B100 injection settings exploration CFD results

In both evaluated engine operating conditions (A100 and B100) the results observed in Figs. 4.2 and 4.3 show that the SoI advance and the IP increase combination leads to decreasing the ISFC with an increment of NO_x emission causing the well known trade off relation between these two engine outputs. In terms of the Dwell and the Post quantity there is not impact neither on the ISFC or NO_x in the simulated ranges. The Post quantity which is one parameter mainly defined to help to increase the soot oxidation at the end of combustion shows a slight influence in medium speed A100 operating condition a trend which is lost when passing to high speed B100 point.

4.2.1.1 Simplification of the main factors to be experimentally tested

After identifying the engine outputs main trends observed in the evaluated ranges for each DoE factor, another big utility of the DoE methodology is the simplification of factors based on their interactions and influence in each output. In order to simplify the number of entrance variable in the experimental activity a Pareto diagram must be constructed per each operating conditions studied through the 3D CFD model. Figs. 4.4 and 4.5 depicts the statistical effect of each factor in each engine output based on the coefficients of each factor or factor interaction allowing in this way to discard the lowest effects factors.

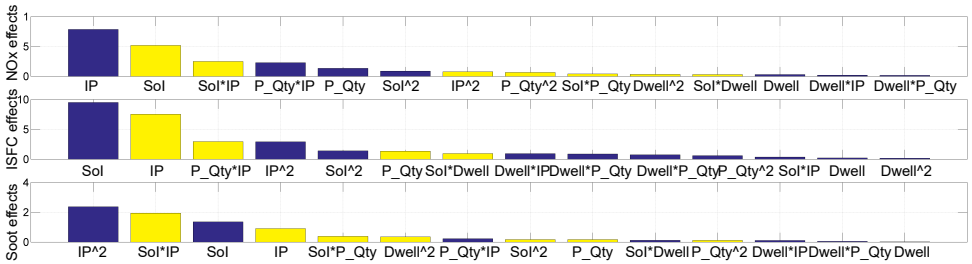

Figure 4.4: A100 factor effects in the engine outputs

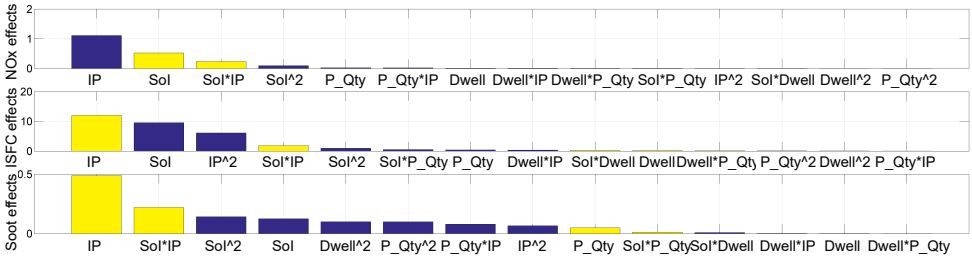

Figure 4.5: B100 factor effects in the engine outputs

In a multi-injection strategy as the currently studied, it is not always evident to identify the effects of each injection parameter for its simplification hence the used DoE methodology is a very powerful tool in order to optimize the test campaign. As could be noticed in Figs. 4.4 and 4.5 in both Pareto diagrams, all the effects were placed in the positive side in order to identify in a better way the predominant factors over the others and their interactions, but the negative effects are identified as yellow bars. The SoI and the IP placed in the left side of the diagram are the main factors affecting directly the NO_x, ISFC and soot emission in both engine conditions A100 and B100,

then for the experimental section 4.2.2 both factors will be deeper analyzed using a classic parametric testing approach.

4.2.2 Experimental study of the SOI and the IP

With the conclusions obtained in the section of 3D CFD simulations, several parametric studies are proposed in this subsection in order to identify a set of injection parameters which optimize the NO_x, the BSFC and the soot emission over all the engine conditions defined in the actual regulation. A total of 7 engine operating conditions are included in the standard procedure and the test matrix of each one is described in Table 4.3. These kind of parametric studies are widely used in the engine research as the works performed by Nabi et al. [8]. or Benajes et al. [9].

	IP [bar]	SoI (Main) [CAD]	Dwell [CAD]	Post Qty [mg/cc]
A100	**500**-600-700	351-353-355-357-**359**-361-363	5.5	19
A75	**375**-475-575	353-355-357-359-**361**-363-365	5.5	19
A50	**340**-440-540	354-356-358-360-**362**-364-366	11	4.6
B100	**820**-920-1020	348.5-350.5-352.5-354.5-**356.5**-358.5-360.5	12	4.9
B75	**690**-790-890	353.5-355.5-357.5-359.5-**361.5**-363.5-365.5	12	19
B50	**580**-680-780	354-356-358-360-**362**-364-366	12	10
B10	**600**-700-800	350-352-354-356-**358**-360-362	12	10

Table 4.3: Injection settings of the parametric experimental study

The experimental results are classified by engine speed grouping the medium speed (A points) and the rated engine speed (B Points) separately in each subsection. The main discussed results in the section are the pollutants (NO_x and soot) and the engine efficiency (BSFC) as a function of the injection pressure and the start of injection and the standard reference point in each map is identified by a yellow circle.

4.2.2.1 Study in the medium engine speed

The engine test carried out over the medium speed engine conditions (A points) are composed of 21 points which set a grid generated from the combination of the injection pressure and the SoI.

In the case of A50 engine point, the results observed on Fig. 4.6 keeps the trade-off relation between the BSFC and the NO_x emission, as it was observed

through the CFD simulations, but in terms of soot there is an interesting behavior which brakes the trade-off expected after the CFD simulations between the NO_x and the soot. In this case for the earliest SoI there is high soot in a relatively zone of high NO_x as could be noticed in the Fig. 4.6 which could lead to a simultaneously reduction of both emissions. The evaluated ranges for the injection pressure and start of injection combination set 3 possible scenarios for the choosen engine outputs:

- Best efficiency scenario: Reduction of 16% in BSFC and 28% in soot with an associated increase of 128% in NO_x.
- Best NO_x scenario: Reduction of 8% in NO_x with an associated increase of 8% in BSFC and 4% in soot.
- Best soot scenario: Reduction of 84% in soot and 4% in BSFC with an associated increase of 39% in NO_x.

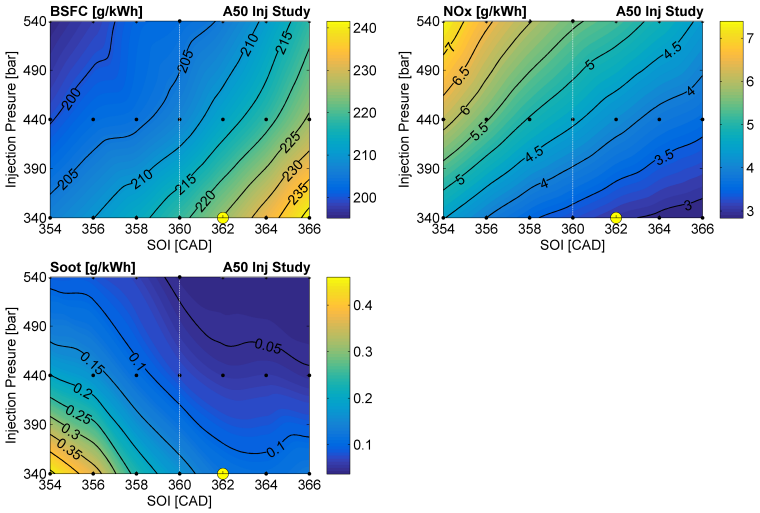

Figure 4.6: A50 injection experimental parametric study

In the case of A75 engine point, the results observed on Fig. 4.7 do not only keep the trade-off relation between the BSFC and the NO_x emission as described by Benajes et al. [10], but in terms of soot the interesting behavior breaking the NO_x-soot trade-off observed in the A50 engine condition is preserved when evaulating the SoI dependency. In the same way than previous depicted for A50 engine conditions the evaluated ranges for the injection pressure and start of injection combination set 3 possible scenarios for the chosen engine outputs:

- Best efficiency scenario: Reduction of 15% in BSFC with an associated increase of 145% in NO_x and 12% in soot.
- Best NO_x scenario: Reduction of 16% in NO_x with an associated increase of 8% in BSFC and 7% in soot.
- Best soot scenario: Reduction of 82% in soot and 3% in BSFC with an associated increase of 46% in NO_x.

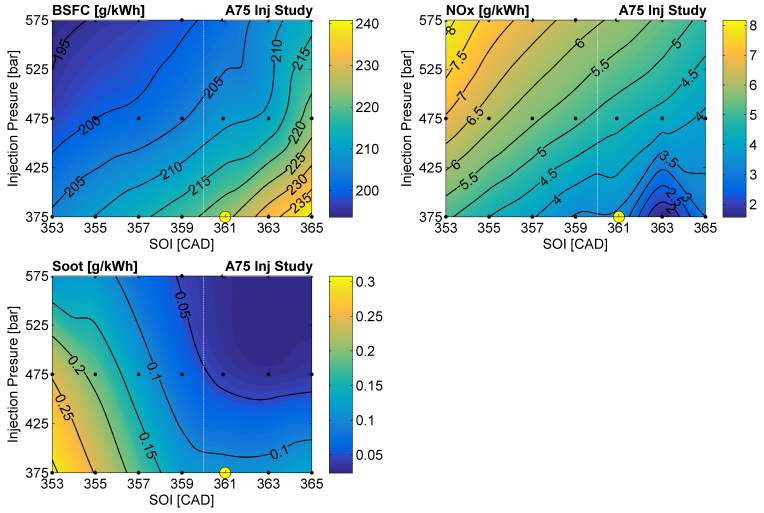

Figure 4.7: A75 injection experimental parametric study

Centering now in the full load A100 engine point, the results observed on Fig. 4.8 preserves the trade-off relation between the BSFC and the NO_x emission as expected, but in terms of soot the interesting relation is confirmed when evaluating the SoI dependency, it continues breaking the NO_x-soot trade-off identified through the CFD simulations as observed in previous partial load engine conditions. The 3 possible scenarios for the chosen engine outputs in the A100 engine condition are:

- Best efficiency scenario: Reduction of 9% in BSFC with an associated increase of 92% in NO_x and 33% in soot.
- Best NO_x scenario: Reduction of 8% in NO_x with an associated increase of 9% in BSFC and 3% in soot.
- Best soot scenario: Reduction of 67% in soot and 3% in BSFC with an associated increase of 38% in NO_x.

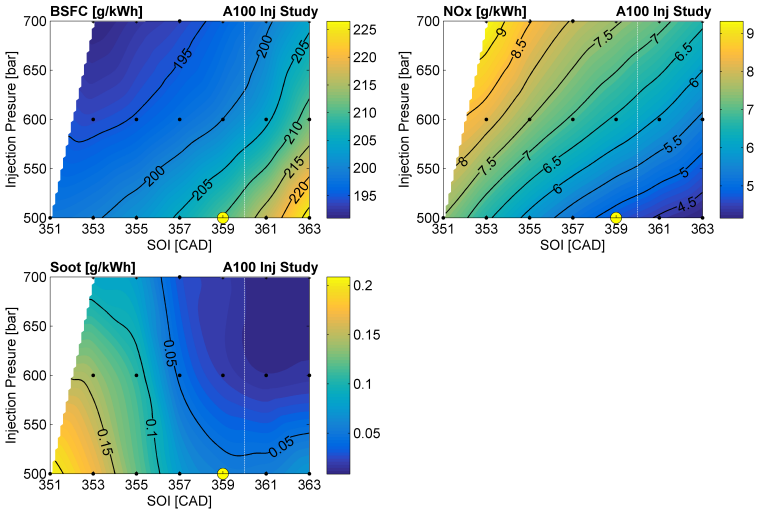

Figure 4.8: A100 injection experimental parametric study

4.2.2.2 Study in the high engine speed

In the same way than the engine test carried out over the medium speed engine conditions (A points) the rated speed study is composed of 21 points which set a grid generated from the combination of the injection pressure and the SoI. The structure of the shown results is equal than medium speed points defining per each engine operating conditions 3 possible scenarios from each engine output optimization.

Beginning with the lowest load point, the B10 engine point, the results observed on Fig. 4.9 keep the trade-off relation between the BSFC and the NO_x emission, but in terms of soot, the behavior where NO_x-soot trade-off is broken observed in the medium speed points, for the SoI is preserved. In the same way than previous depicted engine conditions the evaluated ranges optimization could lead to 3 possible scenarios for the chosen engine outputs:

- Best efficiency scenario: Reduction of 10% in BSFC with an associated increase of 116% in NO_x and 68% in soot.
- Best NO_x scenario: Reduction of 7% in NO_x and 53% in soot with an associated increase of 6% in BSFC.
- Best soot scenario: Reduction of 76% in soot keeping the BSFC with an associated increase of 10% in NO_x.

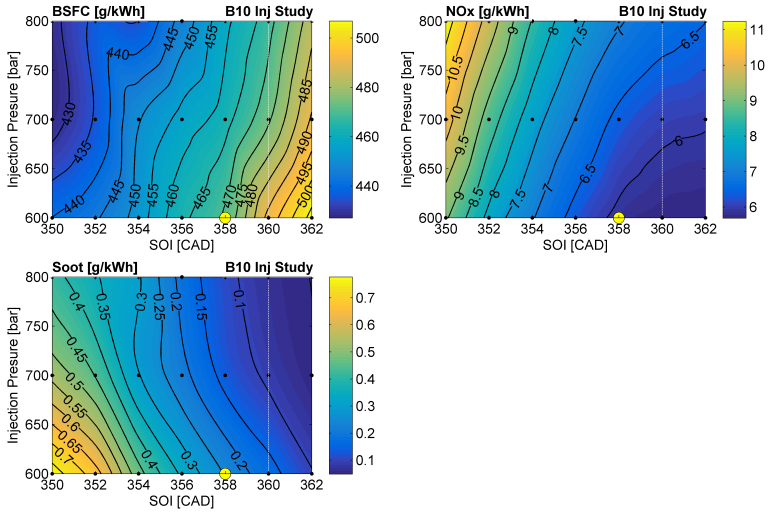

Figure 4.9: B10 injection experimental parametric study

In the case of B50 engine point, the results observed on Fig. 4.10 do not only keep the trade-off relation between the BSFC and the NO_x emission as expected, but in terms of soot the interesting behavior breaking the NO_x-soot trade-off observed in all the previous engine operating condition begins to disappear leading to the traditional behavior of these to engine emissions observed trough the CFD simulation and discussed by Yadav et al. [11]. The possible scenarios for the evaluated ranges in this engine condition are:

- Best efficiency scenario: Reduction of 17% in BSFC and 63% in soot with an associated increase of 88% in NO_x.
- Best NO_x scenario: Reduction of 15% in NO_x with an associated increase of 11% in BSFC and 31% in soot.
- Best soot scenario: Reduction of 69% in soot and 1% BSFC with an associated increase of 9% in NO_x.

Evaluating now the B75 engine point, the results observed on Fig. 4.11 maintains the trade-off relation between the BSFC and the NO_x emission as expected, but in terms of soot the NO_x-soot trade-off is recovered for the start of injection dependency leading to high soot emission when the NO_x emission is lower. The 3 possible scenarios for the evaluated engine condition with the studied parameters combination are:

- Best efficiency scenario: Reduction of 18% in BSFC and 45% in soot with an associated increase of 109% in NO_x.

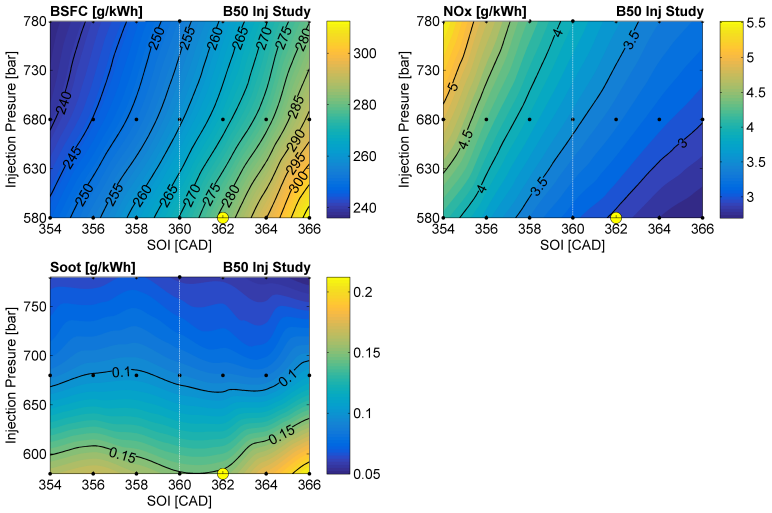

Figure 4.10: B50 injection experimental parametric study

- Best NO_x scenario: Reduction of 4% in NO_x with an associated increase of 10% in BSFC and 64% in soot.
- Best soot scenario: Reduction of 64% in soot and 1% BSFC with an associated increase of 9% in NO_x.

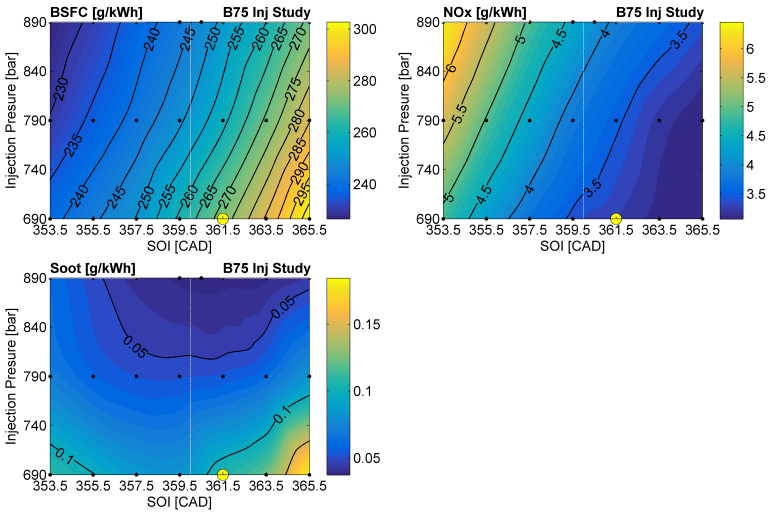

Figure 4.11: B75 injection experimental parametric study

In order to end with the experimental approach the full load B100 engine point is evaluated. As could be observed on Fig. 4.12, B100 operating condition

preserves the trade-off relation between the BSFC and the NO_x emission a trend expected which is maintained along all the tested engine conditions an parameters combination. In terms of soot the NO_x-soot trade-off the same trend recovered in B75 engine condition is confirmed. With the evaluated ranges for the injection pressure and start of injection combination the 3 possible scenarios for the chosen engine outputs are:

- Best efficiency scenario: Reduction of 13% in BSFC and 67% in soot with an associated increase of 150% in NO_x.
- Best NO_x scenario: Reduction of 9% in NO_x with an associated increase of 3% in BSFC and 25% in soot .
- Best soot scenario: Reduction of 67% in soot and 13% the BSFC with an associated increase of 25% in NO_x.

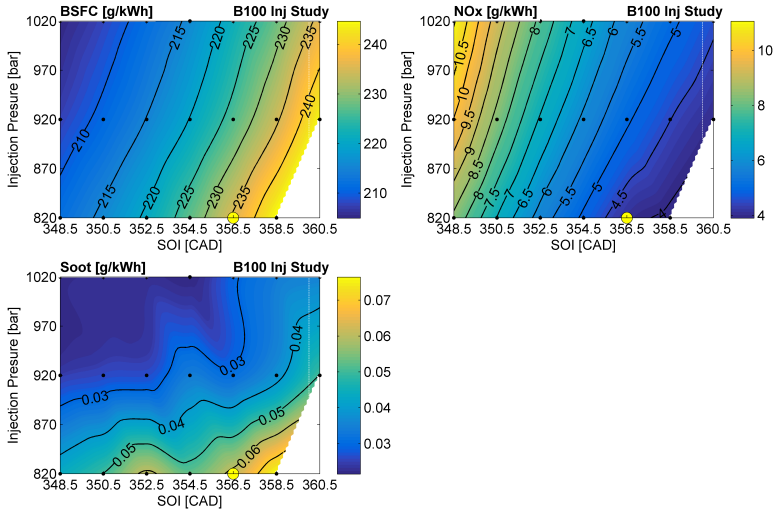

Figure 4.12: B100 injection experimental parametric study

A complete summary of all scenarios observed for each tested operating condition could be observed in Table 4.4. In this table there are 3 group of columns each group per scenario (the best NO_x, the best soot and the best BSFC) and the percentage of reduction or increase is highlighted by the green or red color respectively. As the combination of parameters is not equal per each operating conditions a set of ideas are summarized to conclude with the parametric experimental study.

- The best NO_x scenario was found in the lowest injection pressure combined with delayed SoI for all tested operating conditions.

Operating	Best NO_x [%]			Best Soot [%]			Best BSFC [%]		
Condition	NO_x	Soot	BSFC	Soot	BSFC	NO_x	BSFC	NO_x	Soot
A50	-8	4	8	-84	-4	39	-16	128	-28
A75	-16	7	8	-82	-3	46	-15	145	12
A100	-8	3	9	-67	-3	38	-9	92	33
B10	-7	-52	6	-76	-1	10	-10	88	68
B50	-15	31	11	-69	-1	11	-17	88	-63
B75	-4	62	10	-64	-1	9	-18	109	-45
B100	-9	25	3	-67	-13	25	-13	150	-67

Table 4.4: Summary of scenarios under IP-SoI strategies All Operating conditions

- The best BSFC scenario was found in the highest injection pressure combined with the early SoI for all tested operating conditions.
- The best soot scenario was found always in the highest injection pressure but in this case from medium speed engine conditions until B10 the minimum soot was found in the delayed SoI but for B50, B75 and B100 it moves to earliest SoI.

4.3 The combustion hardware matching

After experimental study in section 4.2.2, the 3D CFD model configured for injection parameters exploration could be double checked and how is the case, it serves to virtually explore the advantages of the combustion hardware matching as a cost-effective pollutant control strategy. In first instance, the selection of B100 operating engine conditions (Full power) was defined as the center of the study due its implication in terms of mechanical and thermal constraints, then the first short discussion of the double calibration process is done comparing the experimental results with the injection DoE results. The next subsection is the combustion hardware study where a set of geometrical parameters are studied through the 3D CFD model with a similar DoE methodology than used in the section 4.2.1.

4.3.1 Double calibration of the 3D CFD model

In first instance, the experimental parametric test studied in section 4.2 serve to double check the injection parameters CFD simulations comparing the

injection DoE factors combination with the parametric test matrix. In this case the results after the initial calibration could be completed and considered like a second calibration with the objective to give robustness to the CFD model which is used to simulate the different hardware configuration in this section 4.3.

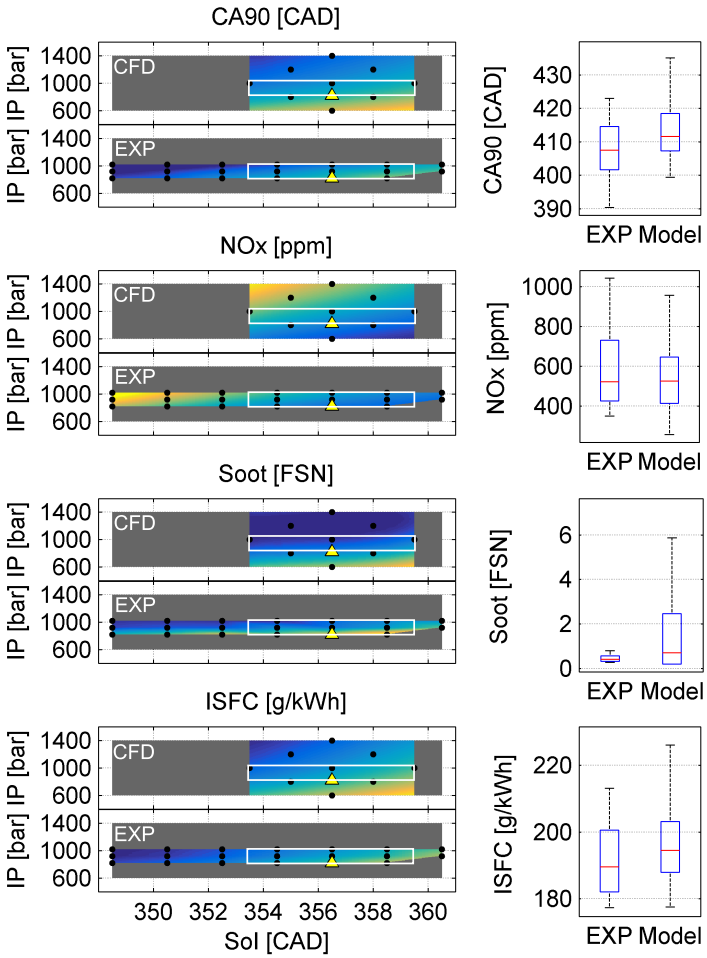

Figure 4.13: B100 Comparison 3D-CFD simulations and experimental study

As observed in Fig. 4.13. While the CFD DoEs exploration is wider in IP, the parametric study focuses on the SoI and its effects in the four engine outputs. In spite of the different parameter target exploration there is a common area in the study zone for both variables which is identified with a white rectangle at each figure. as previously described The Dwell and Post Quantity, variables studied by CFD DoEs are not considered in the parametric

tests due to negligible affectation detected through the 3D CFD simulation and DoE methodology then in this case the Dwell and Post quantity were fixed in the standard reference values.

For the B100 operating engine conditions Fig. 4.13 shows that CFD DoEs results are consistent with obtained experimental results. All the trends are well described by the model and the numerical output for three of four selected variables (CA90, NO_x and ISFC) are in the same ranges. Only in case of the soot ranges the differences detected in the first calibration process described in section 3.3.4 are preserved thus the model continues with the soot emission overestimation.

4.3.2 Combustion hardware 3D CFD simulations

The same DoE technique and the response surface method coupled with the CFD model serve to explore the engine performance and emissions under four parameters related with the combustion hardware a methodological approach which is applied by Benajes et al. [12]. The study of the combustion chamber geometry and its components is performed changing different geometrical parameters of the piston and nozzle configuration as shown Fig. 4.14. In this case two parameters related to the piston bowl shape as diameter (d/B) and re-entrant profile (S), the injection hardware (nozzle included angle (NA)) and the air path movement (Swirl number) are the input parameters of the DoE.

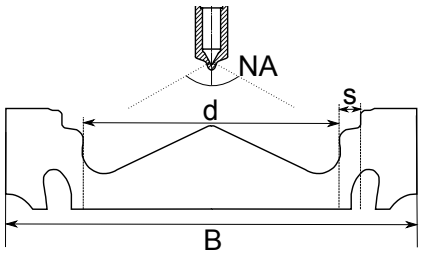

Figure 4.14: Geometry parameters in the DoE definition

It must be defined the standard geometrical parameters in the same way than the nozzle angle and the swirl number. These reference values are described in Table 4.5. After definition of standard parameters the hardware DoE is defined as a central composite design of 4 factors and α=2 same kind of DoE than previous discussed with the injection settings in section 4.2.1. There are 5 levels of each factor and the maximum an minimum ranges could be identified in the same table.

	d/B	S	NA	SN
	[-]	[mm]	[deg]	[-]
Reference	0.62	2.86	150	1.4
min	0.57	0	144	0.6
max	0.67	5.72	156	2.2
α	2	2	2	2

Table 4.5: B100 DoE: Combustion geometry factors and ranges

The DoE results could be observed in Fig. 4.15 which is divided in two columns (same structure of the injection settings DoE): the left column shows the effects of bowl geometry (d/B and S) and nozzle included angle (NA) and the right one the effects of bowl geometry (d/B and S) and swirl number respectively. All the parameters are evaluated in the selected engine outputs: engine efficiency (ISFC) and NO_x-soot emissions.

Focusing on the observed trends, it can be seen how increasing bowl diameter (d/B) leads to slight reductions on ISFC while the impact in NO_x could be attenuated by the Nozzle angle matching a behavior matching the observed by Li et al. [13]. or Kakaee et al. [14]. Additionally, increasing the re-entrant shape of the bowl (S) is a parameter which depends of Nozzle angle because with a narrow angle it decreases ISFC and the contrary effect appears with a wider angle. In terms of soot a low re entrant shape of the bowl (S) combined with lower bowl diameter (d/B) and a wider nozzle angle is a bad matching because this geometrical configuration maximize the soot formation.

Switching to the most relevant trends observed when swirl is studied (right column in Fig. 4.15), there is a decrease of ISFC also independently from the values of the other input parameters when a high swirl number is used. A corresponding trend in NO_x appears and the trade-off behavior is observed when increasing the swirl number leads to NO_x increases independently of the other variables. In terms of soot emission the trend observed when the nozzle angle is wider is maintained as the swirl is increased a combination which leads to highest values in soot emission.

4.3.2.1 Simplification and exploration of the main factors

After the description of the engine outputs main trends observed in the evaluated ranges for each DoE factor, the simplification of factors based on their interactions is a big utility of the DoE methodology as it was done for the injection parameters in section 4.2.1. Fig. 4.16 depicts the Pareto diagram

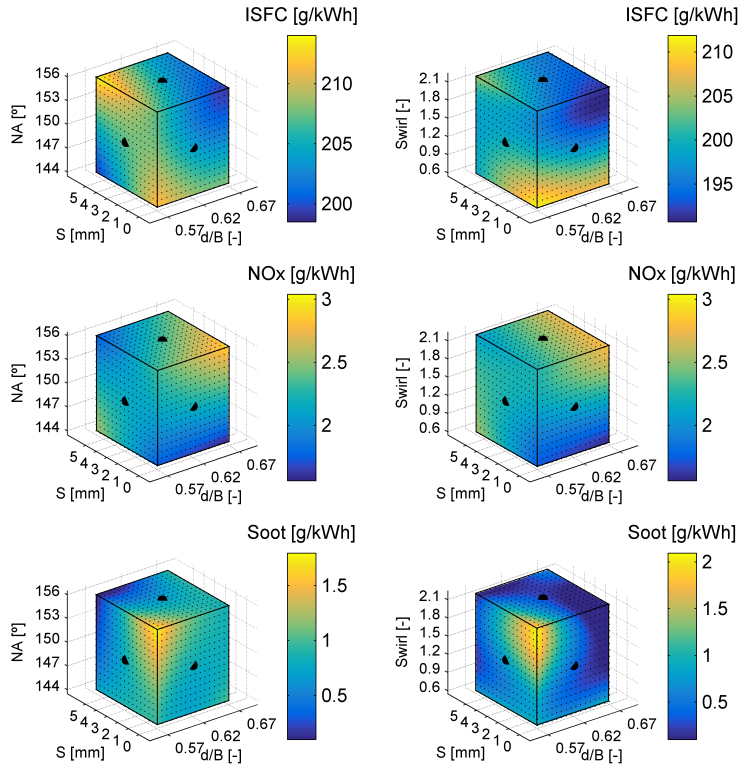

Figure 4.15: B100 3D-CFD simulation results DoE:Geometrical parameters

where the statistical effect of each factor in each engine output based on its coefficients could be defined allowing in this way to discard the lowest effects factors. In the Pareto diagram observed in Fig. 4.16 all the effects were placed in the positive side in order to identify in a better way the predominant factors over the others and their interactions, in the same plot the negative effects of the factors could be identified as yellow bars. The d/B relation and the Swirl number which are placed in the left side of the diagram are the main factors affecting directly the NO_x, ISFC, and the soot emission. The same plot give indication about the effect sense, as an example increasing in d/B relation leads to increase NO_x emission (Positive: purple bar) and at the same time it leads to reductions in soot emission (Negative: yellow bar).

Centering the analysis in d/B relation and the Swirl number factors, and keeping in mind the values definition in the configured engine described in the line reference of the Table 4.5, these factors behavior could be deeper studied as is shown in Fig. 4.17 allowing to conclude with a set of general ideas to use hardware configuration and geometry as a cost-effective control emission tool.

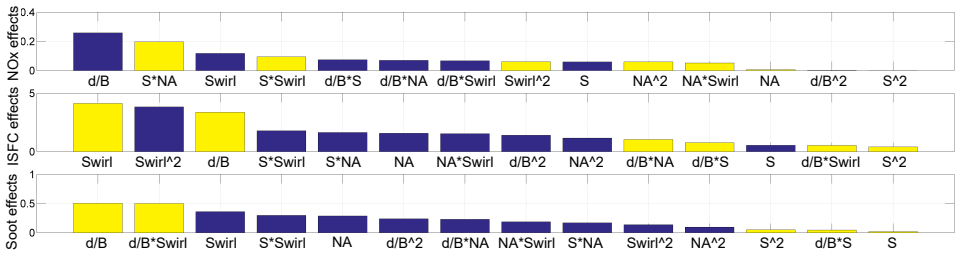

Figure 4.16: B100 geometrical factors effects in the engine outputs

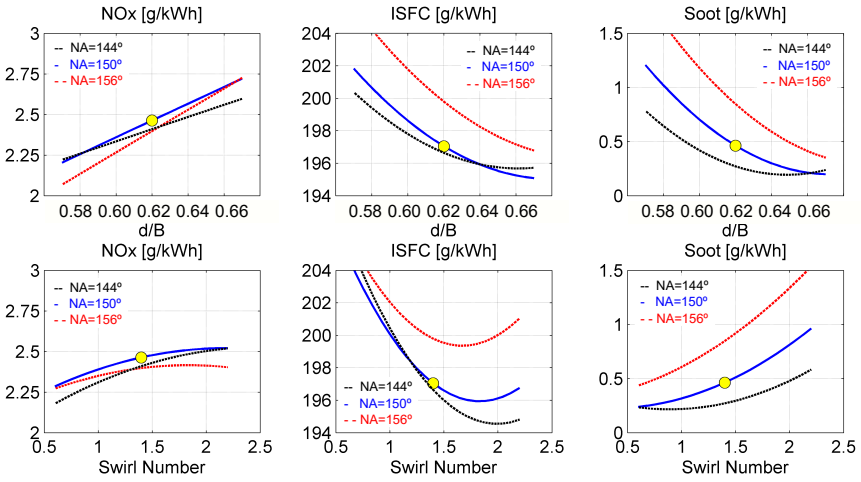

Figure 4.17: Geometrical effects comparison

In first instance for the d/B relation the main conclusions obtained through the DoE methodology in the 3D CFD simulated ranges are:

- The d/B=0.52 relation which is the current piston bowl relation is near to the optimum ISFC for the current NA, S and Swirl number as could be observed in Fig. 4.17 from where it could be establish than the geometric design was favored to keep lower ISFC knowing in advance than NO_x could be controlled by delaying the multi-injection strategy.

- In the previous described scenario keeping constant the others current engine factors (S, NA and swirl) the reduction of the d/B relation leads to reduce the NO_x emission with a consequent penalization in terms of of ISFC.

- There is not trade off relation between the ISFC and the soot emission in this case greater d/B relation leads to decrease the ISFC and soot simultaneously.

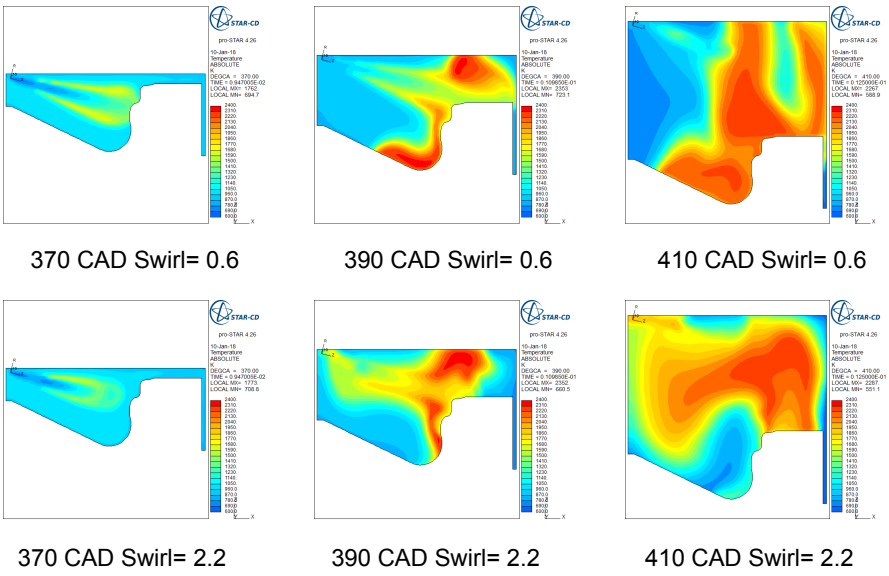

Figure 4.18: Incylinder temperature during combustion phase

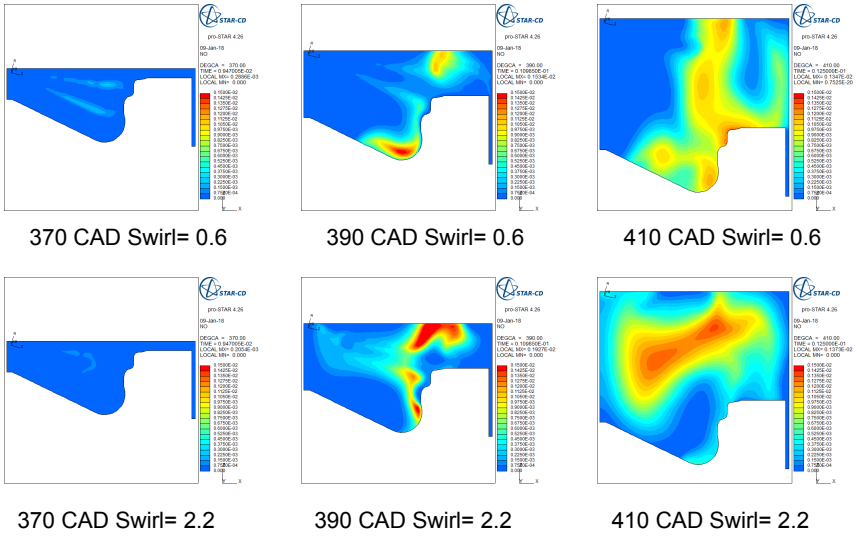

Figure 4.19: Incylinder NO_x during combustion phase

Moving the focus to the Swirl number which is a complex factor in the design process, the 3D CFD simulations bring the opportunity to analyze the pollutant formation in a detailed way describing the formation inside the combustion chamber as could be observed for NO_x Fig. 4.19. This process

could be linked with others interesting incylinder variables like the local temperature which is estimated by the model as depict in Fig. 4.18.

Figure. 4.18 shows the incylinder temperature in 3 different time steps represented as function of CAD 370, 390 and 410 which are the selected angles for the 2 limits simulated Swirl conditions. As could be identified in this figure, the local temperatures reached by a high Swirl number leads to increase the incylinder local temperature distribution. The increase of the local temperature is highly related to increase in the NO_x emission as observed in Fig. 4.19 where the highest Swirl number case is correspondent with the highest NO_x formation case as the results obtained by Li et al. [15].

After studying the Swirl behavior in the current engine configuration, the main conclusions obtained through the DoE methodology in the 3D CFD simulated ranges are:

- The Swirl number=1.5 which is the current engine Swirl is near to the optimum ISFC for the current d/B piston relation, NA and S as could be identified in Fig. 4.17. From where it could be establish than the geometric design was favored to keep lower BSFC from air motion point of view.
- As mentioned in the Pareto Diagram selection, the NA does not have a big influece in the NO_x behavior for the evaluated ranges, perhaps it recover importance when the ISFC soot emissions are evaluated.

Although the combustion hardware matching is a cost-effective pollutant control strategy with an interesting potential as previously observed, unfortunately has not been experimental validated in the thesis development due to high cost in the implementation of hardware modification for only one engine unit.

4.A Appendix: DoE: Central composite design description

The practical steps needed for planning and conducting a DoE test campaign as defined in the doctoral Thesis of De Lima Daniela [16] which in this chapter is used to explore the injection settings (injection pressure and SoI) and the combustion hardware can be summarized as follows:

- *Selection of the response variables.* This step requires choosing the group of entrance engine parameters that are going to be modeled along the DoE, with the aim of characterizing the combustion process, as well as the engine performance indicators in terms of emissions and efficiency. Particularly for this case: Injection pressure, Dwell, SoI or PostQty or bowl shape (diameter (d/B) and re-entrant profile (S)), the injection hardware (nozzle included angle (NA)) and the air path movement (Swirl number) to describe the engine performance through the engine ouputs indicators: NO_x, soot and ISFC.

- *Choice of factors and ranges.* For this investigation, the number of factors has been set to 4 to keep a relatively simple design with reasonable total number of tests as could be observed in Table 4.6. The ranges for each factor are selected based on experience gained prior to this investigation from performing fast screening tests in the engine.

- *Choice of design.* The type of DoE has to be chosen depending on the number of factors, the assumed form of the influence of a factor on a given response (i.e. linear, quadratic...), and accordingly, the number of levels chosen for the factors. For this investigation, a Central Composite Design (CCD) was selected to build the test plan, to be able to have a polynomial (second degree) mathematical model for the responses, including all possible second order interactions between the factors. The CCD is composed of 3 sequences: a test in the center of the field (at the midpoint of the range of each factor) replicated several times to estimate the variance of repeatability, an orthogonal "full-factorial" design (with 2 levels per factor) that gives the form of the model and the influence of the factors, and finally two additional "star" or axial tests on the axis of each factor at a distance α from the center of the design (selected based on criteria such as rotability) to measure the quadratic effect of the factors and their interactions. The final design gives a test plan with a total of 5 levels for each factor.

	Factor1	Factor2	Factor3	Factor4
-α	F1-α	F2-α	F3-α	F4-α
-1	F1-1	F2-1	F3-1	F4-1
REF	F1 REF	F2 REF	F3 REF	F4 REF
+1	F1+1	F2+1	F3+1	F4+1
+α	F1+α	F2+α	F3+α	F4+α

	Factor1	Factor2	Factor3	Factor4
1	F1REF	F2REF	F3REF	F4REF
2	F1-1	F2-1	F3-1	F4-1
3	F1-1	F2-1	F3-1	F4+1
4	F1-1	F2-1	F3+1	F4-1
5	F1-1	F2-1	F3+1	F4+1
6	F1-1	F2+1	F3-1	F4-1
7	F1-1	F2+1	F3-1	F4+1
8	F1-1	F2+1	F3+1	F4-1
9	F1-1	F2+1	F3+1	F4+1
10	F1+1	F2-1	F3-1	F4-1
11	F1+1	F2-1	F3-1	F4+1
12	F1+1	F2-1	F3+1	F4-1
13	F1+1	F2-1	F3+1	F4+1
14	F1+1	F2+1	F3-1	F4-1
15	F1+1	F2+1	F3-1	F4+1
16	F1+1	F2+1	F3+1	F4-1
17	F1+1	F2+1	F3+1	F4+1
18	F1+α	F2REF	F3REF	F4REF
19	F1-α	F2REF	F3REF	F4REF
20	F1REF	F2+α	F3REF	F4REF
21	F1REF	F2-α	F3REF	F4REF
22	F1REF	F2REF	F3+α	F4REF
23	F1REF	F2REF	F3-α	F4REF
24	F1REF	F2REF	F3REF	F4+α
25	F1REF	F2REF	F3REF	F4-α

Table 4.6: DoE Points Factors and levels combination

- *Test plan execution.* For the selected 4 factors, the CCD test plan gives a total of 25 points with the combination of all levels as described in Table 4.6, 16 points of the orthogonal design, 8 "star" points and the central reference point. The tests must be performed in the most rigorous way, and in a random run order, to ensure that the model meets certain statistical assumptions and also to reduce possible influence of other "noise" parameters that are not included in the study.

- *Statistical analysis.* After performing the tests, the mathematical models are built and fitted to the data measured for each response. Accordingly, different plots and statistical metrics are generated to assess the fit of the model and evaluate its predictive capability. The results from the fitted model helps to determine which terms of the model have a relevant effect over the measured response, and which terms can be neglected or excluded from the model. For this purpose Pareto diagrams are very useful allowing to simplify in a statically controlled way the fitted models identifying the main factors in the effects of engine outputs.

Bibliography

[1] Shi Y. and Reitz R. D. "Optimization study of the effects of bowl geometry, spray targeting, and swirl ratio for a heavy-duty diesel engine operated at low and high load". *International Journal of Engine Research*, Vol. 9 n^o 4, pp. 325–346, 2008.

[2] Khoobbakht G., Najafi G., Karimi M. and Akram A. "Optimization of operating factors and blended levels of diesel, biodiesel and ethanol fuels to minimize exhaust emissions of diesel engine using response surface methodology". *Applied Thermal Engineering*, Vol. 99, pp. 1006–1017, 2016.

[3] Beatrice C., Napolitano P. and Guido C. "Injection parameter optimization by DoE of a light-duty diesel engine fed by Bio-ethanol/RME/diesel blend". *Applied Energy*, Vol. 113, pp. 373–384, 2014.

[4] Taghavifar H., Jafarmadar S., Taghavifar H. and Navid A. "Application of DoE evaluation to introduce the optimum injection strategy-chamber geometry of diesel engine using surrogate epsilon-SVR". *Applied Thermal Engineering*, Vol. 106, pp. 56–66, 2016.

[5] Reitz R. D. and Ehe J. "Use of in-cylinder pressure measurement and the response surface method for combustion feedback control in a diesel engine". *Proceedings of the Institution of Mechanical Engineers, Part D: Journal of Automobile Engineering*, Vol. 220 n^o 11, pp. 1657–1666, 2006.

[6] Shi Y. and Reitz R. D. "Assessment of Optimization Methodologies to Study the Effects of Bowl Geometry, Spray Targeting and Swirl Ratio for a Heavy-Duty Diesel Engine Operated at High-Load". *SAE International Journal of Engines*, Vol. 1 n^o 1, pp. 537–557, 2008.

[7] Cocker D. R., Shah S. D., Johnson K., Miller J. W. and Norbeck J. M. "Development and Application of a Mobile Laboratory for Measuring Emissions from Diesel Engines. 1. Regulated Gaseous Emissions". *Environmental Science & Technology*, Vol. 38 n^o 7, pp. 2182–2189, 2004.

[8] Nabi Md. N., Zare A., Hossain F. M., Bodisco T. A., Ristovski Z. D. and Brown R. J. "A parametric study on engine performance and emissions with neat diesel and diesel-butanol blends in the 13-Mode European Stationary Cycle". *Energy Conversion and Management*, Vol. 148, pp. 251–259, 2017.

[9] Benajes J., Molina S., Novella R. and Belarte E. "Evaluation of massive exhaust gas recirculation and Miller cycle strategies for mixing-controlled low temperature combustion in a heavy duty diesel engine". *Energy*, Vol. 71, pp. 355–366, 2014.

[10] Benajes J., Molina S., Novella R., Amorim R., Hamouda H. B. H. and Hardy J. P. "Comparison of two injection systems in an HSDI diesel engine using split injection and different injector nozzles". *International Journal of Automotive Technology*, Vol. 11 n^o 2, pp. 139–146, 2010.

[11] Yadav J. and Ramesh A. "Injection strategies for reducing smoke and improving the performance of a butanol-diesel common rail dual fuel engine". *Applied Energy*, Vol. 212, pp. 1–12, 2018.

[12] Benajes J., Novella R., Pastor J. M., Hernández-López A., Hasegawa M., Tsuji N., Emi M., Uehara I., Martorell J. and Alonso M. "Optimization of the combustion system of a medium duty direct injection diesel engine by combining CFD modeling with experimental validation". *Energy Conversion and Management*, Vol. 110, pp. 212–229, 2016.

[13] Li J., Yang W. M., An H., Maghbouli A. and Chou S. K. "Effects of piston bowl geometry on combustion and emission characteristics of biodiesel fueled diesel engines". *Fuel*, Vol. 120, pp. 66–73, 2014.

[14] Kakaee A. H., Nasiri-Toosi A., Partovi B. and Paykani A. "Effects of piston bowl geometry on combustion and emissions characteristics of a natural gas/diesel RCCI engine". *Applied Thermal Engineering*, Vol. 102, pp. 1462–1472, 2016.

[15] Li X., Qiao Z., Su L., Li X. and Liu F. "The combustion and emission characteristics of a multi-swirl combustion system in a DI diesel engine". *Applied Thermal Engineering*, Vol. 115, pp. 1203–1212, 2017.

[16] de Lima D. *Analysis of combustion concepts in a poppet valve two-stroke downsized compression ignition engine designed for passenger car applications.* Doctoral Thesis, Universidad Politécnica de Valencia, Departamento de Máquinas y Motores Térmicos, 2016.

Chapter 5

Strategies focused on air management

Contents

5.1 Introduction

In this chapter are evaluated the strategies related with the engine air management proposed in the chapter 2. In the first section is developed the procedure to select the engine hardware between a group of candidates using the 1D simulation tool GT Power. Through 1D engine model configured and validated in section 3.3.3 coupled with the air management maps, different options are evaluated for each strategy defining one profile per strategy to be finally machining and tested. Later in the second section, the experimental validation of each chosen Miller or iEGR cam profile over a group of engine operating conditions, classified by part load or full load, help to define the main characteristics of each camshaft as well that all the particularities in the combustion process and engine emissions as discussed in the research done by Bermúdez et al. [1]. Finally in third section all the legislation point are tested and compared with standard reference results showing the real potential of these cost-effective control emission strategies.

5.2 Camshaft strategies simulation and selection

In the current section is discussed the procedure performed to select one camshaft profile per strategy (Miller or iEGR) between a group of candidates proposed which are proposed after the bibliographical research performed in chapter 2 and wih the agreement of the constructor. The results are compared in the air management maps framework and they are defined in the main criteria helping to chose the profiles to be machined and tested.

5.2.1 Engine operating conditions selection

The selection of the engine operating conditions where the candidates camshaft profiles are evaluated was done focusing on full Load which are the extreme conditions of all the engine map in terms of thermo-mechanical constraints. Two full load engine conditions were selected as is shown in Fig. 5.1 one at medium speed an the other one in high speed. The two engine points are defined by the torque and speed values which were maintained constant for all simulated and tested air management strategies.

In terms of injection pressure as well as the number and timing of injections the conditions were defined for all the selected operating points as shown in Table 5.1. These injection settings were maintained constant in all the study and they are the same settings used with the standard camshaft in the case of

Miller camshaft profile. In the case of iEGR strategy and due to engine thermo-mechanical constraints the injection settings (injection pressure and timing) were modified as observed on Table 5.1. increasing the injection pressure or delaying the start of injection.

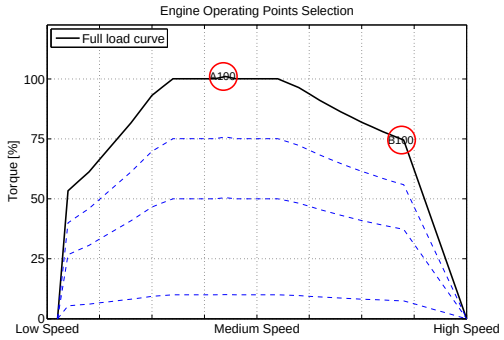

Figure 5.1: Engine operating conditions for Camshaft profile simulation and selection

Inj Settings Fulll Load			
	NoI [-]	IP [bar]	SoI(Main) [CAD]
A100 Miller	3	500	359
A100 iEGR	3	735	357
B100 Miller	2	820	356.5
B100 iEGR	2	950	356.5

Table 5.1: Injection settings of selected operating conditions at full load

5.2.2 Internal EGR camshaft profile selection

The standard camshaft profile was measured directly on the engine, installing a linear displacement transducer which allows to measure the cam profile using the lift of intake and exhaust valves a procedure described in section 3.5. the measured standard profile is represented on black in Fig. 5.2 and it is an input on the engine model. At this point with the aim to explore different air management strategies and select the "Optimal camshaft profile to be manufactured" the 1D engine model is used in order to simulate 7 iEGR profiles varying the exhaust valve aperture and the rebreathing angle location during intake stroke as studied by Luján [2]. This profiles candidates are represented in Fig. 5.2 as a cyan, green or blue curves depending the case for each air management strategy.

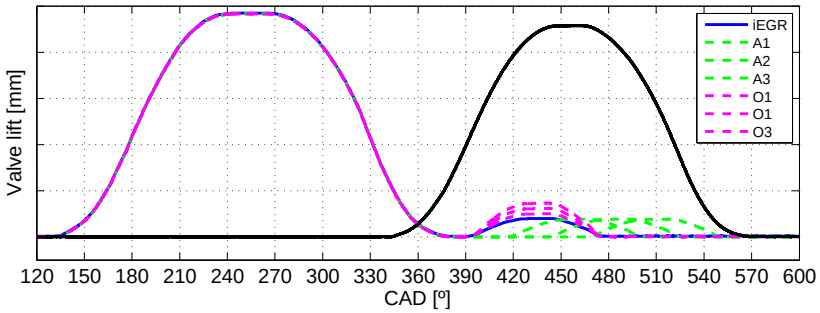

Figure 5.2: iEGR simulated camshaft profiles

Based on the results observed on Fig. 5.3, in case of iEGR, the selection of the optimal camshaft profile is done for the A100 operating condition. The blue camshaft profile is the chosen one because it is on the limit in the A/F relation (Blue diamond) which set the conditions to avoid an excessive richness and a low quantity of iEGR. The main characteristics of the selected iEGR camshaft profile are opening the exhaust valve during 90 CAD while the intake valve is open as is shown in Fig. 5.2 allowing to get inside the cylinder the exhaust gases in a process strongly dependent on the intake and exhaust manifolds pressure conditions as described by Schwoerer et al. [3] or Balaji et al. [4].

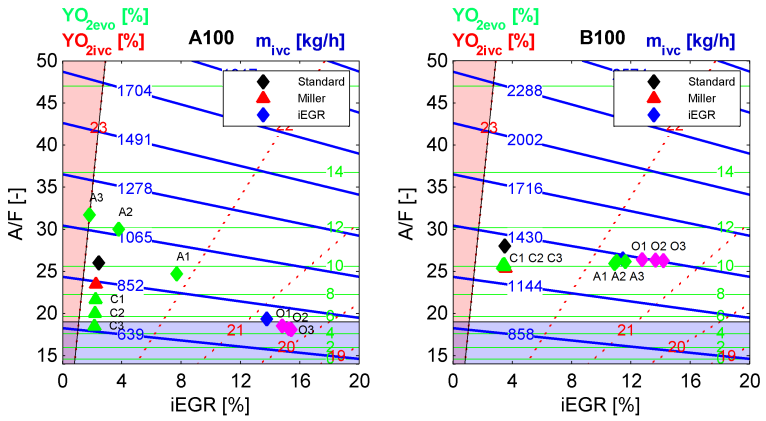

Figure 5.3: 1D Simulation results of camshaft profiles candidates

5.2.3 Miller camshaft profile selection

In the same way than for iEGR strategy described in the last subsection, The measured standard profile is represented as a black curve in Fig. 5.4

and it is an input on the 1D engine model parametrisation. Likewise the same methodology for Miller profile simulation was performed with the aim to explore the different possible Miller configurations searching the "Optimal camshaft profile to be manufactured". For this camshaft profile, the air management strategies simulated are four different Miller profiles changing the intake valve closing as represented in green and red on Fig. 5.4.

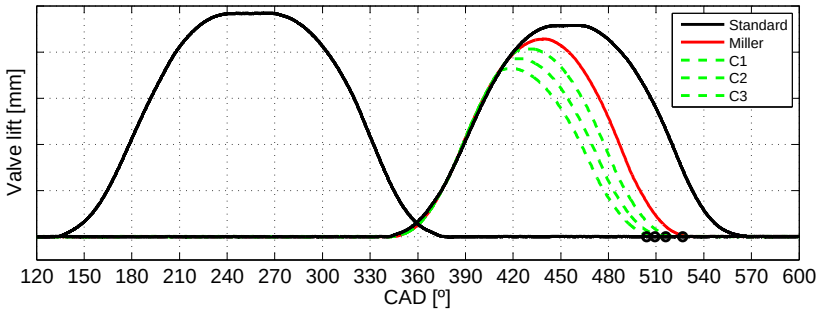

Figure 5.4: Miller simulated camshaft profiles

Evaluating the results of the different Miller profiles observed on Fig. 5.3. It is possible to select the Miller camshaft profile to be manufactured between all the simulated options selecting the plotted red triangle (Red camshaft profile in Fig. 5.4 as the chosen one. The main reasons to select it between the others camshaft profiles could be observed at engine operating conditions A100 which is the same point where the iEGR profile was chosen. In this case for Miller, the advancing of intake valve closing was selected with the objective to keep a similar mass at intake valve closing compared to iEGR camshaft as well as not affect the fuel consumption in big measure. In Comparison to the standard camshaft, the selected Miller profile is changing the angle of intake valve closing from 560 CAD to 530 CAD as is show in Fig. 5.4.

5.3 Experimental validation of selected camshaft profiles

After the selection of one camshaft profile per strategy performed in the previous section, now it is the time to validate the 1D simulation results trough the engine testing of the machined profiles. First of all they are defined the part load and full load engine operating conditions where are evaluated the cam profiles to later study the engine performance and emissions giving a discussion of the obtained results classifying them by engine load (Part load results and Full load results).

5.3.1 Operating conditions of the experimental validation

Together with full load engine operating conditions described to evaluate and select the cam profiles in section 5.2, Another 4 part load conditions are added in the study in order to validate experimentally the behavior of the engine in terms of performance and emissions as observed in Fig. 5.5. The description of the part load injection settings was done in the chapter 4 and they were kept constant regardless the kind of tested camshaft profile.

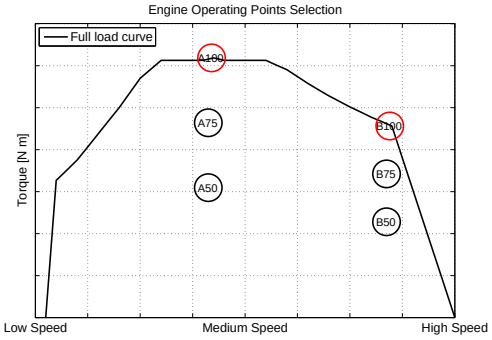

Figure 5.5: Engine operating conditions for Camshaft profile experimental evaluation

5.3.2 Part load experimental exploration of selected camshaft profiles

In this subsection are evaluated the Miller and iEGR camshaft profiles results over the part load engine operating conditions. The subsection is structured in order of the event time occurrence in the engine operation, describing in first place the compression stroke in-cylinder conditions, later the Combustion process study and finally the discussion of the behavior of each camshaft profile in the engine performance and emissions.

Compression stroke in-cylinder conditions: The compression in-cylinder behavior is independent from the injection parameters but totally affected by the gas exchange processes conditions. In case of Miller camshaft profile, advancing the IVC shortens the duration of the intake process which reduces the total air mass flow trough the engine which is equivalent to the reduction of effective compression ratio. For iEGR camshaft profile the total mass flow is reduced like the Miller one but the reason in this case is the opening of exhaust valve when the intake valve is opened reducing the fresh air quantity in the cylinder. In this part of the analysis, the objective is

to determine all the thermodynamic conditions from the intake valve closing until beginning of combustion, in order to compare the influence of each tested camshaft profile in the thermodynamic behavior of the compression stroke.

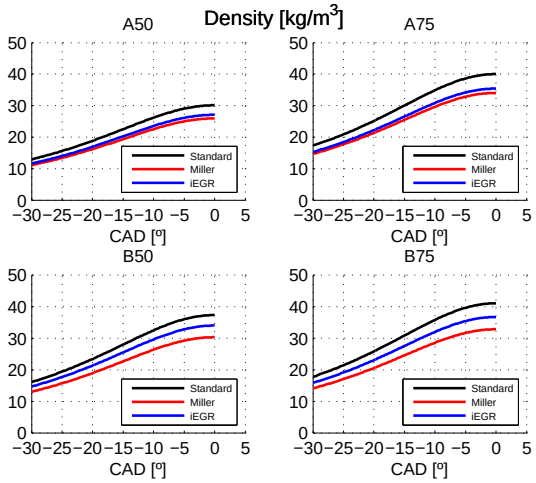

Figure 5.6: Part load in-cylinder density under selected Miller and iEGR camshaft profiles

As previously mentioned the first notorious consequence of producing Miller cycle by advancing IVC is a reduction on the trapped air mass, this explains the results in terms of density on the four evaluated engine points compared to the standard camshaft profile density behavior as shown in Fig. 5.6. As the intake valve was closed earlier, there is an slight expansion of the in-cylinder charge which is the cause of a lower initial pressure on the compression process. This is equivalent to reduce the compression ratio CR and the effect can be noticed at the end of the compression stroke where the maximal pressure is reduced in all part load points compared with the standard camshaft Fig. 5.7. These results in terms of in-cylinder pressure are equivalent to those obtained by Benajes et al. [5]. With the reduction in terms of pressure and despite the density decrease a reduction of mean in-cylinder temperature was expected as is shown in Fig. 5.8.

In case of iEGR camshaft, the density behavior shown in Fig. 5.6 is mainly explained by the in-cylinder temperature which is increased by the internal recirculation of exhaust gases causing a density reduction as shown on Fig. 5.8. Considering a similar intake manifold pressure at beginning of the compression process for both iEGR and standard camshafts, there is a pressure reduction at the end of the stroke despite the temperature increase caused by iEGR profile as observed on Fig. 5.7. This pressure reduction is explained by the

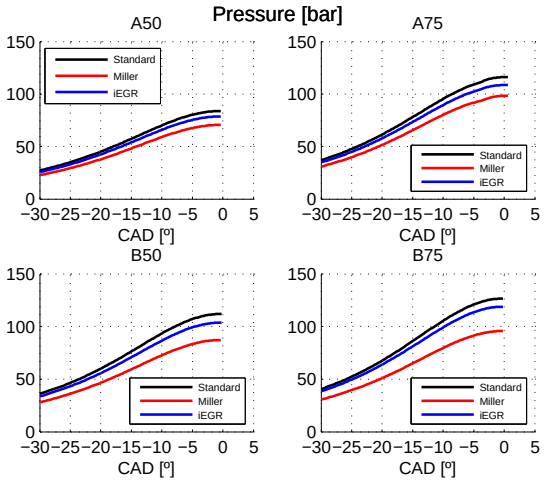

Figure 5.7: Part load in-cylinder Pressure under selected Miller and iEGR camshaft profiles

density decrease added to the in cylinder air dilution with CO_2 and H_2O (with higher Cp with respect to N_2 and O_2).

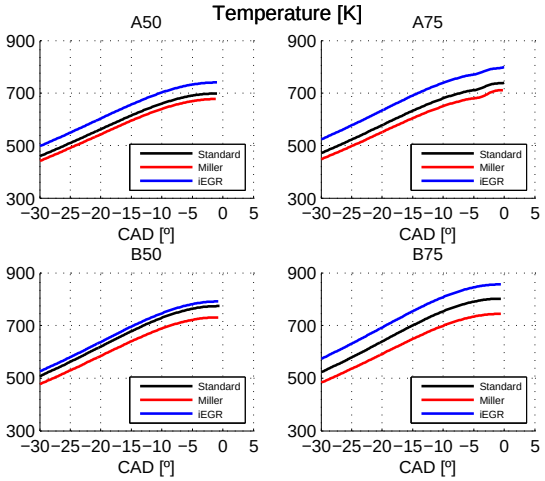

Figure 5.8: Part load in-cylinder mean temperature under selected Miller and iEGR camshaft profiles

Combustion process study: The combustion process is now described to well understand the phenomena that occurs inside the combustion chamber and its influence on the engine efficiency and the pollutant formation. The combustion results are classified at medium load on Fig. 5.9 and medium-high load Fig. 5.10. On the combustion process different variables have

been selected as a tracer of the phenomena: the oxygen concentration, the density, the HRR and the adiabatic temperature are plotted as function of mass fraction burned which evolves from 0% to 100%.

In the case of oxygen concentration could be observed that is always higher with the standard profile in four tested engine conditions for the same mass fraction burned. The application of the air management strategies not only affect the trapped mass and consequently the density, but also affects the evolution of the oxygen concentration. This effect is remarked on the medium speed conditions A50 and A75 in the case of iEGR camshaft profiles.

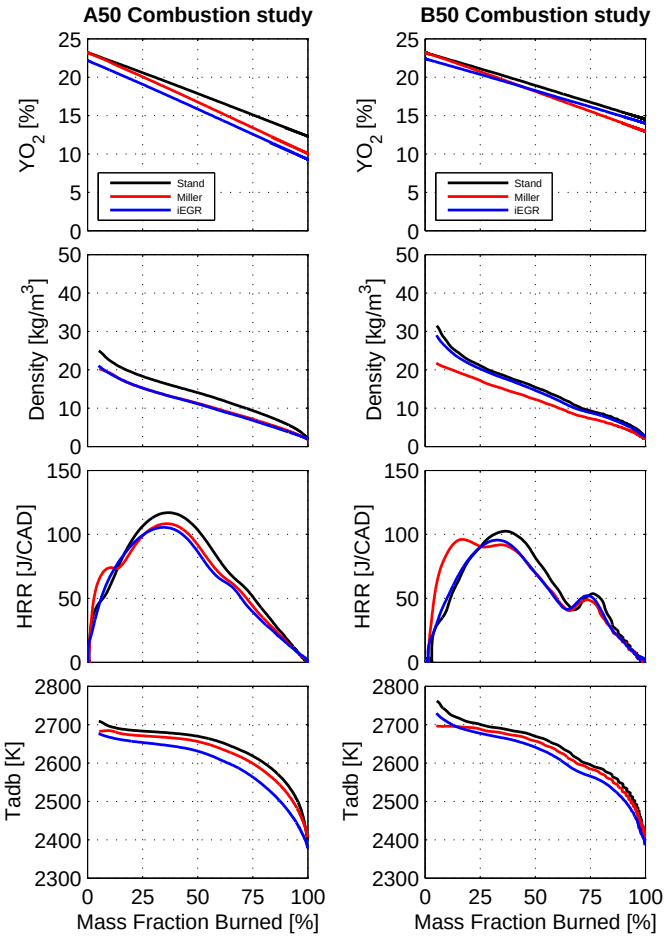

Figure 5.9: Combustion study of A50 and B50 engine operating conditions

Centering now on the HRR and based on the mixture process both strategies slow down the combustion speed as is shown on the reduction of

maximum peak on HRR, again with the iEGR profile and in the medium speed points this decrease is remarked.

The last combustion variable selected as indicator was the adiabatic flame temperature, this is the temperature reached in the spray reaction surface and it is one of the main controls in the chemical processes on the formation of NO_x and soot. It is not a measured variable due to difficulty to measure in an engine without optical access, but on Fig. 5.9 and Fig. 5.10 it is shown the theoretical one calculated from the chemical equilibrium having in account the combustion residuals products and the dissociation effects.

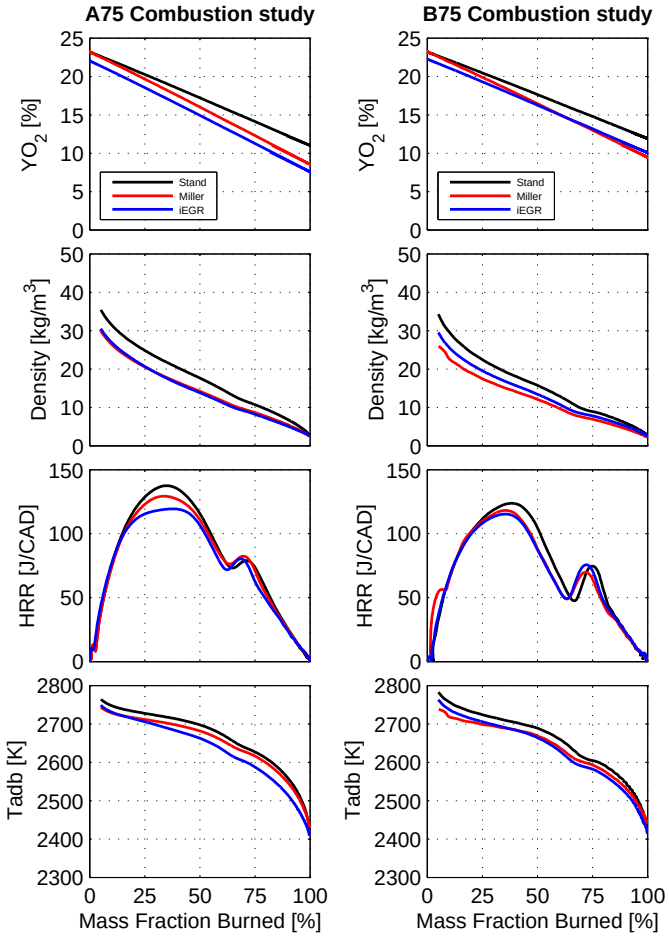

Figure 5.10: Combustion study of A75 and B75 engine operating conditions

The adiabatic temperature decreases with the Miller profile due to reduction on the in-cylinder temperature at the same oxygen concentration at combustion beginning but in case of iEGR in spite of the temperature

increase the reduction of oxygen concentration causes a decrease even bigger than Miller profile. This is an effect over again remarked on the medium speed conditions A50 and A75.

Pollutant emissions and engine efficiency: Studying now the pollutant results and the engine efficiency in part load operating conditions could be observed that NO_x emission was reduced in all the points tested with Miller camshaft as well as iEGR as is shown on Fig. 5.11 and Fig. 5.12. This effect is due to the reduction of adiabatic flame temperature during combustion process specially before the end of injection where most of thermal NO_x is formed as proposed by Benajes et al. [6]. The Miller and the iEGR camshafts allow the reduction of flame temperature acting on two different ways on the combustion process:

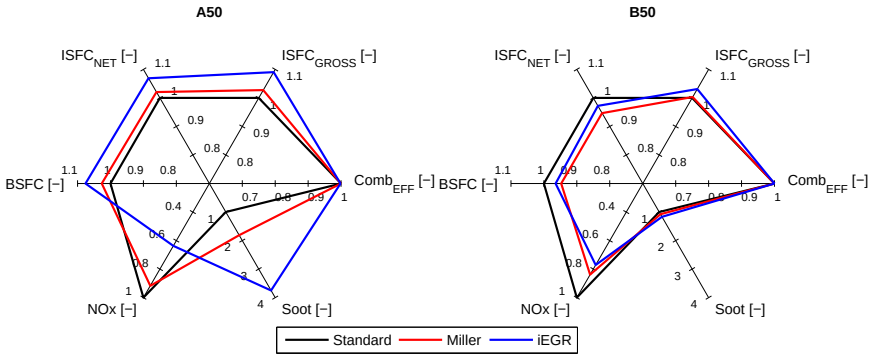

Figure 5.11: Pollutants and engine efficiency at part load A50 and B50

- With Miller camshaft, the main modification is the reduction on the maximum temperature of the combustion chamber due to lower pressure at start compression stroke. This reduction of temperature helps to have a cooler combustion in the surroundings of the spray, which leads to reduce NO_x formation.

- In case of iEGR camshaft, the reduction of NO_x emissions is mainly explained by the reduction of oxygen concentration. This reduction is achieved by the internal re circulation of exhaust gases which contain less oxygen than fresh air. At the end the combustion temperature is reduced despite the fact that the end compression temperature shown in Fig. 5.8 is higher.

Exploring in detail the results in terms of NO_x emissions, this pollutant reduction with iEGR camshaft is more notorious than Miller which is not affected by the engine speed as much as the iEGR does.

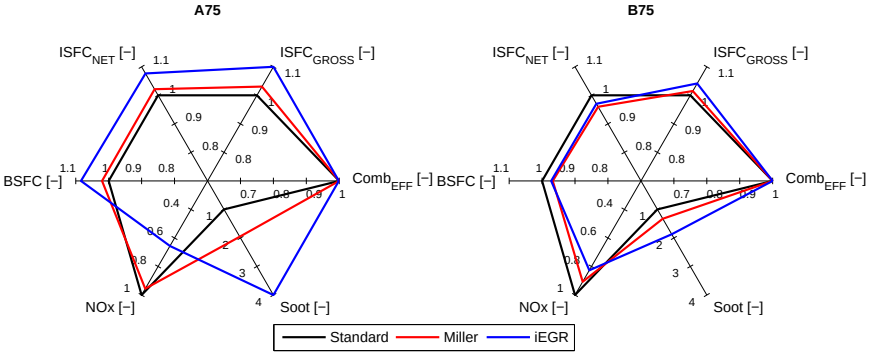

Figure 5.12: Pollutants and engine efficiency at part load A75 and B75

Consequently with the results in NO_x emissions the well known trade off is completed by increase in soot emissions. The strong reduction of NO_x achieved by the iEGR camshaft is compensated by a notorious increment in soot emission, specially at medium engine speed (A points on Fig. 5.11 and Fig. 5.12). Focusing on these results A50 and A75 points shows a combustion deterioration for iEGR camshaft leading to do not reach the soot oxidation temperatures when the mass fraction burned is near to 100%. Picket et al. [7] describes that the soot formation occurs inside the envelope of the diffusion flame on the high temperature and fuel-rich region after the lift-off length, then the increase on the ambient temperature added to lower concentration of O2 with iEGR camshaft promotes this formation in the same way than developed work by Ladommatos et al. [8].

Engine efficiency: The engine efficiency was evaluated from fuel consumption point of view and compared in the spider diagrams as shown on Fig. 5.11 and Fig. 5.12. This kind of diagrams helps to have a complete picture of the engine behavior in the selected parameters related with pollutants and efficiency. The $ISFC_{GROSS}$, $ISFC_{NET}$ and BSFC are compared for all air management configuration at the four tested part load engine conditions. Both tested strategies at the medium speed points (A points) reduces the engine efficiency in a percentage between the 2% and the 8%, showing the same trend as reported in previous works by Benajes et al. [9] where the changes introduced by the camshafts in the gas exchange conditions deteriorates the combustion process in a similar way. When the analysis is translated to high speed (B points) an opposite effect is found, there is a reduction in the

fuel consumption BSFC which cause the improving of the engine efficiency even with the increase noticed on the ISFC_{GROSS} caused by the combustion deterioration. This behavior could be explained by the ISFC_{NET} where the pumping loop is added.

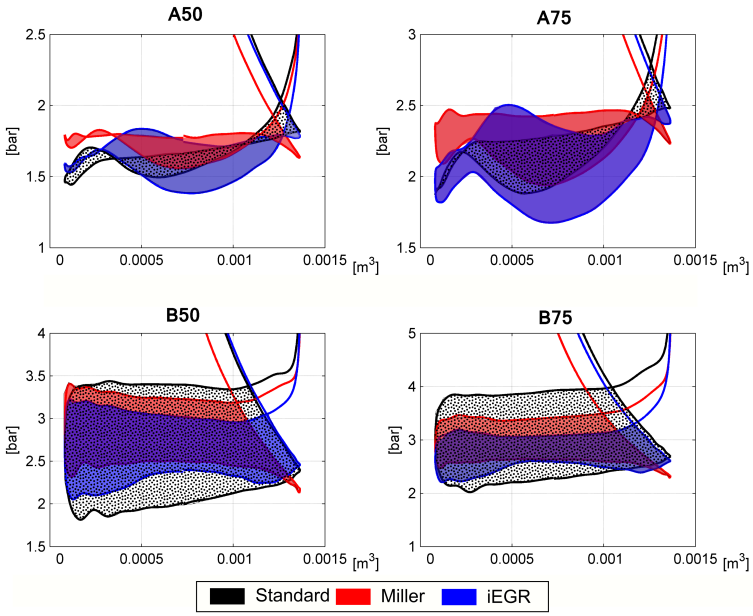

Figure 5.13: P-V Diagram (pumping loop) in part load engine operating conditions

To better understand this fuel consumption behavior the indicators diagrams under part load tested operating conditions are shown on Fig. 5.13. In this plot the pumping loop is zoomed in order to observe the modifications caused by each camshaft profile since it is this loop that fully explains the behavior in fuel consumption and consequently in the engine efficiency.

Camshaft	A50		A75	
	PMEP [bar]	PMEP in BMEP [%]	PMEP [bar]	PMEP in BMEP [%]
Standard	-0.03	-0.3	0.082	0.5
Miller	0.04	0.4	0.22	1.4
iEGR	0.18	1.8	0.42	2.8

Table 5.2: Pumping mean effective pressure comparison for A part load points

At medium speed (A points), there is a high volumetric efficiency then the engine work used to perform the gas exchange process is not so big than at high speed. the Table 5.2 summarize the pumping loop value under each camshaft configuration. In this case Miller and iEGR improves the pumping loop changing from spending engine work to contribute to global BMEP in a

Camshaft	B50		B75	
	PMEP [bar]	PMEP in BMEP [%]	PMEP [bar]	PMEP in BMEP [%]
Standard	-1.38	-16.1	-1.68	-13.9
Miller	-0.82	-9.5	-0.93	-7.7
iEGR	-0.81	-9.4	-0.74	-6.1

Table 5.3: Pumping mean effective pressure comparison for B part load points

low percentage not representative on the BSFC. At high speed (B points), the Table 5.3 shows the same trend of medium speed points. The pumping loop is improved but in this case reducing the amount of engine work spent to do the gases exchange process contributing in a big percentage to global BMEP and notoriously reducing the $ISFC_{NET}$. This is the main reason to have an improvement on the BSFC then with the two air management strategies tested efficiency at high speed is increased.

5.3.3 Full load validation of selected camshaft profiles

In the same way than previous part load subsection now they are evaluated the Miller and iEGR camshaft profiles over the full load engine operating conditions. The subsection is structured in order of the event time occurrence in the engine operation, describing in first place the intake valve closing conditions compared through the air management maps framework, later the Combustion process study are detailed and finally the discussion of the behavior of each camshaft profile in the engine performance and emissions.

Determination of intake valve closing conditions: In order to visualize the relationship between different operating parameters the results of tested strategies are placed in the same engine maps described in the simulation and selection section in the Fig. 5.3. As explained before, the air management maps allow to compare many settings of engine operation: the Y_{O2} concentration at intake and exhaust as well as the A/F and internal EGR. In this maps the red iso-lines defines the Y_{O2} concentration at the intake valve closing while the green iso-lines are the Y_{O2} concentration at exhaust valve opening (a set of parameters which are constant independently of each operating condition). The blue iso-lines depict the mass flow at the intake valve closing and they are calculated for each particular standard engine point. As the two air management profiles were selected in these full load conditions through the simulation discussed in section 5.2, now it is possible to validate experimentally the results obtained by the 1D GT Power model as is shown

on Fig. 5.14 which show a good agreement between the simulations and the tested behavior engine.

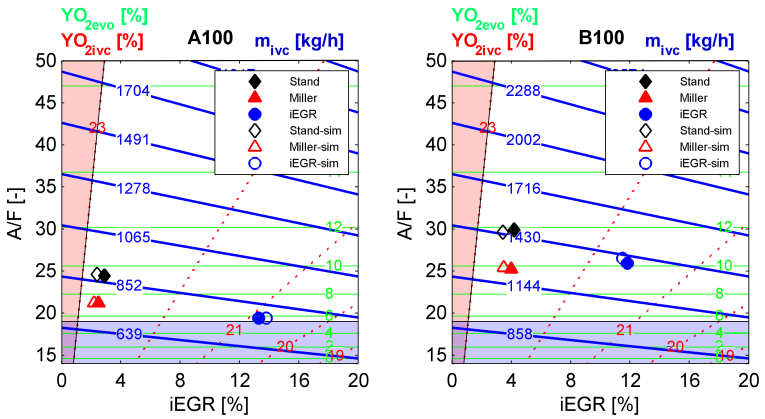

Figure 5.14: Experimental and 1D Simulation results of selected camshaft profiles

Combustion process study: The combustion study is performed in the same way than partial load by analyzing the oxygen concentration, the density, the HRR and the adiabatic flame temperature as observed on Fig. 5.15. In both cases the A100 and B100 the injection settings were defined for each profile as described on Table 5.1, then the comparison must have in account the increase in injection pressure for iEGR camshaft profile compared with the reference. In a similar way than part load points the application of the air management strategies not only affect the trapped mass and consequently the density, but also affects the evolution of the oxygen concentration during combustion.

The main difference in combustion process between part load and full load conditions is remarked in the HRR and T_{adb} behavior. Centering on the HRR and based on the mixture process the rise up caused by the injection pressure increase on standard profile iEGR contrast with the HRR on standard profile under Miller injection conditions which has a lower injection pressure. Focusing now on adiabatic flame temperature the improvement on mixture process due to injection pressure increases the adiabatic flame temperature for iEGR then the effect of this air management strategy is mitigated. In case of Miller strategy the results are similar than explained in part load.

Pollutant emissions and engine efficiency: The Pollutants and engine efficiency under both camshaft strategies are depicted in Fig. 5.16. The Miller

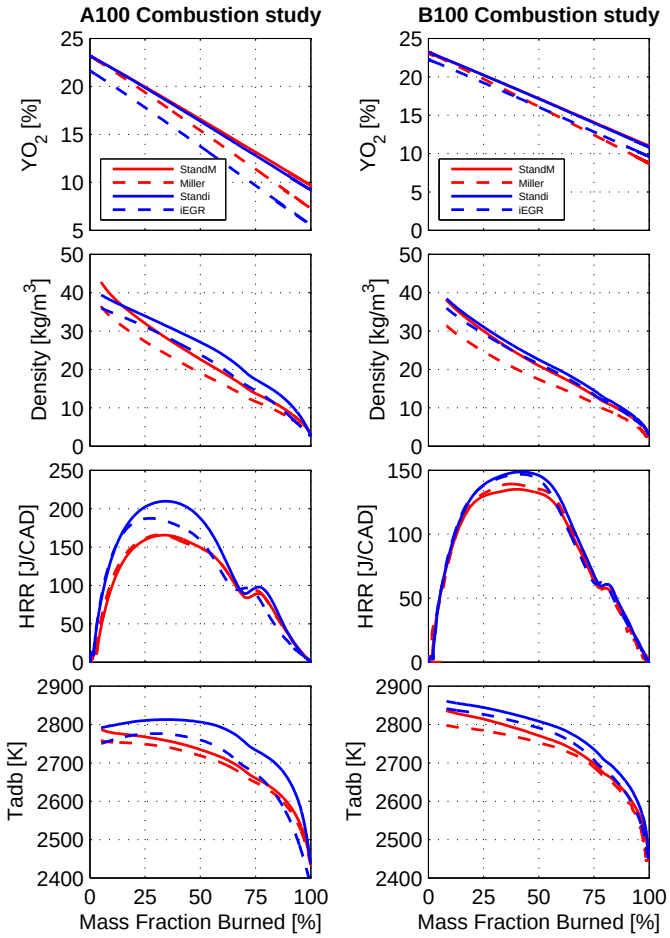

Figure 5.15: Combustion study of A100 and B100 engine operating conditions

and the iEGR camshaft profiles preserve the combustion efficiency reached by the standard profile as described on Fig. 5.16, then the CO and HC pollutants are not increased in high measure. With respect NO_x emissions, the adiabatic flame temperature described on combustion study explains the behavior shown on Fig. 5.16, where are compared the two air management strategies with the standard one. In this case and due to injection pressure increase with iEGR profile, the NO_x reduction is not the highest with this profile.

In terms of soot emission the notorious increase caused by the iEGR profile in part load points is reduced due to improvement on mixture process achieved by the raise of the injection pressure. In case of Miller profile the richness near to the lift off is reduced because it decreases the density and the temperature of the gas in the combustion chamber. Despite this reduction in the soot

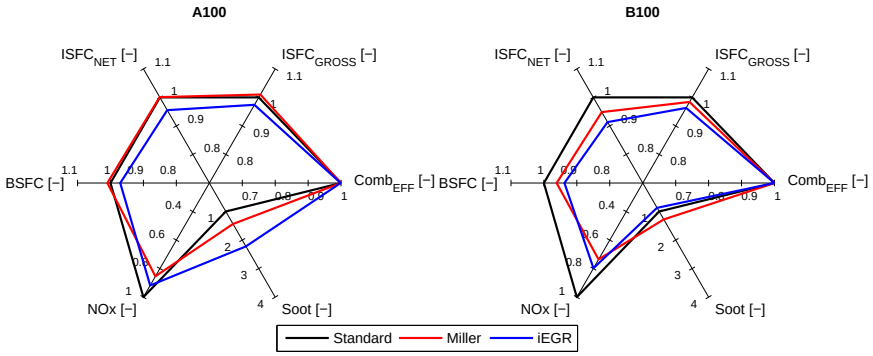

Figure 5.16: Pollutants and engine efficiency at Full load A100 and B100

formation conditions, there is a soot increment which confirms the affectation in the soot oxidation process in the same way than part load points.

Engine efficiency: The engine efficiency behavior at full load is explained in a similar way than part load points trough the spider diagrams, in case of the A100 operating condition the fuel consumption shown on Fig. 5.16 is not so affected by the Miller strategy which contrast with the iEGR profile where the increment on injection pressure helps to improve the mixture process making a faster combustion reducing the ISFC_{GROSS} reflected on the BSFC. In case of B100 the high speed point, the reduction on the pumping loop as explained on part load section added to the increase on injection pressure in the case of iEGR profile helps to have a notorious improvement in the ISFC_{GROSS}, ISFC_{NET} and consequently on BSFC as observed on Fig 5.16. It should be clarified that in the previous analysis the iEGR camshaft profile is not being fairly compared, since from the beginning and in order to fullfill the load requirements it requires the modification of the injection parameters in the values previously described.

5.3.4 Transient effects discussion

The transient behavior comparison is described on Fig. 5.17. In this case only the results of A50 and A75 operating condition are discussed due to the modification in the injection settings for iEGR strategy at full load. The well known tip-in transient test as proposed by Hagena et al. [10] and Kirchen et al. [11] it is performed instantaneously changing the pedal position from 0% to 50% and 75% respectively.

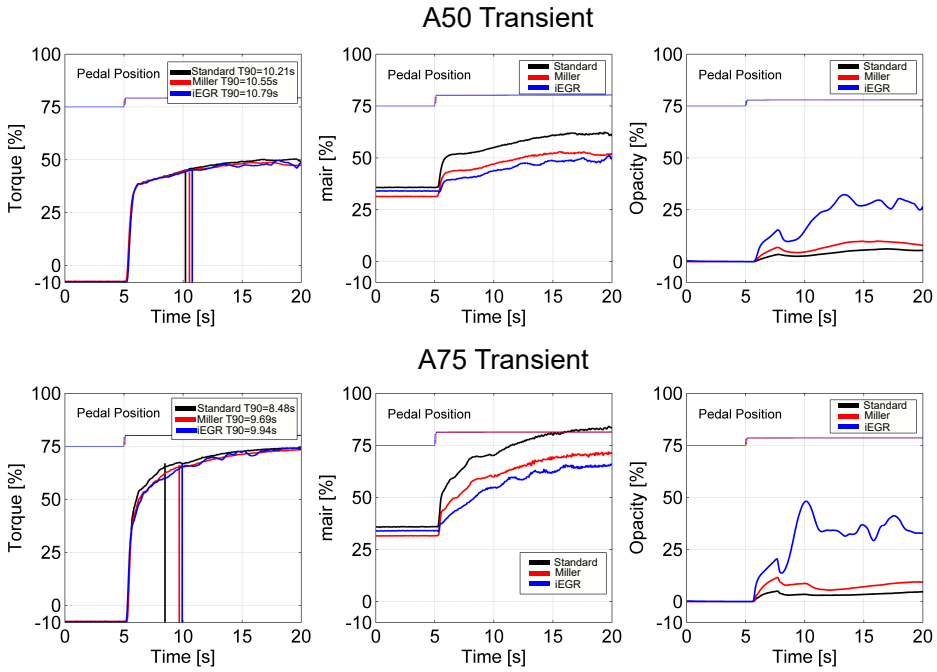

Figure 5.17: Transient engine behavior under selected air management strategies

The Torque, air mass flow and opacity are recorded during 20s under each air management configuration obtaining the next results:

- The first studied variable is the Torque, in this case with both tested air management strategies (Miller and iEGR) there is an increase on the T90 time which is the required time to achieve the 90% of target Torque. The maximum increment is of 1.5s in iEGR strategy case in A75 mode.
- In case of air mass flow, the transient study is coherent with the results obtained in the steady test. There is a reduction of fresh air flow into the engine when is operated in any of different camshaft profiles different to the standard one.
- A notorious increase on opacity with the iEGR strategy and in less quantity with Miller profile is observed, the reduction in the A/F relation due to reduction in air mass flow leads to increase the richness of the mixture causing the raise of the opacity. In case of A50 engine point the increment is under 30% which is an acceptable increase of the opacity peak. The A75 engine condition must be re-calibrated in order to avoid the peak near to the 50% which is the maximum allowed peak value (Emission standard ISO 8178).

5.4 Miller and iEGR camshafts profiles cycle testing

After individually exploring the consequences of using the selected air management strategies in subsection 5.2 and subsection 5.3, now in the current subsection are compared all the regulated engine points under the tested strategies, allowing to compare them with the standard camshaft profile in order to globally evaluate their behavior and potential.

The camshaft strategies behavior is discussed over all the cycle points dividing it in 2 parts, in first place, the verification of the injection settings used in each engine operating conditions coupled with the mechanical limits fulfillment. In second place, the pollutants emission and the engine fuel consumption summary under each camshaft profile strategy as perfomed by Yanowitz et al. [12].

5.4.1 Points definition and mechanical limits

5.4.1.1 Test injection settings evaluation

The injection settings comparison between the tested Miller and iEGR camshaft profiles and the standard one is done in Fig. 5.18. As could be observed, any modification of the injection settings was performed during the experimental evaluation of Miller thus the results obtained in this case are caused by the direct application of the air management strategy. In the case of iEGR camshaft, the modification of the injection settings at full load compared with the reference difficult reasoning the air management strategy behavior at this points.

5.4.1.2 Evaluated mechanical limits

The evaluation of the engine mechanical limits is done in Fig. 5.19. The Turbospeed, the In-cylinder pressure and the intake and exhaust manifolds pressure and temperatures are verified for all the engine operating conditions. As observed for all evaluated mechanical limits they are under the reference defined by the manufacturer as the critical level of thermo-mechanical strength.

As previously described in the strategies selection subsection as well than in the chapter 4, the full load points A100 and B100 are the critical engine operating conditions in the process of concepts design from a mechanical

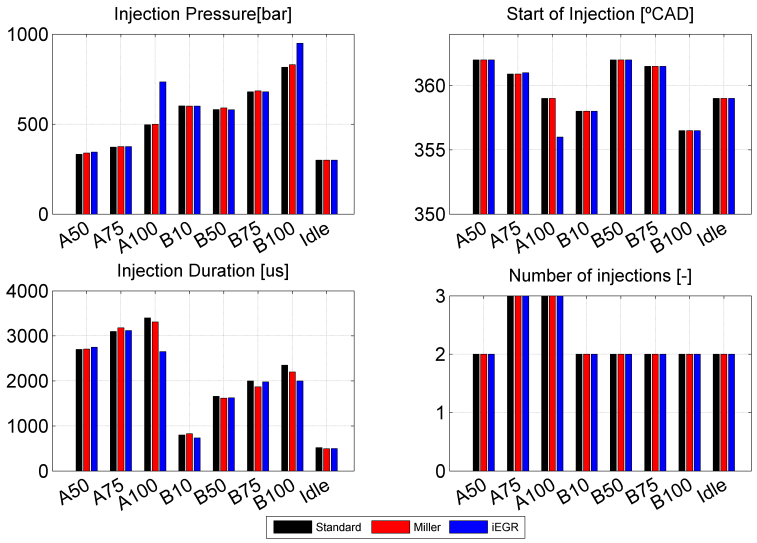

Figure 5.18: Injection settings definition with Miller and iEGR camshaft profiles

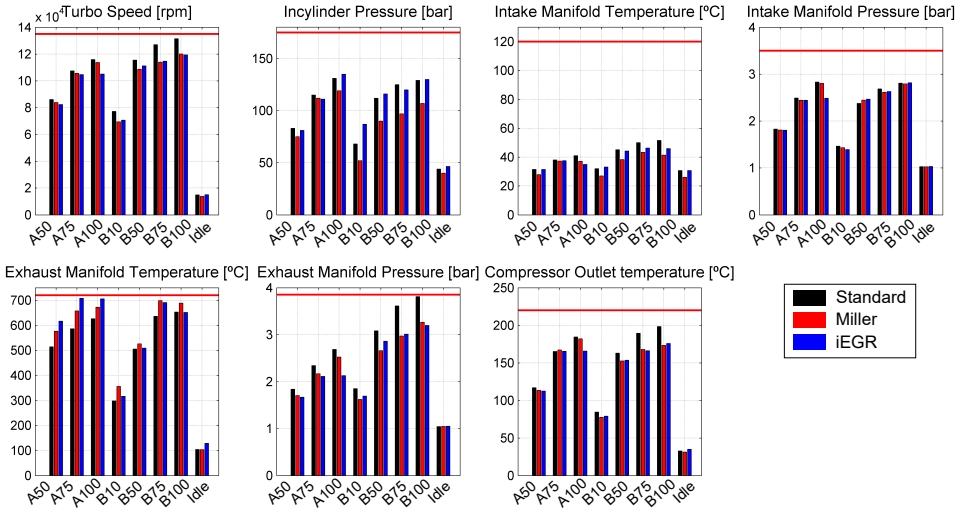

Figure 5.19: Mechanical limits under Miller and iEGR camshaft profiles

resistance point of view. Particularly at these points is where all the simulations discussed along the thesis (3D CFD simulations or 1D simulations) were performed.

Likewise the results depict in Fig. 5.19 help to evaluate the reasons which leads to modify the injection settings of the iEGR camshaft profiles as discussed in subsection 5.4.1.1. Having in mind the high exhaust manifold temperature observed in the A75 and B75 engine operating conditions, if long

injection pattern is kept under this strategy and the engine load is increased, it could exceed the temperature limits suggested by the manufacturer for this kind of engine.

5.4.2 Pollutants and engine efficiency

As particularly studied for each point in subsection 5.3, the pollutants and the engine fuel consumption are depicted in Fig. 5.20 allowing to summarize the pros and cons of using the Miller and iEGR strategies as a cost-effective solution in the Diesel engine emission control.

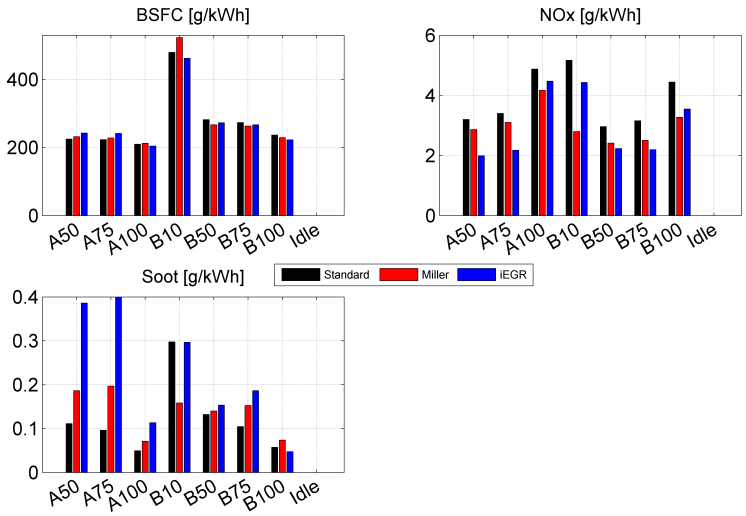

Figure 5.20: Engine emissions and efficiency under Miller and iEGR strategies

Based on the results obtained trough each tested air management strategy, it is possible to build the Table 5.4. In this table are summarized the percentage of gain or loss in the engine pollutants and the engine efficiency from the fuel consumption point of view. Looking at the complete picture which this table give us the main conclusions obtained from all the study using the air management strategies could be described:

- Concerning NO_x emission in Fig. 5.20 could be observed how all the camshaft strategies are focused in the NO_x reduction.
- In most of part load engine operating conditions except the B10 point the highest reduction in terms of NO_x emission are achieved by the iEGR camshaft profile being penalized by the high increase of Soot and fuel consumption in medium speed points.

- In terms of engine efficiency based on the engine fuel consumption, both camshaft have demonstrated the important influence of the pumping loop in the high speed operating conditions (B points) both in partial loads and full load as explained in section 5.3.
- The BSFC is improved as well than NO_x emission in the high speed engine conditions a very interesting behavior of the tested air management strategies.
- The NO_x reduction achieved by the tested air management strategies is higher than the obtained by the injection settings explored in the chapter 4. If it is considered than the air management strategies causes a total effect over all the engine map and the injection settings could be used as a local tuning (point by point) there is an interesting optimization way combining the strategies studied in chapter 4 and chapter 5 which are the basic idea explored in the next chapter 6.

Operating	Miller camshaft[%]			iEGR camshaft [%]		
Condition	NO_x	Soot	BSFC	NO_x	Soot	BSFC
A50	-10	67	3	-38	247	8
A75	-9	104	2	-36	374	8
A100	-15	43	1	-8	129	-3
B10	-46	-47	9	-14	0	-4
B50	-19	6	-5	-25	16	-3
B75	-21	46	-4	-30	78	-2
B100	-26	28	-3	-20	-18	-6

Table 5.4: Results under Miller and iEGR strategies compared with the standard one

Bibliography

[1] Bermúdez V., Molina S., Novella R. and Estepa D. "Experimental Study of Two Air Management Strategies for Emissions Control in Heavy Duty Engines at Medium to High Loads". *Energy & Fuels*, Vol. 31 n^o 9, pp. 10011–10022, 2017.

[2] Luján JM. *Recirculación interna de gases de combustión en motores Diesel sobrealimentados*. Doctoral Thesis, Universidad Politécnica de Valencia, Departamento de Máquinas y Motores Térmicos, 1998.

[3] Schwoerer J., Dodi S., Fox M., Huang S. and Yang Z. "Internal EGR Systems for NOx Emission Reduction in Heavy-Duty Diesel Engines". *SAE Technical Paper-2004-01-1315*, 2004. doi:10.4271/2004-01-1315.

[4] Balaji J., Ganesh Prasad M. V., L. Navaneetha R.., Bandaru B. and Ramesh A. "Modelling and Experimental Study of Internal EGR System for NOx Control on an Off-Road Diesel Engine". *SAE Technical Paper-2014-01-2645*, 2014. doi:10.4271/2014-01-2645.

[5] Benajes J., Serrano J.R., Molina S. and Novella R. "Potential of Atkinson cycle combined with EGR for pollutant control in a HD diesel engine". *Energy Conversion and Management*, Vol. 50, pp. 174–183, 2008.

[6] Benajes J., Novella R., García A. and Arthozoul S. "The role of in-cylinder gas density and oxygen concentration on late spray mixing and soot oxidation processes". *Energy*, Vol. 36 n^o 3, pp. 1599–1611, 2011.

[7] Pickett L. M. and Siebers D. L. "Soot in diesel fuel jets: effects of ambient temperature, ambient density, and injection pressure". *Combustion and Flame*, Vol. 138 n^o 1-2, pp. 114–135, 2004.

[8] Ladommatos N., Song H. and Zhao H. "Measurements and predictions of diesel soot oxidation rates". *Proceedings of the Institution of Mechanical Engineers, Part D: Journal of Automobile Engineering*, Vol. 216 n^o 8, pp. 677–689, 2002.

[9] Benajes J., Molina S., Martín J. and Novella R. "Effect of advancing the closing angle of the intake valves on diffusion-controlled combustion in a HD diesel engine". *Applied Thermal Engineering*, Vol. 29, pp. 1947–1954, 2009.

[10] Hagena J. R., Filipi Z. and Assanis D. N. "Transient Diesel Emissions: Analysis of Engine Operation During a Tip-In". *SAE Technical Paper-2006-01-1151*, 2006. doi:10.4271/2006-01-1151.

[11] Kirchen P., Obrecht P. and Boulouchos K. "Soot Emission Measurements and Validation of a Mean Value Soot Model for Common-Rail Diesel Engines during Transient Operation". *SAE Technical Paper-2009-01-1904*, 2009. doi:10.4271/2009-01-1904.

[12] Yanowitz J., Graboski M. S. and McCormick R. L. "Prediction of In-Use Emissions of Heavy-Duty Diesel Vehicles from Engine Testing". *Environmental Science & Technology*, Vol. 36 n^o 2, pp. 270–275, 2002.

Chapter 6

Potential of the cost-effective strategies combination

Contents

6.1 Introduction

The previous discussed strategies focused on injection-combustion in chapter 4, and in the air management in chapter 5, have demonstrated their efficacy in order to control engine emissions, increase the engine efficiency and in some cases both of them in the same way than previous performed works by Balaji et al. [1] or Benajes et al. [2]. As mentioned in the air management strategies conclusions these strategies are not mutually exclusive enabling the possibility of combining both in order to define the potential of these cost-effective strategies. The main structure of this chapter begins with the description of the injection-combustion parameters combined with the Miller strategy results discussing in a separate way the medium speed and the high speed engine operating conditions. The second subsection keeps the structure of the first one but in this case the discussion is focused in the iEGR air management strategy and the injection-combustion combination. The last subsection helps to define the global behavior of each strategies combination weighing each engine point as defined in the emissions legislation, in this framework the real limits of each cost-effective engine definition could be depicted.

6.2 The injection parameters and the Miller strategy combination

As mentioned in the air management strategies chapter 5, the combination of a global engine strategy like the Miller one with a local optimization trough the injection parameters as performed by Park et al. [3] could lead to improve the engine emissions, increase the engine efficiency and in some cases both of them. In this section the Miller air management strategy is combined with the injection parameters exploration through a set of parametric studies in the same way than performed in chapter 4, for the standard air management definition.

6.2.1 Miller Parametric study definition

In chapter 5, Miller camshaft profile was evaluated in the standard injection setting defined per each engine operating condition. The evaluation results have shown that full load points A100 and B100 were in risk of engine thermo-mechanical limits violation being the main reason to keep this parametric exploration centered in the part load points as observed in Table 6.1. In the

same table the engine operating conditions are separated in medium and high speed engine a classification which is kept along the chapter development for results evaluation.

	IP [bar]	SoI (Main) [CAD]	Dwell [CAD]	Post Qty [mg/cc]
A50	**340**-360-380-400	359-360-361-**362**-363-364	11	4.6
A75	**375**-400-425-450	357-358-359-360-**361**-362-363	5.5	19
B10	950-1050-1150	354-355-356-357-**358**	12	10
B50	**580**-630-680	356-357-358-359-360-361-**362**	12	10
B75	**690**-720-750	357-358-359-360-**361.5**	12	19

Table 6.1: Injection settings of the parametric experimental study Miller strategy

The Miller camshaft exploration done in chapter 5 shows how this air management strategy helps to reduce the NO_x emissions in all tested engine operating conditions a trend described in the work performed by Bermúdez et al. [4] hence in the same way than performed in chapter 4, different scenarios could be established per each engine point depending on the path of the injection parameters optimization. The path of searching minimal emissions with high impact in the engine fuel consumption is not explored in the research work then the NO_x emission is the key parameter in the optimization and look for ISO-NO_x conditions compared with the standard engine definition could help to improve even more the engine efficiency. With strategies ISO-NO_x objective in the optimization two scenarios per engine point are possible:

- One scenario under ISO-NO_x conditions with the optimal BSFC but negative consequences in the Soot behavior depending of each operating condition due to.
- One scenario under ISO-NO_x conditions with interesting results in BSFC and the best results in the Soot behavior thanks to optimization is done in the highest tested injection pressure.

6.2.2 Medium engine speed parametric study

In the case of the A50 engine operating condition the parametric study results, as observed in Fig. 6.1, it depicts two scenarios when the ISO-NO_x condition are evaluated. The combination of increase of the injection pressure plus delaying the SOI leads to moderate reduction of BSFC coupled with

moderate reduction in Soot. Keeping the standard injection pressure and advancing the SOI leads to interesting reduction of BSFC maintaining the reference Soot emission value.

- Reduction of 1% in BSFC, increase of 44% of soot compared with reference at ISO-NO_x.
- Increase of 2.5% in BSFC, increase of 15% of soot compared with reference at ISO-NO_x.

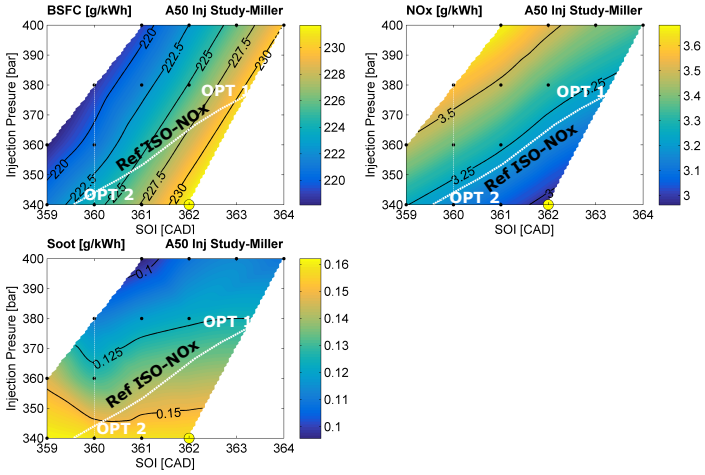

Figure 6.1: A50 Miller ISO-NO_x optimization

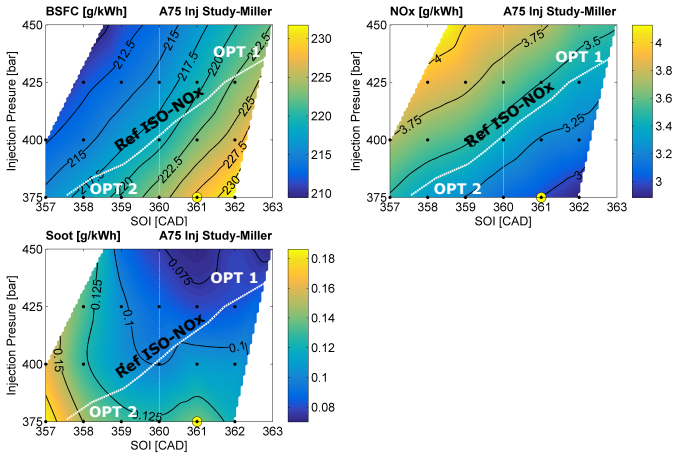

Figure 6.2: A75 Miller ISO-NO_x optimization

Centering now in the A75 engine operating conditions, from the parametric study results observed in Fig. 6.2 similar conclusions than previously discussed

A50 engine point could be extracted. In this way, the injection pressure increase could not reach high levels due to ISO-NO_x closeness.

- Reduction of 3% in BSFC and increase of 71% in Soot compared with reference at ISO-NO_x.
- Similar level of BSFC and reduction of 16% in Soot compared with reference at ISO-NO_x.

6.2.3 High engine speed parametric study

The high engine operating points called B points are evaluated in the current subsection. Unlike the medium speed points the high speed engine points allow to increase the injection pressure with interesting consequences in the fuel consumption an the Soot behavior.

Beginning for B10 engine operating condition the parametric study results observed in Fig. 6.3 depict two optimization ways when the ISO-NO_x is reached. Similarly the medium speed points, the SOI indicates the two optimization paths but in this case with early SOI angles.

- Reduction of 12% in BSFC and 76% in Soot compared with reference at ISO-NO_x.
- Reduction of 14% in BSFC and 89% in Soot compared with reference at ISO-NO_x.

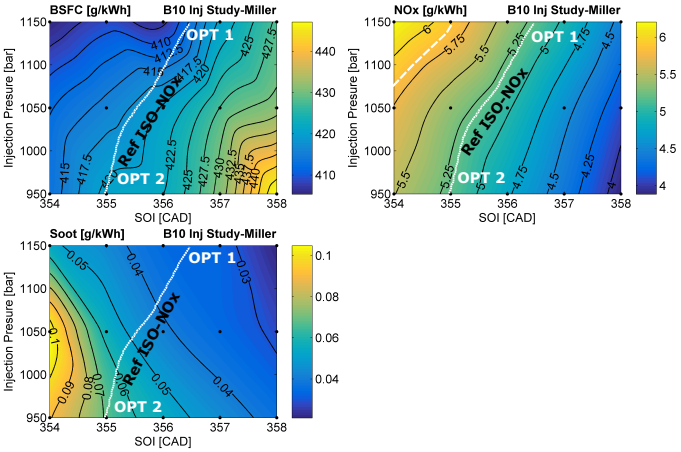

Figure 6.3: B10 Miller ISO-NO_x optimization

Focusing now in the B50 operating condition, the results observed in Fig. 6.4 continue with the trend observed in the previous discussed B10 point. The ISO-NO_x reference conditions is found with a combination of high injection pressure and early SOI allowing the reduction of fuel consumption.

- Reduction of 14% in BSFC and increase of 21% compared with reference at ISO-NO_x.
- Reduction of 14% in BSFC and reduction in 37% in Soot compared with reference at ISO-NO_x.

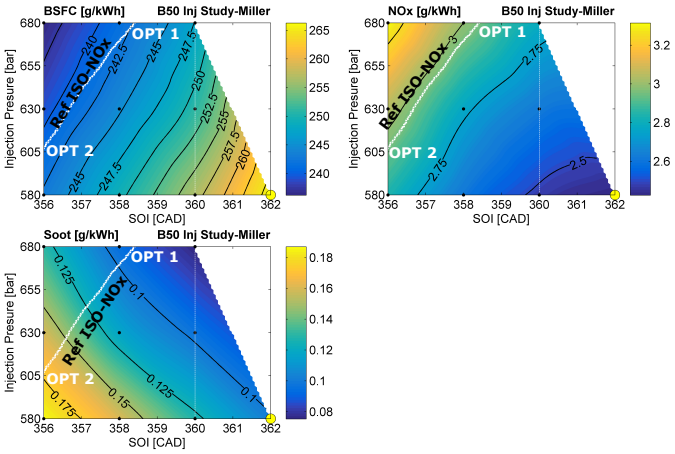

Figure 6.4: B50 Miller ISO-NO_x optimization

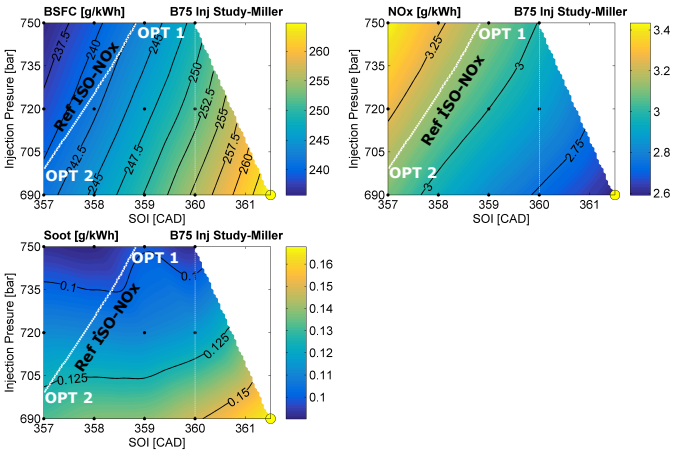

Figure 6.5: B75 Miller ISO-NO_x optimization

The highest engine load evaluated in the high engine speed is the B75 operating condition. B75 point results are depicted in Fig. 6.5. As could be

observed, the trend described in previous discussed points leads to the same combination of injection parameters advancing the SOI combined with the injection pressure increase in order to reach the ISO-NO_x reference.

- Reduction of 12% and increase of 20% in Soot compared with reference at ISO-NO_x.
- Reduction of 11% in BSFC and 6% in Soot compared with reference at ISO-NO_x.

6.2.4 Summary of Miller strategy study

In the previous subsection are detailed the parametric studies performed combining the Miller air management strategy and the injection-combustion parameters. Both of them cost-effective strategies give the opportunity to optimize the engine emissions and efficiency. The Table 6.2 summarize the optimization performed at ISO-NO_x at each engine operating condition.

Operating	Optimization 1[%]			Optimization 2 [%]		
Condition	NO_x	Soot	BSFC	NO_x	Soot	BSFC
A50	ISO	15	2.5	ISO	44	-1
A75	ISO	-16	0	ISO	71	-3
B10	ISO	-89	-14	ISO	76	-12
B50	ISO	-37	-14	ISO	27	-4
B75	ISO	-6	-11	ISO	20	-12

Table 6.2: Results under Miller strategy at reference ISO-NO_x conditions

A set of conclusions could be extracted from the summary Table 6.2 which are now detailed.

- In the medium engine speed points A50 and A75 where the ISO-NO_x does not allow to increase the injection pressure the gains in the BSFC are not as important as the high engine speed points.
- At really low load as the B10 engine operating condition, the Miller camshaft profile allow the highest increase in the injection pressure value which leads to obtain important benefits of using this air management strategy in this engine zone.
- The high influence of the pumping loop improvement under the Miller air management strategy helps to reduce even more the fuel consumption

in both evaluated optimization a result which match the previously published by Benajes et al. [5].

6.3 The injection parameters and the iEGR strategy combination

In the same way than Miller camshaft strategy, in the chapter 5, iEGR profile was evaluated in the standard injection setting defined per each engine operating condition. The evaluation results have shown that the strategy mainly helps to reduce the NO_x emission even in a higher level than Miller camshaft but risking at the same time exceeding the thermo-mechanical limits in the full load engine condition as the work performed by Schwoerer et al. [6]. This is the main reason as the Miller profile to keep this parametric exploration centered in the part load points as observed in Table 6.3. In the same table the engine operating conditions are separated in medium and high speed engine a classification which is kept along the section development for the results evaluation.

6.3.1 iEGR Parametric study definition

In chapter 5, iEGR camshaft profile was evaluated in the standard injection setting defined per each engine operating condition. The evaluation results have shown that full load points A100 and B100 were in risk of engine thermo-mechanical limits violation as the Miller camshaft profile. This is the main reason to keep the parametric exploration centered in the part load points as observed in Table 6.3. In the same table the engine operating conditions are separated in medium and high speed engine a classification which in a similar way than previous described subsection.

	IP [bar]	SoI (Main) [CAD]	Dwell [CAD]	Post Qty [mg/cc]
A50	450-500-550	357-358-359-360-361-**362**-363-364	11	4.6
A75	500-550-600	356-357-358-359-360-**361**-362	5.5	19
B10	**600**-675-750	354-355-356-357-**358**-359-360	12	10
B50	680-755-830	358-359-360-361-**362**-363	12	10
B75	780-880-980	357-358-359-360-361-362-363	12	19

Table 6.3: Injection settings of the parametric experimental study iEGR strategy

As the Miller camshaft exploration done in previous section different scenarios could be established per each engine point depending on the path of the injection parameters optimization. The path of searching minimal emissions with high impact in the engine fuel consumption is not explored in the research work then the NO_x emission is the key parameter in the optimization and look for ISO-NO_x conditions compared with the standard engine definition could help to improve even more the engine efficiency. With the ISO-NO_x strategy defined as the objective in the optimization, two scenarios per engine point could be obtained:

- One scenario under ISO-NO_x conditions with the optimal BSFC but negative consequences in the Soot behavior depending of each operating condition due to.
- One scenario under ISO-NO_x conditions with interesting results in BSFC and the best results in the Soot behavior thanks to optimization is done in the highest tested injection pressure.

6.3.2 Medium engine speed parametric study

Using the iEGR camshaft profile, the parametric study of the A50 engine operating condition could be observed in Fig. 6.6. In this plot could be identified the ISO-NO_x condition reached by the combination of the increase of the injection pressure plus advancing the SOI. with this parameters combination the optimization scenarios are described.

- Reduction of 5% in BSFC and increase of 150% in Soot compared with reference at ISO-NO_x.
- Reduction of 4% in BSFC and 5% in Soot compared with reference at ISO-NO_x.

In the case of A75 engine operating condition the parametric study results observed in Fig. 6.7. depict two optimization way when the ISO-NO_x is reached similarly than previous studied operating conditions.

- Reduction of 6% in BSFC and increase of 160% in Soot compared with reference at ISO-NO_x.
- Reduction of 4% in BSFC and 5% in Soot compared with reference at ISO-NO_x.

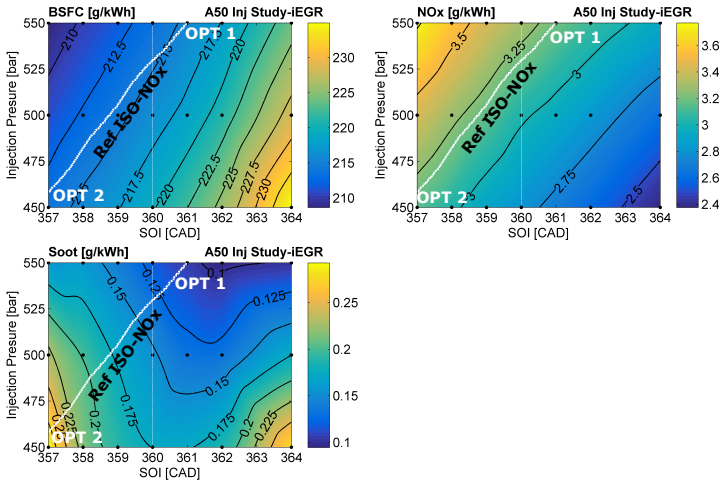

Figure 6.6: A50 iEGR ISO-NO_x optimization

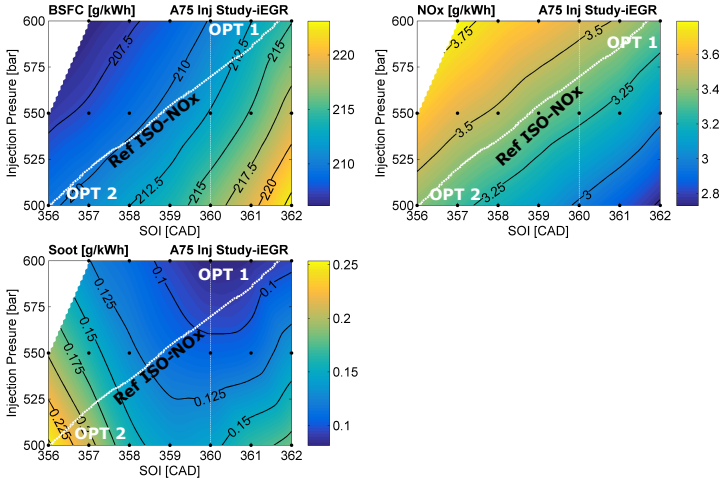

Figure 6.7: A75 iEGR ISO-NO_x optimization

6.3.3 High engine speed parametric study

The high engine operating points B points are evaluated in the current subsection. The injection pressure increase leads to interesting consequences in the fuel consumption an the Soot behavior. This injection parameters definition added to improvement in the pumping loop leads to improve even more the BSFC.

The B10 operating condition optimization results could be observed in Fig. 6.8. Depending of parameter combination the two optimization paths in this engine point are described.

- Reduction of 8% in BSFC and increase of 78% in Soot compared with reference at ISO-NO_x.
- Reduction of 10% in BSFC and 33% in Soot compared with reference at ISO-NO_x.

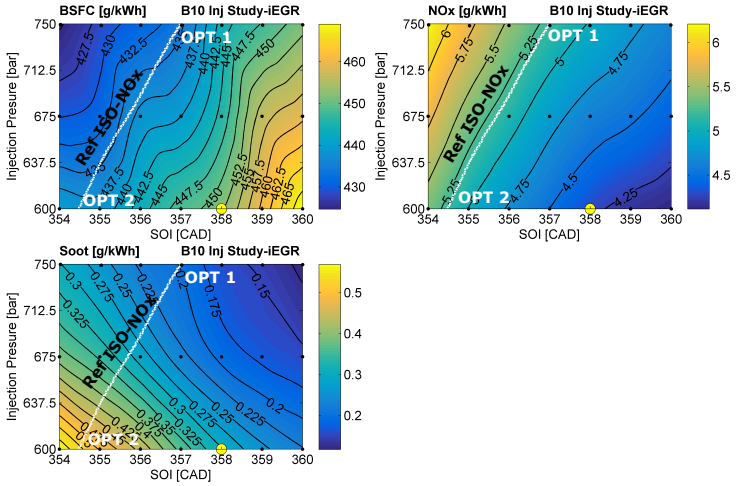

Figure 6.8: B10 iEGR ISO-NO_x optimization

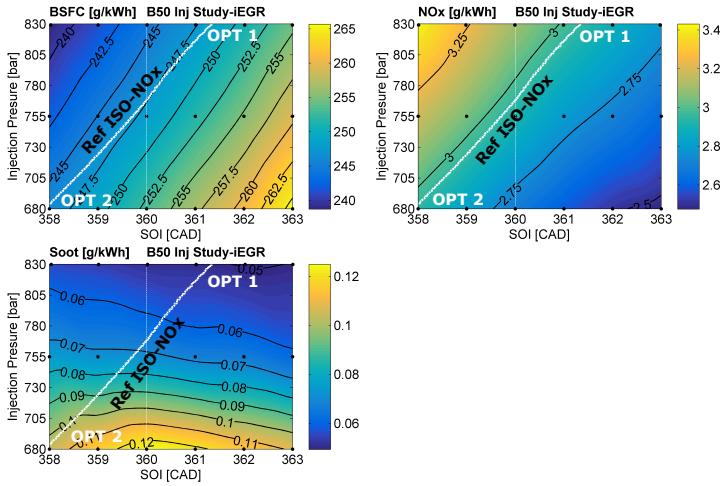

Figure 6.9: B50 iEGR ISO-NO_x optimization

Focusing now in the B50 operating condition, the results observed in Fig. 6.9 continue with the trend observed in the previous discussed B10 point. The ISO-NO_x reference conditions is found with a combination of high injection pressure and early SOI allowing the reduction of fuel consumption.

- Reduction of 13% in NO_x and reduction of 27% in Soot compared with reference at ISO-NO_x.
- Reduction of 12% in NO_x and 64% in Soot compared with reference at ISO-NO_x.

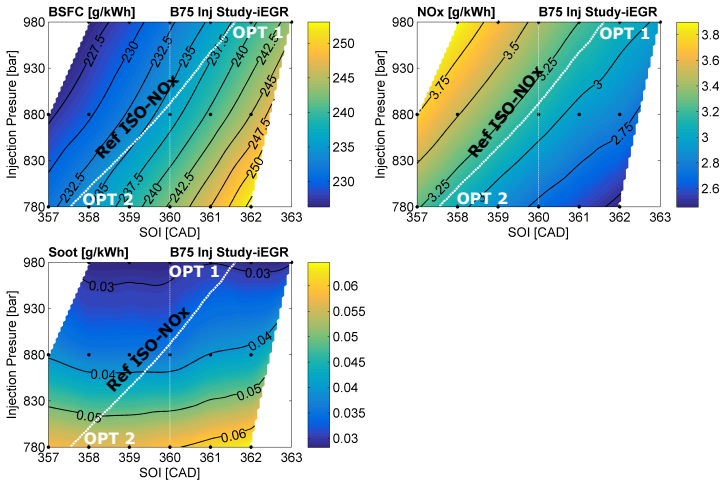

Figure 6.10: B75 iEGR ISO-NO_x optimization

The highest engine load evaluated in the high engine speed is the B75 operating condition. B75 point results are depicted in Fig. 6.10. As could be observed, the trend described in previous discussed points leads to the same combination of injection parameters advancing the SOI combined with the injection pressure increase in order to reach the ISO-NO_x reference.

- Reduction of 15% in NO_x and reduction of 44% in Soot compared with reference at ISO-NO_x.
- Reduction of 13% in NO_x and 72% in Soot compared with reference at ISO-NO_x.

6.3.4 Summary of iEGR strategy study

In the same way than performed for Miller profile in the previous section, they are detailed the parametric studies performed combining the iEGR air management strategy and the injection-combustion parameters. The Table 6.4 summarize the optimization performed at ISO-NO_x at each engine operating condition.

Operating	Optimization 1[%]			Optimization 2 [%]		
Condition	NO_x	Soot	BSFC	NO_x	Soot	BSFC
A50	ISO	-5	-4	ISO	150	-5
A75	ISO	-5	-4	ISO	160	-6
B10	ISO	-33	-10	ISO	78	-8
B50	ISO	-64	-12	ISO	-27	-13
B75	ISO	-72	-13	ISO	-44	-15

Table 6.4: Results under iEGR strategy at reference ISO-NO_x conditions

The iEGR air management strategy combined with the injection parameters optimization give us a set of conclusions which could be extracted from the summary Table 6.2.

- Differently than Miller, in the medium engine speed points A50 and A75 where the ISO-NO_x condition allow the increase of the injection pressure, it helps to obtain gains in the BSFC combined with Soot improvements.
- At low load B10 engine operating condition, the iEGR is not as good as the Miller camshaft profile allow which allow highest increase in the injection pressure in this engine zone.
- The high influence of the pumping loop improvement under the iEGR air management strategy helps to reduce even more the fuel consumption in both evaluated optimization.

6.4 Strategies optimization comparison

After all regulated engine operating condition optimization under each studied camshaft profile a complete comparison of the strategies is proposed in the current section. For this purpose the emission framework discussed in the chapter 1 is used like a reference to define the limits and benefits of each strategy. The comparison is done classifying the optimization results in the structure maintained along the chapter dividing them by engine speed.

6.4.1 Medium engine speed conditions

The three operating conditions at medium engine speed previously discussed are evaluated under each camshaft strategy. As could be observed in Fig. 6.11 (A50, A75 and A100) these are the plots where the standard air

management strategy is compared with the Miller and iEGR camshaft and their optimization. In the left side of the plot are placed the results in a NO_x-Soot trade-off which defines the limits of each EURO legislation and in the right side the diagram bar helps to compare the fuel consumption being in blue the standard hardware and in white after the injection optimization with each tested camshaft.

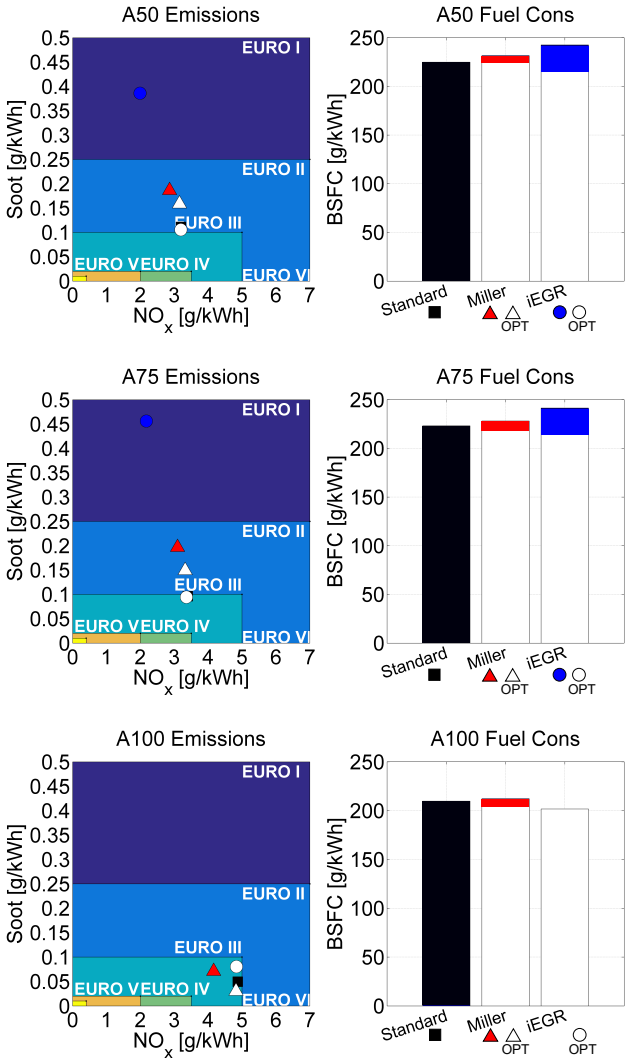

Figure 6.11: Medium engine speed all strategies and optimization

- The standard hardware at A50 operating condition is on the limit of EURO III regulation and neither iEGR or Miller optimized strategies

could improve the current emissions trade off. The potential of the iEGR strategy is identified in the BSFC due to fuel consumption reduction at ISO-NO_x condition keeping the same emission levels than standard reference.

- Similarly than A50 operating condition the A75 point is on the limit of EURO III regulation and neither iEGR or Miller optimized strategies could improve the current emissions trade off. The potential of the iEGR strategy is identified in the BSFC due to fuel consumption reduction at ISO-NO_x condition keeping the same emission levels than standard reference.

- In the full load A100 operating condition slight reduction in Soot emission could be reached with the Miller optimized profile at ISO-NO_x, combined with slight improvement in the fuel consumption.

6.4.2 High engine speed conditions

In the case of high engine speed operating conditions, the comparison of each studied air management strategy is done in the current subsection. Fig. 6.12 and Fig. 6.13 allow to put in the same framework the Miller and the iEGR results and their optimization. The Low load and medium load results (B10 and B50) are compared in the Fig. 6.12 while the high and full load (B75 and B100) are depicted in the Fig. 6.13. As in the medium speed engine points, in the left side of the plot are placed the results in a NO_x-Soot trade-off which defines the limits of each EURO legislation and in the right side the diagram bar helps to compare the fuel consumption.

- The standard hardware at low load B10 operating condition is not well optimized and the pollutants trade off is in the EURO I zone. The iEGR and Miller optimized strategies could improve the current emissions trade off with interesting potential in the fuel consumption reduction at ISO-NO_x condition reducing the Soot emission levels compared with the reference.

- In the medium load B50 operating condition improvements in Soot emission could be reached with the Miller and the iEGR optimized profile at ISO-NO_x. These pollutant improvement are combined with several in reduction in the fuel consumption.

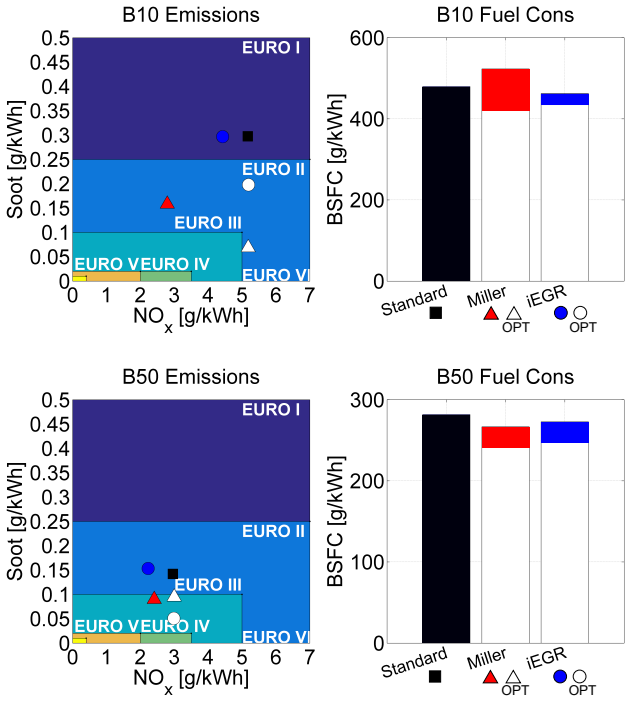

Figure 6.12: B10 and B50 comparison under all strategies and optimization

- The B75 operating condition only the iEGR optimized strategy could improve the standard emissions trade off. The potential of both optimized strategies is identified in the BSFC due to fuel consumption reduction at ISO-NO_x.
- In the high speed full load B100 operating condition slight reduction in Soot emission could be reached with the iEGR optimized profile at ISO-NO_x. As all the previous engine points the cost-effective strategies show a good potential in the engine efficiency.

6.5 Weighing of the Miller and iEGR strategies

The previous section 6.2 and 6.3 are dedicated to understand and quantify the use of the air management strategies and their optimization through the injection settings parameter specifically for each operating condition. Later in section 6.4 the optimized engine points are compared in a common emission legislation framework. Perhaps this emission legislation defines a pollutants limit for all the engine operation range. For this purpose each studied engine

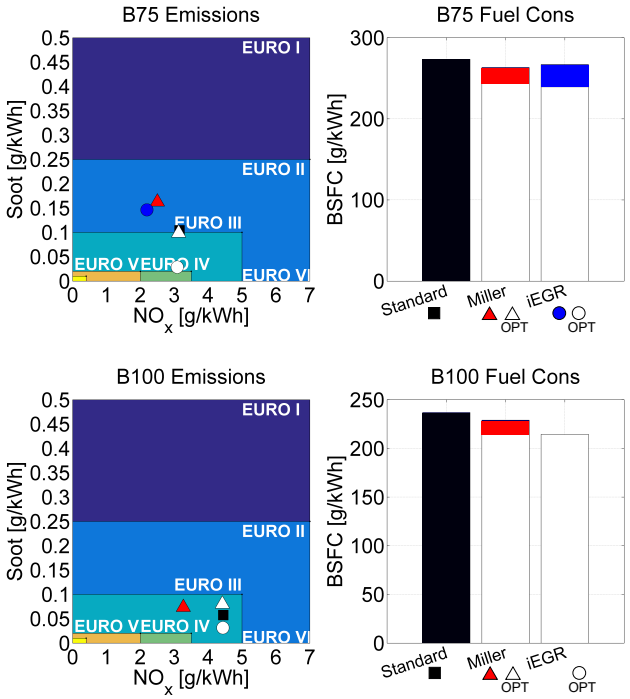

Figure 6.13: B75 and B100 comparison under all strategies and optimization

point has a weight in the normative ISO. [7] thus in the current section the weighing of all the studied engine points is discussed.

6.5.1 Engine operating conditions weighing

First of all they are defined each engine point weight as described by the ISO emission legislation [7]. The Fig. 6.14 depicts per each operating condition the factor which affects the emissions value. After the weighing of all the emissions values per each operating point they are added defining in this way the total engine emissions in NO_x and Soot. Despite is not regulated in the legislation the same weighing procedure could be applied over the engine fuel consumption. In this way it could be compared the improvements or affectations in the pollutants with the engine efficiency.

6.5.2 Cost-Effective strategies limits

The results of weighing procedure are shown in Fig. 6.15. The plot keeps the structure of one by one results description as it is done in the section

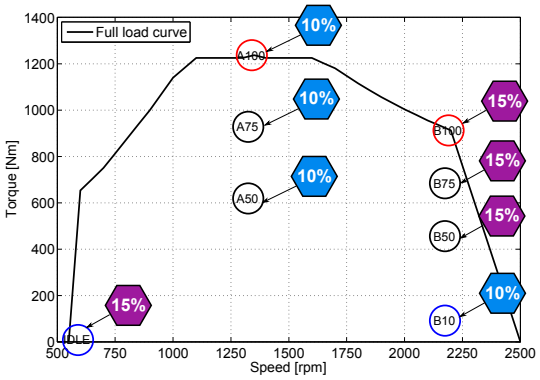

Figure 6.14: Engine operating conditions weigths

6.4 allowing to compare the final engine definition in the emission legislation framework. In this plot are compared the engine pollutants under the standard engine hardware, the integration of air management modification and their optimization. For each studied cases added to emissions the engine efficiency could be evaluated trough the comparison of the engine fuel consumption. Based on Fig. 6.15, the main conclusions of the strategies comparison could be extracted.

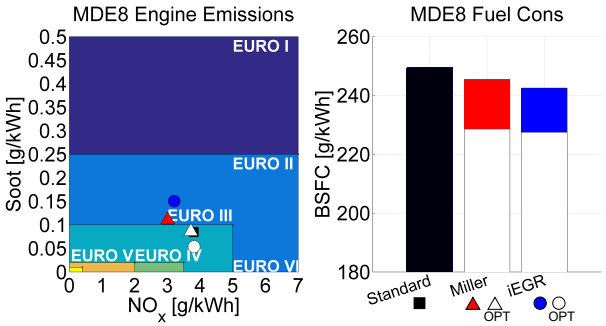

Figure 6.15: Cost-Effective engine definition comparison

- The Miller and iEGR air management strategies have not enough potential to evolve in an stringent emission legislation framework as EURO IV o later ones. Without injection parameters optimization the Miller air management strategy is the cost-effective one which less emission affectation compared with the Standard reference. With this strategy there are gains in terms of NO_x emission and BSFC with slight penalization in the Soot.

- Integrating another cost-effective strategy as the injection parameters optimization, it is possible to preserve (Miller profile) or reduce the Soot emissions (iEGR profile) keeping the ISO-NO_x standard reference value.
- There is an interesting potential in terms of BSFC improvements by using these cost-effective strategies. The engine fuel consumption could be reduced between 8% and 10% with a good optimization work.
- The characteristic of the optimization process is the injection pressure increase which leads to better mix process. The combination of better mixing process with the pumping loop reduction is the main reason to obtain these important BSFC reduction.

Bibliography

[1] Balaji J., Ganesh Prasad M. V., L. Navaneetha R.., Bandaru B. and Ramesh A. "Modelling and Experimental Study of Internal EGR System for NOx Control on an Off-Road Diesel Engine". *SAE Technical Paper-2014-01-2645*, 2014. doi:10.4271/2014-01-2645.

[2] Benajes J., Molina S., Martín J. and Novella R. "Effect of advancing the closing angle of the intake valves on diffusion-controlled combustion in a HD diesel engine". *Applied Thermal Engineering*, Vol. 29, pp. 1947–1954, 2009.

[3] Park S., Kim Y., Woo S. and Lee K. "Optimization and calibration strategy using design of experiment for a diesel engine". *Applied Thermal Engineering*, Vol. 123, pp. 917–928, 2017.

[4] Bermúdez V., Molina S., Novella R. and Estepa D. "Experimental Study of Two Air Management Strategies for Emissions Control in Heavy Duty Engines at Medium to High Loads". *Energy & Fuels*, Vol. 31 n^o 9, pp. 10011–10022, 2017.

[5] Benajes J., Serrano J.R., Molina S. and Novella R. "Potential of Atkinson cycle combined with EGR for pollutant control in a HD diesel engine". *Energy Conversion and Management*, Vol. 50, pp. 174–183, 2008.

[6] Schwoerer J., Dodi S., Fox M., Huang S. and Yang Z. "Internal EGR Systems for NOx Emission Reduction in Heavy-Duty Diesel Engines". *SAE Technical Paper-2004-01-1315*, 2004. doi:10.4271/2004-01-1315.

[7] International standards ISO. *ISO 8178-4 recopricating internal combustion engines - exhasut emissions measurement*. ISO International standards, 2007.

Chapter 7

Conclusions and future work

Contents

7.1 Introduction

The research work presented on this thesis represents a contribution to the evaluation of cost-effective emission control strategies in the development and optimization of the combustion system of an stringent pollutant framework in emerging markets which are passing from EURO III to EURO IV emission limits. This final chapter outlines the main conclusions and scientific contributions of this research work, and highlights the most relevant results obtained along the different stages of this investigation, with the aim of proposing new research paths in heavy duty Diesel engines and their pollutant control strategies. In a second step, new possible research directions are formulated together with the recommendation of future tasks and studies, which are based on the knowledge and experience acquired along the practical execution and posterior analysis of the different studies proposed in this investigation.

7.2 Summary of thesis development and main conclusions

Before summarizing the most relevant outcomes and contributions achieved by the thesis, it might by useful to take back the global context and the general objectives proposed for this investigation. As it was discussed in chapter 1, this research work has been established in a difficult context marked by the growing technological challenges for the heavy duty Diesel engine industry, which has to be in constant evolution to face and successfully overcome more severe legislation for the regulated emissions (NO_x, Soot, HC and CO). All of this is added to the already complex and rapidly changing regional and global markets specially in emerging markets where the cost of the platforms plays a key role in the technological integration.

From the literature review performed on chapter 2, it was possible to understand the fundamental aspects related to the physical and chemical mechanisms occurring inside the combustion chamber of a direct injection CI Diesel engine, in the frame of mixing-controlled conventional Diesel combustion. In this case, the ignition and combustion of the cylinder charge typically occur while the fuel is still being injected and mixed with the surrounding air, so the combustion rate is controlled by the injection and air entrainment rate into the fuel spray, and the fuel-air mixture spans a wide range of local equivalence rations and temperatures along the combustion process, which promote the formation of both NO_x and Soot emissions.

After identifying the main process in the conventional Diesel combustion which are directly related in the NO_x and Soot formation, the literature review described in the same chapter allow to identify the main technological answer which the industry has faced the multiple challenges proposed by the different emission legislation policies. In an emerging markets environment the cost of each technology must be defined in order to define the cost-effective strategies which help to control the described Diesel engine pollutants. After this evaluation a set of cost-effective pollutant control strategies are proposed and placed in a scientific context where the main contributions of the research community are described giving the first approach to later define a set of theoretical and experimental tools in order to evaluate these strategies in one specific platform.

In the chapter 3, all the theoretical and experimental tools are described. The experimental tools and methodologies are detailed in order to have a complete overview of all the equipment and procedures which allow to evaluate the selected strategies, while in the theoretical description the different used models are depicted with all the calibration process.

The chapters 4, 5 and 6 could be grouped as the thesis results chapters and their conclusions are discussed separately in the next subsections.

7.2.1 The injection parameters exploration

As discussed in chapter 4, Electronically controlled fuel injection system allows controlling multiple injection strategies such as: the control of injection timing, pilot injection, post injection and injection pressure. As shown in the chapter development, this flexibility raise the challenge to manage with all these parameters in the design and calibration process of the combustion system in the heavy duty CI engines. In this chapter, the geometrical configuration of the combustion chamber and the injection parameters bring the opportunity to optimize the combustion system achieving low levels on emissions and improvements on engine efficiency. Hence in a framework of restrictive legislation for emerging markets optimizing this injection variables is an interesting cost-effective measure to control pollutants keeping the legislation levels. The main conclusions obtained from this chapter are now detailed.

- As expected based on the bibliographical research, the best NO_x scenario was found and quantified in the lowest injection pressure combined with delayed SoI for all tested operating conditions.

- Similar to previous conclusion, as expected based on the bibliographical research, the best BSFC scenario was found in the highest injection pressure combined with the early SoI for all tested operating conditions.
- The best Soot scenario was found always in the highest injection pressure having different behavior when SoI is evaluated. In this case from medium speed engine conditions until B10 the minimum soot was found in the delayed SoI but for B50, B75 and B100 it moves to earliest SoI.
- The Swirl number=1.5 which is the current engine Swirl is near to the optimum ISFC for the current d/B piston relation, NA and S as could be identified in Fig. 4.17. From where it could be establish than the geometric design was favored to keep lower BSFC from air motion point of view.
- As mentioned in the Pareto Diagram selection discussed in the chapter 4, the NA does not have a big influence in the NO_x behavior for the evaluated ranges, perhaps it recover importance when the ISFC Soot emissions are evaluated.

Although the combustion hardware matching is a cost-effective pollutant control strategy with an interesting potential as previously observed, unfortunately has not been experimental validated in the thesis development due to high cost in the implementation of hardware modification for only one engine unit.

7.2.2 The air management strategies

The chapter 5 is dedicated to the strategies related with the engine air management. In this case the first section allow to develop the procedure to select the engine hardware between a group of candidates using the 1D simulation tool GT Power. Through 1D engine model configured and validated in section 3.3.3 coupled with the air management maps, different options are evaluated for each strategy defining one profile per strategy to be finally machining and tested.

Later in the second section, the experimental validation of each chosen Miller or iEGR cam profile over a group of engine operating conditions, classified by engine load, help to define the main characteristics of each camshaft as well that all the particularities in the combustion process and engine emissions a work which is detailed in the paper published by Bermúdez et al. [1]. The main conclusions obtained from this chapter are now detailed.

- Concerning NO_x emission in Fig. 5.20 could be observed how all the camshaft strategies are focused in the NO_x reduction.

- In most of part load engine operating conditions except the B10 point the highest reduction in terms of NO_x emission are achieved by the iEGR camshaft profile being penalized by the high increase of Soot and fuel consumption in medium speed points.

- In terms of engine efficiency based on the engine fuel consumption, both camshaft have demonstrated the important influence of the pumping loop in the high speed operating conditions (B points) both in partial loads and full load as explained in section 5.3.

- The BSFC is improved as well than NO_x emission in the high speed engine conditions a very interesting behavior of the tested air management strategies.

- The NO_x reduction achieved by the tested air management strategies is higher than the obtained by the injection settings explored in the chapter 4. If it is considered than the air management strategies causes a total effect over all the engine map and the injection settings could be used as a local tuning (point by point) there is an interesting optimization way combining the strategies studied in chapter 4 and chapter 5 which are the basic idea explored in the chapter 6.

7.2.3 Potential of the cost-effective strategies combination

In the the previous subsection were discussed the effects of the injection-combustion and the air management which have demonstrated their efficacy in order to control engine emissions, increase the engine efficiency and in some cases both of them. As mentioned in the air management strategies conclusions these strategies are not mutually exclusive enabling the possibility of combining both in order to define the potential of these cost-effective strategies.

The Miller and iEGR strategies were combined with the injection-combustion parameters with interesting results individually described as well as, the engine global behavior was evaluated weighing each engine point as defined in the emissions legislation. this is the proposed methodology in order to evaluate the real limits of each cost-effective engine definition and the main conclusions obtained from this chapter are now detailed.

- The Miller and iEGR air management strategies have not enough potential to evolve in an stringent emission legislation framework as EURO IV o later ones. Without any injection parameters optimization the Miller air management strategy is the cost-effective one which less emission affectation compared with the Standard reference. With this strategy there are gains in terms of NO_x emission and BSFC with slight penalization in the Soot.

- Integrating another cost-effective strategy as the injection parameters optimization, it is possible to preserve in the case of Miller profile or reduce the Soot emissions for the iEGR one, keeping the ISO-NO_x standard reference value.

- There is an interesting potential in terms of BSFC improvements by using these cost-effective strategies. The engine fuel consumption could be reduced between 8% and 10% with a good optimization work.

- The main characteristic of the optimization process is the injection pressure increase which leads to better mix process. The combination of better mixing process with the pumping loop reduction is the main reason to obtain these important BSFC reductions.

7.3 Future work and new research paths

Besides the fully work performed to study and quantify experimentally the real effect of the selected cost-effective pollutant control strategies discussed in Fig. 2.6, some of them were not addressed during this developed work and the potential to go deep in their knowledge remains as a future work.

- As mentioned before, although the combustion hardware matching is a cost-effective pollutant control strategy with an interesting potential as described in chapter 4, unfortunately has not been experimental validated in the thesis development due to high cost in the implementation of hardware modification for only one engine unit. Hence Some efforts could be interesting to do as a future work to experimentally validate these results.

- Integrating another cost-effective strategy as the geometric variable turbo as part of the air handling system. The traditional turbochargers have a narrow operational range which leaves low-speed and high-torque operating conditions with less air than required for the most efficient

combustion. Geometric variable turbo could provide the right amount of air under a wider range of engine operating conditions combined with the including at low speed and high torque and could be combined with the injection settings and hardware optimization as well with the different camshaft profiles.

- Integrating another cost-effective strategy as the EGR cooled or not cooled. An EGR system which recirculates a portion of exhaust gas back to the engine's cylinders. Nowdays EGR is the most widely used technology for in-cylinder NO_x reduction in Diesel-powered engines therefore it could be interesting to evaluate the possible combination of EGR and the air management strategies as a Miller cycle in a stringent emission legislation framework for emerging markets.

7.3.1 The potential in CO_2 reduction

Until 2017, a European Union regulatory procedure to determine and certify the CO_2 emissions and fuel consumption of heavy-duty vehicles did not exist. Heavy-duty vehicles are currently responsible for about a quarter of the CO_2 emissions from road transportation in the European Union as discussed in chapter 1, and are set to increase by as much as 10% by 2030, representing 32% of the on-road CO_2 emissions in 2030 [2]. To attain the EU target of reducing CO_2 emissions from transport by 60% in 2050 compared with 1990 levels, it is necessary to introduce policy measures that accelerate the introduction of energy-efficient heavy-duty vehicles into the market.

The first of these policy measures is the introduction of a certification procedure for the CO_2 emissions and fuel consumption of heavy-duty vehicles. Regulation (EC) No 595/20095 mandated the European Commission to develop such a certification procedure as discussed on May 2017, during the 67th meeting of the Technical Committee Motor Vehicles. In this committee the different member states of the European Union unanimously adopted a draft implementing act put forward by the European Commission on the certification of the CO_2 emissions and fuel consumption of heavy-duty vehicles.

Starting January, 2019, heavy-duty vehicles belonging to one of the four vehicle groups with the highest contribution to on-road freight carbon emissions will be certified for their CO_2 emissions and fuel consumption. Six additional heavy-duty vehicle groups will be required to be certified for CO_2 emissions and fuel consumption by January, 2020.

Due to diversity of configurations in the heavy-duty sector and associated this diversity testing challenges, carrying out the CO_2 certification in the same

way as passenger and light commercial vehicles is not viable. Therefore, a simulation-based approach was selected to determine the CO_2 emissions and fuel consumption of the heavy-duty vehicles. Internationally, the use of component testing and vehicle simulation for the CO_2 certification of heavy-duty vehicles is not a new approach; the United States, Canada, China, and Japan use vehicle simulation in some form for certification in their heavy-duty vehicle CO_2 standards. In the EU, Directive 2007/46/EC established the general framework that allows virtual testing in the type-approval process.

The methodology for certification of CO_2 emissions from heavy-duty vehicles is based on tests of the individual components of the vehicle and a subsequent simulation of fuel consumption and CO_2 emissions of the entire vehicle. This approach offers the possibility to accurately capture the highly diverse characteristics of the vehicle configuration and their influence on fuel consumption and CO_2 emissions, without heavily increasing the complexity and the costs for each certification.

As one of the central parts in the development of the CO_2 certification procedure the committee has launched the development of a "Vehicle Energy Consumption calculation Tool" (VECTO). VECTO simulates CO_2 emissions and fuel consumption based on vehicle longitudinal dynamics using a driver model for backward simulation of target speed cycles. The required load to be delivered by the internal combustion engine is calculated based on the driving resistances, the power losses in the drivetrain system and the power consumption of the vehicle auxiliary units. Engine speed is determined based on a gear shift model, the gear ratios and the wheel diameter. Fuel consumption is then interpolated from an engine fuel map. CO_2 emissions are calculated based on fuel consumption and reference fuel specifications [3].

As demonstrated with the cost-effective strategies evaluated along this thesis, these kind of approaches have not a great potential to fulfill more exigent pollutant emission regulation policies later than EURO IV, but as discussed in the conclusions, they have demonstrated an interesting capacity to reduce the engine fuel consumption improving the engine efficiency. Hence in a framework of regulated CO_2 emission as depicted in this section background, the future European legislation could need improvements of engine fuel consumption which lead to reduce these engine CO_2 emissions and the cost-effective strategies evaluated in this research work could help to accomplish these new exigences.

Bibliography

[1] Bermúdez V., Molina S., Novella R. and Estepa D. "Experimental Study of Two Air Management Strategies for Emissions Control in Heavy Duty Engines at Medium to High Loads". *Energy & Fuels*, Vol. 31 n^o 9, pp. 10011–10022, 2017.

[2] ICCT POLICY UPDATE. *Certification of CO2 emissions and fuel consumption of on-road heavy-duty vehicles in the european union.* The international council of clean transportation, 2017.

[3] Rexeis M., Quaritsch M., Hausberger S., Silberholz G., Kies A., Steven H. and Vermeulen R. *VECTO tool development: Completion of methodology to simulate Heavy Duty Vehicles' fuel consumption and CO2 emissions.* European Comission, 2017.

Bibliography

-.
AVL 364 angular encoder.
Available technical information in http://www.avl.com. (cited on p. 51)

-.
AVL 415 Smoke meter.
Available technical information in http://www.avl.com. (cited on p. 54)

-.
AVL 439 Smoke meter.
Available technical information in http://www.avl.com. (cited on p. 54)

-.
AVL 733S fuel balance.
Available technical information in http://www.avl.com. (cited on p. 52)

-.
Horiba MEXA 7100 DEGR exhaust gas analyzer.
Available technical information in http://www.ats.horiba.com. (cited on p. 53)

-.
Kistler 4045A10 transducer.
Available technical information in http://www.kistler.com. (cited on p. 52)

-.
Kistler 46125c transducer.
Available technical information in http://www.kistler.com. (cited on p. 52)

-.
Linear Transducer WAL by HBM.
Available technical information in https://www.hbm.com. (cited on p. 55)

-.
Sensyflow FMT500IG hotfilm anemometer.
Available technical information in http://www.abb.com. (cited on p. 52)

-.
Yokogawa DL708E oscillographic recorder.
Available technical information in http://www.yokogawa.com. (cited on p. 50)

Abouri D., Zellat M., Duranti S. and Ravet F.
Advances in combustion modeling in Star-CD:Validation of ECFM CLE-H model to engine analysis.
SAE International, 2008. (cited on p. 69)

Agarwal A. Kumar, Srivastava D. K., Dhar A., Maurya R. K., Shukla P. C. and Singh A. P.
Effect of fuel injection timing and pressure on combustion, emissions and performance characteristics of a single cylinder diesel engine.
Fuel, Vol. 111, pp. 374–383, 2013. (cited on p. 31)

Agency European Environment.
Emissions of primary PM2.5 and PM10 particulate matter.
European Environment Agency, 2010. (cited on p. 3)

air technology center (MD-12) Clean.
Nitrogen oxides (NOx), why and how they are controlled.
Environmental Protection Agency, 1999. (cited on p. 4)

Angelberger C., Poinsot T. and Delhay B.
Improving Near Wall Combustion and Wall Heat Transfer Modeling in SI Engine Computations.
SAE International, 1997.
972881. (cited on p. 69)

Armas O.
Diagnóstico experimental del proceso de combustión en motores Diesel de inyección directa.
Doctoral Thesis, Universidad Politécnica de Valencia, Departamento de Máquinas y Motores Térmicos, 2005. (cited on p. 60)

Arrègle J., López J. J., García J. M. and Fenollosa C.
Development of a zero-dimensional Diesel combustion model. Part 1: Analysis of the quasi-steady diffusion combustion phase.
Applied Thermal Engineering, Vol. 23 n^o 11, pp. 1301–1317, 2003. (cited on p. 23)

Arrègle J., López J. J., García J. M. and Fenollosa C.
Development of a zero-dimensional Diesel combustion model: Part 2: Analysis of the transient initial and final diffusion combustion phases.
Applied Thermal Engineering, Vol. 23 n^o 11, pp. 1319–1331, 2003. (cited on p. 23)

Association Manufacturers Emission Controls.
Emission Control Technologies for Diesel-Powered Vehicles.
Manufacturers of Emission Controls Association, 2007. (cited on p. 8)

Badami M., Mallamo F., Millo F. and Rossi E. E.
Influence of Multiple Injection Strategies on Emissions, Combustion Noise and BSFC of a DI Common Rail Diesel Engine.
SAE International, 2002. (cited on p. 31)

Balaji J., Ganesh Prasad M. V., L. Navaneetha R.., Bandaru B. and Ramesh A.
Modelling and Experimental Study of Internal EGR System for NOx Control on an Off-Road Diesel Engine.
SAE Technical Paper-2014-01-2645, 2014.
doi:10.4271/2014-01-2645. (cited on pp. 38, 104, 126)

Beatrice C., Napolitano P. and Guido C.
Injection parameter optimization by DoE of a light-duty diesel engine fed by Bio-ethanol/RME/diesel blend.
Applied Energy, Vol. 113, pp. 373–384, 2014. (cited on p. 77)

Beatrice C., Rispoli N., Di Blasio G., atrianakos G., Kostoglou M., Konstandopoulos A. G., Imren A., Denbratt I. and Palacin R.
Emission Reduction Technologies for the Future Low Emission Rail Diesel Engines: EGR vs SCR.
SAE Technical Paper-, 2013.
2013-24-0087. (cited on p. 25)

Beatrice C., Rispoli N., Di Blasio G., Konstandopoulos A. G., Papaioannou E. and Imren A.
Impact of Emerging Engine and After-Treatment Technologies for Improved Fuel Efficiency and Emission Reduction for the Future Rail Diesel Engines.
Emiss. Control Sci. Technol, 2016.
DOI 10.1007/s40825-016-0035-1. (cited on p. 30)

Benajes J., López J. J., Novella R. and García A.
Advanced methodology for improving testing efficiency in a single-cylinder research Diesel engine.
Experimental Techniques, doi: 10.1111/j.1747-1567.2007.00296.x, 2007.
(cited on p. 56)

Benajes J., Molina S., Martín J. and Novella R.
Effect of advancing the closing angle of the intake valves on diffusion-controlled combustion in a HD diesel engine.
Applied Thermal Engineering, Vol. 29, pp. 1947–1954, 2009. (cited on pp. 112, 126)

Benajes J., Molina S., Novella R., Amorim R., Hamouda H. B. H. and Hardy J. P.
Comparison of two injection systems in an HSDI diesel engine using split injection and different injector nozzles.
International Journal of Automotive Technology, Vol. 11 n^o 2, pp. 139–146, 2010.
(cited on p. 82)

Benajes J., Molina S., Novella R. and Belarte E.
Evaluation of massive exhaust gas recirculation and Miller cycle strategies for mixing-controlled low temperature combustion in a heavy duty diesel engine.
Energy, Vol. 71, pp. 355–366, 2014. (cited on pp. 36, 81)

Benajes J., Novella R., García A. and Arthozoul S.
The role of in-cylinder gas density and oxygen concentration on late spray mixing and soot oxidation processes.
Energy, Vol. 36 n^o 3, pp. 1599–1611, 2011. (cited on p. 111)

Benajes J., Novella R., Pastor J. M., Hernández-López A., Hasegawa M., Tsuji N., Emi M., Uehara I., Martorell J. and Alonso M.
Optimization of the combustion system of a medium duty direct injection diesel engine by combining CFD modeling with experimental validation.
Energy Conversion and Management, Vol. 110, pp. 212–229, 2016. (cited on p. 90)

Benajes J., Serrano J.R., Molina S. and Novella R.
Potential of Atkinson cycle combined with EGR for pollutant control in a HD diesel engine.
Energy Conversion and Management, Vol. 50, pp. 174–183, 2008. (cited on pp. 107, 132)

Bermúdez V., Molina S., Novella R. and Estepa D.
Experimental Study of Two Air Management Strategies for Emissions Control in Heavy Duty Engines at Medium to High Loads.
Energy & Fuels, Vol. 31 n^o 9, pp. 10011–10022, 2017. (cited on pp. 102, 127, 148)

Blumberg K. O., Wals M. P. and Charlotte P.
Low-sulfur gasoline & Diesel: The key to lower vehicle emissions.
The international council of clean transportation (ICCT), 2003. (cited on p. 7)

Boulouchos K. and Stebler H.
Combustion Features and Emissions of a DI-Diesel Engine with Air Path Optimization and Common Rail Fuel Injection.
SAE Technical Paper, 1998.
981931. (cited on p. 36)

Briani M., Fraioli V., Migliaccio M., Di Blasio G., Lucchini T. and Ettorre D.
Multi-Dimensional Modeling of Combustion in Compression Ignition Engines Operating with Variable Charge Premixing Levels.
SAE Technical Paper-, 2011.
2011-24-0027. (cited on p. 69)

Bruneaux G.
Mixing Process in High Pressure Diesel Jets by Normalized Laser Induced Exciplex Fluorescence Part I: Free Jet.
SAE International, 2005. (cited on p. 23)

Chan T. L. and Cheng X. B.
Numerical Modeling and Experimental Study of Combustion and Soot Formation in a Direct Injection Diesel Engine.
Energy & Fuels, Vol. 21 n^o 3, pp. 1483–1492, 2007. (cited on p. 69)

Chartier C., Aronsson U., Andersson, Ö.and Egnell R., Collin R., Seyfried H., Richter M. and Aldén M.
Analysis of Smokeless Spray Combustion in a Heavy-Duty Diesel Engine by Combined Simultaneous Optical Diagnostics.
SAE International, 2009. (cited on p. 20)

Cocker D. R., Shah S. D., Johnson K., Miller J. W. and Norbeck J. M.
Development and Application of a Mobile Laboratory for Measuring Emissions from Diesel Engines. 1. Regulated Gaseous Emissions.
Environmental Science & Technology, Vol. 38 n^o 7, pp. 2182–2189, 2004. (cited on p. 78)

Correas D.
Estudio Teórico-Experimental del chorro libre diesel isotermo.
Doctoral Thesis, Universidad Politécnica de Valencia, Departamento de Máquinas y Motores Térmicos, 1998. (cited on p. 17)

de Lima D.
Analysis of combustion concepts in a poppet valve two-stroke downsized compression ignition engine designed for passenger car applications.
Doctoral Thesis, Universidad Politécnica de Valencia, Departamento de Máquinas y Motores Térmicos, 2016. (cited on pp. 63, 96)

de Risi A., Donateo T. and Laforgia D.
Optimization of the Combustion Chamber of Direct Injection Diesel Engines.
SAE International, 2003. (cited on p. 34)

Dec J. E.
A Conceptual Model of DI Diesel Combustion Based on Laser-Sheet Imaging*.
SAE International, 1997. (cited on pp. 16, 18, 20)

Dec J. E. and Canaan R. E.
PLIF Imaging of NO Formation in a DI Diesel Engine1.
SAE International, 1998. (cited on p. 22)

Dec J. E. and Coy E. B.
OH Radical Imaging in a DI Diesel Engine and the Structure of the Early Diffusion Flame.
SAE International, 1996. (cited on p. 20)

Dec J. E. and Tree D. R.
Diffusion-Flame / Wall Interactions in a Heavy-Duty DI Diesel Engine.
SAE International, 2001. (cited on p. 22)

Desantes J. M., Benájes J., Molina S. and González C. A.
The modification of the fuel injection rate in heavy-duty diesel engines. Part 1: Effects on engine performance and emissions.
Applied Thermal Engineering, Vol. 24 n^o 17, pp. 2701–2714, 2004. (cited on p. 32)

Desantes J. M., Benájes J., Molina S. and González C. A.
The modification of the fuel injection rate in heavy-duty diesel engines: Part 2: Effects on combustion.
Applied Thermal Engineering, Vol. 24 n^o 17, pp. 2715–2726, 2004. (cited on p. 32)

Desantes J. M., López J. J., García J. M. and Pastor J. M.
Evaporative Diesel Spray Modeling.
Atomization and Sprays, Vol. 17 n^o 3, pp. 193–231, 2007. (cited on p. 18)

Dodge L. G., Simescu S., Neely G. D., Maymar M. J., Dickey D. W. and Savonen C. L.
Effect of Small Holes and High Injection Pressures on Diesel Engine Combustion.
SAE International, 2002. (cited on p. 31)

Fjällman J.
GT-Power Report.
KTH Mechanics., 2014. (cited on p. 67)

Flynn P. F., Durrett R. P., Hunter G. L., zur Loye A. O., Akinyemi O. C., Dec J. E. and Westbrook C. K.
Diesel Combustion: An Integrated View Combining Laser Diagnostics, Chemical Kinetics, And Empirical Validation.
SAE International, 1999. (cited on pp. 16, 18, 21)

Galindo J., Serrano J. R., Arnau F. J. and Piqueras P.
Description and analysis of a one-dimensional gas-dynamic model with independent time discretization.
Proceedings of the ASME Internal Combustion Engine Division 2008 Spring Technical Conference, 2008. (cited on p. 65)

Gamma Technologies INC.
GT Suite Flow theory manual Version 7.5.
Gamma Technologies, Inc., 2014. (cited on p. 65)

Ge H.W., Shi Y., Reitz R. D., Wickman D. D. and Willems W.
Optimization of a HSDI Diesel Engine for Passenger Cars Using a Multi-Objective Genetic Algorithm and Multi-Dimensional Modeling.
SAE International Journal of Engines, Vol. 2 n^o 1, pp. 691–713, 2009. (cited on p. 33)

Gimeno J.
Desarrollo y aplicacion de la medida del flujo de cantidad de movimiento de un chorro diesel.
Doctoral Thesis, Universidad Politécnica de Valencia, Departamento de Máquinas y Motores Térmicos, 2008. (cited on p. 17)

Gonca G., Sahin B., Parlak, A.and Ust Y., Ayhan, V.and Cesur I. and Boru B.
Theoretical and experimental investigation of the Miller cycle diesel engine in terms of performance and emission parameters.
Applied Energy, Vol. 138, pp. 11–20, 2015. (cited on p. 36)

Habchi C., Lafossas F. A., Béard P. and Broseta D.
Formulation of a One-Component Fuel Lumping Model to Assess the Effects of Fuel Thermodynamic Properties on Internal Combustion Engine Mixture Preparation and Combustion.
SAE International, 2004.
2004-01-1996. (cited on p. 69)

Hagena J. R., Filipi Z. and Assanis D. N.
Transient Diesel Emissions: Analysis of Engine Operation During a Tip-In.
SAE Technical Paper-2006-01-1151, 2006.
doi:10.4271/2006-01-1151. (cited on p. 117)

Hermens S.
Influence of diesel injector nozzle geometry on the injection and combustion process.
Doctoral Thesis, Universidad Politécnica de Valencia, Departamento de Máquinas y Motores Térmicos, 2008. (cited on p. 17)

Hernández Vera I.
Soot modeling in flames and Large-Eddy Simulations of thermo-acoustic instabilities.
2011. (cited on p. 71)

Higgins B., Siebers D. L. and Aradi A.
Diesel-Spray Ignition and Premixed-Burn Behavior.
SAE International, 2000. (cited on p. 20)

Hiwase S. D., Moorthy S., Prasad H., Dumpa M. and Metkar R. M.
Multidimensional Modeling of Direct Injection Diesel Engine with Split Multiple Stage Fuel Injections.
Procedia Engineering, Vol. 51, pp. 670–675, 2013. (cited on p. 31)

Huh KY. and Gosman AD.
A phenomenological model of diesel spray atomization.
Proceedings of the international conference on multiphase flows, 1991. (cited on p. 69)

ICCT POLICY UPDATE.
Certification of CO2 emissions and fuel consumption of on-road heavy-duty vehicles in the european union.
The international council of clean transportation, 2017. (cited on p. 151)

iea International Energy Agency.
CO2 Emissions from Fuel Combustion Highlights.
International Energy Agency iea, 2017. (cited on p. 2)

iea International Energy Agency.
The Future of Trucks Implications for Energy and the Environment.
International Energy Agency iea, 2017. (cited on p. 3)

iea International Energy Agency.
Key world energy statistics.
International Energy Agency iea, 2017. (cited on p. 2)

International standards ISO.
ISO 8178-4 recopricating internal combustion engines - exhasut emissions measurement.
ISO International standards, 2007. (cited on pp. 46, 141)

Issa R. I.
Solution of the implicitly discretised fluid flow equations by operator-splitting.
Journal of Computational Physics, Vol. 62 n^o 1, pp. 40–65, 1986. (cited on p. 70)

Kakaee A. H., Nasiri-Toosi A., Partovi B. and Paykani A.
Effects of piston bowl geometry on combustion and emissions characteristics of a natural gas/diesel RCCI engine.
Applied Thermal Engineering, Vol. 102, pp. 1462–1472, 2016. (cited on p. 91)

Khoobbakht G., Najafi G., Karimi M. and Akram A.
Optimization of operating factors and blended levels of diesel, biodiesel and ethanol fuels to minimize exhaust emissions of diesel engine using response surface methodology.
Applied Thermal Engineering, Vol. 99, pp. 1006–1017, 2016. (cited on p. 76)

Kim T. and Ghandhi J. B.
Quantitative 2-D Fuel Vapor Concentration Measurements in an Evaporating Diesel Spray using the Exciplex Fluorescence Method.
SAE International, 2001. (cited on p. 23)

Kirchen P., Obrecht P. and Boulouchos K.
Soot Emission Measurements and Validation of a Mean Value Soot Model for Common-Rail Diesel Engines during Transient Operation.
SAE Technical Paper-2009-01-1904, 2009.
doi:10.4271/2009-01-1904. (cited on p. 117)

Kohketsu S., Tanabe K. and Mori K.
Flexibly Controlled Injection Rate Shape with Next Generation Common Rail System for Heavy Duty DI Diesel Engines.
SAE International, 2000. (cited on p. 32)

Kosaka H., Aizawa T. and Kamimoto T.
Two-dimensional imaging of ignition and soot formation processes in a diesel flame.
International Journal of Engine Research, Vol. 6 n^o 1, pp. 21–42, 2005. (cited on p. 18)

Kosaka H., Nishigaki T., Kamimoto T., Sano T., Matsutani A. and Harada S.
Simultaneous 2-D Imaging of OH Radicals and Soot in a Diesel Flame by Laser Sheet Techniques.
SAE International, 1996. (cited on p. 22)

Ladommatos N., Song H. and Zhao H.
Measurements and predictions of diesel soot oxidation rates.
Proceedings of the Institution of Mechanical Engineers, Part D: Journal of Automobile Engineering, Vol. 216 n^o 8, pp. 677–689, 2002. (cited on p. 112)

Lapuerta M., Ballesteros R. and Agudelo J. R.
Effect of the gas state equation on the thermodynamic diagnostic of diesel combustion.
Applied Thermal Engineering, Vol. 26 n^o 14-15, pp. 1492–1499, 2006.
(cited on pp. 60, 61)

Lee S. and Park S.
Optimization of the piston bowl geometry and the operating conditions of a gasoline-diesel dual-fuel engine based on a compression ignition engine.
Energy, Vol. 121, pp. 433–448, 2017. (cited on p. 34)

Li J., Yang W. M., An H., Maghbouli A. and Chou S. K.
Effects of piston bowl geometry on combustion and emission characteristics of biodiesel fueled diesel engines.
Fuel, Vol. 120, pp. 66–73, 2014. (cited on p. 91)

Li X., Qiao Z., Su L., Li X. and Liu F.
The combustion and emission characteristics of a multi-swirl combustion system in a DI diesel engine.
Applied Thermal Engineering, Vol. 115, pp. 1203–1212, 2017. (cited on p. 95)

López J.J.
Estudio Teórico-Experimental del chorro libre diesel no evaporativo y de su interacción con el movimiento del aire.
Doctoral Thesis, Universidad Politécnica de Valencia, Departamento de Máquinas y Motores Térmicos, 2003. (cited on p. 17)

Luján JM.
Recirculación interna de gases de combustión en motores Diesel sobrealimentados.
Doctoral Thesis, Universidad Politécnica de Valencia, Departamento de Máquinas y Motores Térmicos, 1998. (cited on pp. 37, 103)

Marchal C.
Soot formation and oxidation modelling in an automotive engine.
Doctoral Thesis, Université d'Orléans, year = 2008. (cited on p. 69)

Martín J.
Aportación al diagnóstico de la combustión en motores Diesel de inyección directa.
Doctoral Thesis, Universidad Politécnica de Valencia, Departamento de Máquinas y Motores Térmicos, 2007. (cited on p. 60)

Meistrick Z., Usko J., Shoyama K., Kijima K., Okazaki T. and Maeda Y.
Integrated Internal EGR and Compression Braking System for Hino's E13C Engine.
SAE Technical Paper, 2004.
2004-01-1313. (cited on p. 38)

Miller J. D. and Façanha C.
The State of clean transport policy.
The international council on clean transportation, 2014. (cited on pp. vi, 2, 3, 4, 5)

Millo F. and Mallamo F.
The Potential of Dual Stage Turbocharging and Miller Cycle for HD Diesel Engines.
SAE Technical Paper-, 2005.
2005-01-0221. (cited on p. 36)

Millo F., Mallamo F., Arnone L., Bonanni M. and Franceschini D.
Analysis of Different Internal EGR Solutions for Small Diesel Engines.
SAE Technical Paper-, 2007.
2007-01-0128. (cited on p. 38)

Mohan B., Yang W. and Chou S. K.
Fuel injection strategies for performance improvement and emissions reduction in compression ignition engines A review.
Renewable and Sustainable Energy Reviews, Vol. 28, pp. 664–676, 2013.
(cited on pp. 30, 31)

Molina S. A.
Influencia de los parámetros de inyección y la recirculación de gases de escape sobre el proceso de combustión en un motor Diesel.
Doctoral Thesis, Universidad Politécnica de Valencia, Departamento de Máquinas y Motores Térmicos, 2003. (cited on pp. 5, 45)

Monsalve J.
Dual-Fuel Compression ignition: Towards clean, highly efficient combustion.
Doctoral Thesis, Universidad Politécnica de Valencia, Departamento de Máquinas y Motores Térmicos, 2016. (cited on p. 62)

Musculus M. P. B., Lachaux T., Pickett L. M. and Idicheria C. A.
End-of-Injection Over-Mixing and Unburned Hydrocarbon Emissions in Low-Temperature-Combustion Diesel Engines.
SAE International, 2007. (cited on pp. vi, 23, 24)

Naber J. D. and Siebers D. L.
Effects of Gas Density and Vaporization on Penetration and Dispersion of Diesel Sprays.
SAE International, 1996. (cited on pp. 17, 18)

Nabi Md. N., Zare A., Hossain F. M., Bodisco T. A., Ristovski Z. D. and Brown R. J.
A parametric study on engine performance and emissions with neat diesel and diesel-butanol blends in the 13-Mode European Stationary Cycle.
Energy Conversion and Management, Vol. 148, pp. 251–259, 2017. (cited on p. 81)

Nishimura T., Satoh K., Takahashi S. and Yokota K.
Effects of Fuel Injection Rate on Combustion and Emission in a DI Diesel Engine.
SAE International, 1998. (cited on p. 32)

Nova I. and Tronconi E.
Urea-SCR Technology for deNOx After Treatment of Diesel Exhausts.
Springer, 2014. (cited on p. 8)

Novella R.
Influencia de los ciclos Atkinson y Miller sobre el proceso de combustión y las emisiones contaminantes en un motor Diesel.
Doctoral Thesis, Universidad Politécnica de Valencia, Departamento de Máquinas y Motores Térmicos, 2009. (cited on pp. 6, 58)

Park S., Kim Y., Woo S. and Lee K.
Optimization and calibration strategy using design of experiment for a diesel engine.
Applied Thermal Engineering, Vol. 123, pp. 917–928, 2017. (cited on p. 126)

Park S. W.
Optimization of combustion chamber geometry for stoichiometric diesel combustion using a micro-genetic algorithm.
Fuel Processing Technology, Vol. 91 n^o 11, pp. 1742–1752, 2010. (cited on p. 32)

Payri F., Olmeda P., Martín J. and García A.
A complete 0D thermodynamic predictive model for direct injection diesel engines.
Applied Energy, Vol. 88 n^o 12, pp. 4632–4641, 2011. (cited on p. 61)

Pickett L. M., Manin J., Genzale C. L., Siebers D. L., Musculus M. P. B. and Idicheria C. A.
Relationship Between Diesel Fuel Spray Vapor Penetration/Dispersion and Local Fuel Mixture Fraction.
SAE International Journal of Engines, Vol. 4 n^o 1, pp. 764–799, 2011. (cited on p. 21)

Pickett L. M. and Siebers D. L.
Soot in diesel fuel jets: effects of ambient temperature, ambient density, and injection pressure.
Combustion and Flame, Vol. 138 n^o 1-2, pp. 114–135, 2004. (cited on p. 112)

Piumetti M., Bensaid S., Fino D. and Russo N.
Catalysis in Diesel engine NOx aftertreatment: a review.
Catalysis, Structure & Reactivity, Vol. 1 n^o 4, pp. 155–173, 2015. (cited on p. 6)

Posada F., Chambliss S. and Blumberg K.
Costs of emission reduction technologies for heavy-duty Diesel vehicles.
The international council on clean transportation, 2016. (cited on p. 29)

Reitz R. D. and Ehe J.
Use of in-cylinder pressure measurement and the response surface method for combustion feedback control in a diesel engine.
Proceedings of the Institution of Mechanical Engineers, Part D: Journal of Automobile Engineering, Vol. 220 n^o 11, pp. 1657–1666, 2006. (cited on p. 77)

Reitz R.D. and Diwakar R.
Structure of High-Pressure Fuel Sprays.
SAE International, 1987.
870598. (cited on p. 69)

Rexeis M., Quaritsch M., Hausberger S., Silberholz G., Kies A., Steven H. and Vermeulen R.
VECTO tool development: Completion of methodology to simulate Heavy Duty Vehicles' fuel consumption and CO2 emissions.
European Comission, 2017. (cited on p. 152)

Ruiz S.
Estudio Teórico-Experimental de los procesos de atomización y de mezcla en los chorros diesel D.I.
Doctoral Thesis, Universidad Politécnica de Valencia, Departamento de Máquinas y Motores Térmicos, 2003. (cited on p. 17)

Salvador F.J.
Estudio teórico experimental de la iflnuencia de la geometría de la tobera de inyección sobre las caracteristicas del flujo interno y del chorro.
Doctoral Thesis, Universidad Politécnica de Valencia, Departamento de Máquinas y Motores Térmicos, 2003. (cited on p. 17)

Schwoerer J., Dodi S., Fox M., Huang S. and Yang Z.
Internal EGR Systems for NOx Emission Reduction in Heavy-Duty Diesel Engines.
SAE Technical Paper-2004-01-1315, 2004.
doi:10.4271/2004-01-1315. (cited on pp. 38, 104, 132)

Serrano J. R., Bermúdez V., Piqueras P. and Angiolini E.
On the impact of DPF downsizing and cellular geometry on filtration efficiency in pre- and post-turbine placement.
Journal of Aerosol Science, Vol. 113 n^o Supplement C, pp. 20–35, 2017. (cited on p. 6)

Shi L., Cui Y., Deng K., Peng H. and Chen Y.
Study of low emission homogeneous charge compression ignition (HCCI) engine using combined internal and external exhaust gas recirculation (EGR).
Energy, Vol. 31 n^o 14, pp. 2665–2676, 2006. (cited on p. 38)

Shi Y. and Reitz R. D.
Assessment of Optimization Methodologies to Study the Effects of Bowl Geometry, Spray Targeting and Swirl Ratio for a Heavy-Duty Diesel Engine Operated at High-Load.
SAE International Journal of Engines, Vol. 1 n^o 1, pp. 537–557, 2008. (cited on p. 77)

Shi Y. and Reitz R. D.
Optimization study of the effects of bowl geometry, spray targeting, and swirl ratio for a heavy-duty diesel engine operated at low and high load.
International Journal of Engine Research, Vol. 9 n^o 4, pp. 325–346, 2008.
(cited on p. 76)

Siebers D. L.
Scaling Liquid-Phase Fuel Penetration in Diesel Sprays Based on Mixing-Limited Vaporization.
SAE International, 1999. (cited on p. 18)

Siebers D. L. and Higgins B.
Flame Lift-Off on Direct-Injection Diesel Sprays Under Quiescent Conditions.
SAE International, 2001. (cited on p. 21)

SIEMENS Corp.
Release notes Star-CD 4.26.
SIEMENS,Corp., 2016. (cited on pp. 69, 70)

Su T. F., Chang C. T., Reitz R. D., Farrell P. V., Pierpont A. D. and Tow T. C.
Effects of Injection Pressure and Nozzle Geometry on Spray SMD and D.I. Emissions.
SAE International, 1995. (cited on p. 31)

Subramanian G., Vervisch L. and Ravet F.
New Developments in Turbulent Combustion Modeling for Engine Design ECFM-CLEH Combustion Submodel.
SAE International, 2007.
2007-01-0154. (cited on p. 69)

Taghavifar H., Jafarmadar S., Taghavifar H. and Navid A.
Application of DoE evaluation to introduce the optimum injection strategy-chamber geometry of diesel engine using surrogate epsilon-SVR.
Applied Thermal Engineering, Vol. 106, pp. 56–66, 2016. (cited on p. 77)

Torregrosa A. J., Olmeda P., Degraeuwe B. and Reyes M.
A concise wall temperature model for DI Diesel engines.
Applied Thermal Engineering, Vol. 26 n^o 11-12, pp. 1320–1327, 2006. (cited on p. 60)

Verschaeren R., Schaepdryver W., Serruys T., Bastiaen M. and Vervaeke, L.and Verhelst S.
Experimental study of NOx reduction on a medium speed heavy duty diesel engine by the application of EGR (exhaust gas recirculation) and Miller timing.
Energy, Vol. 76 n^o 0, pp. 614–621, 2014. (cited on p. 36)

Vervisch P.E., Colin O., Michel J.B. and Darabiha N.
NO Relaxation Approach (NORA) to predict thermal NO in combustion chambers.
Combustion and Flame, Vol. 158 n^o 8, pp. 1480–1490, 2011. (cited on p. 69)

Volvo Group Trucks Technology .
VOLVO D13K460 EURO VI version.
Available technical information in http://http://productinfo.vtc.volvo.se/STPIFiles/Volvo/FactSheet/D13K460, (cited on pp. vi, 7)

Wang Y., Zeng S., Huang J., He Y., Huang X., Lin L. and Li S.
Experimental investigation of applying miller cycle to reduce NOx emission from diesel engine.
Proceedings of the Institution of Mechanical Engineers, Part A: Journal of Power and Energy, Vol. 219 n^o 8, pp. 631–638, 2005. (cited on p. 36)

Weaver L. K.
Carbon monoxide poisoning.
Critical Care Clinics, Vol. 15 n^o 2, pp. 297–317, 1999. (cited on p. 4)

Wickman D. D., Senecal P. K. and Reitz R. D.
Diesel Engine Combustion Chamber Geometry Optimization Using Genetic Algorithms and Multi-Dimensional Spray and Combustion Modeling.
SAE International, 2001. (cited on p. 33)

Woschni G.
A universally applicable equation for the instantaneous heat transfer coefficient in the internal combustion engines.
SAE Paper 670931, 1967. (cited on p. 60)

Yadav J. and Ramesh A.
Injection strategies for reducing smoke and improving the performance of a butanol-diesel common rail dual fuel engine.
Applied Energy, Vol. 212, pp. 1–12, 2018. (cited on p. 85)

Yakhot V. and Orszag S. A.
Renormalization group analysis of turbulence. I. Basic theory.
Journal of Scientific Computing, Vol. 1 n^o 1, pp. 3–51, 1986. (cited on p. 69)

Yanowitz J., Graboski M. S. and McCormick R. L.
Prediction of In-Use Emissions of Heavy-Duty Diesel Vehicles from Engine Testing.
Environmental Science & Technology, Vol. 36 n^o 2, pp. 270–275, 2002. (cited on p. 119)

Zhang L., Ueda T., Takatsuki T. and Yokota K.
A Study of the Effects of Chamber Geometries on Flame Behavior in a DI Diesel Engine.
SAE International, 1995. (cited on p. 32)

Zheng Z. and Yao M.
Mechanism of Oxygen Concentration Effects on Combustion Process and Emissions of Diesel Engine.
Energy & Fuels, Vol. 23 n^o 12, pp. 5835–5845, 2009. (cited on p. 69)